



**Masterthesis**

---

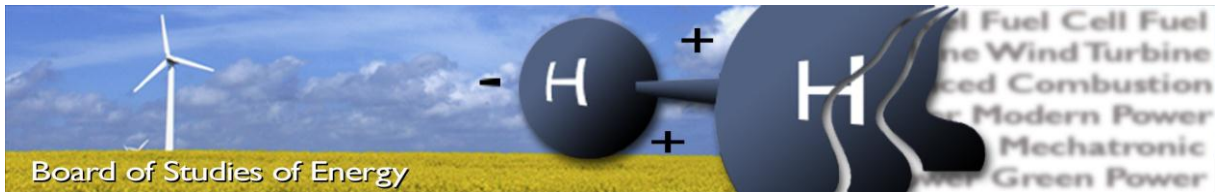
---

**Variable Speed Wind Turbine equipped with a  
Synchronous Generator**

---

---

by  
**Christian Freitag**



**Title:** Variable Speed Wind Turbines equipped with a Synchronous Generator  
**Semester:** 4<sup>th</sup>  
**Semester theme:** Master thesis  
**Project period:** 13.09.10 – 04.01.11  
**ECTS:** 30  
**Supervisor:** Ömer Göksu  
Remus Teodorescu  
Lars Helle  
**Project group:** 954

---

[Christian Freitag]

**SYNOPSIS:**

*This master thesis is initiated by a project proposal from Vestas Wind Systems A/S which is one of the leading manufacturers of wind turbine systems in the world. The proposal deals with DC-DC connected offshore wind farms with a HVDC-link to the shore line which is a promising technical solution regarding the increasing demand of electrical power and the long distances between on- and offshore sites. The main goal is the development of steady state models of an entire wind turbine system with selected AC-DC converters between the generator output and DC-DC connection of the wind turbines.*

Copies: 5  
Pages, total: 80  
Appendix: 1  
Supplements: CD

**By signing this document, each member of the group confirms that all participated in the project work and thereby that all members are collectively liable for the content of the report.**

**Table of contents**

<b>1</b>	<b>Introduction.....</b>	<b>1</b>
1.1	Abstract .....	1
1.2	Importance of wind power.....	1
1.3	Background.....	1
1.4	Objectives of the master thesis.....	1
1.5	Problem statement.....	1
1.6	Outline of the following report .....	2
<b>2</b>	<b>Background information and basics .....</b>	<b>3</b>
2.1	Conversion of wind power to electrical power .....	3
2.1.1	The energy content of the wind .....	3
2.1.2	The amount of power harnessed from the wind .....	4
2.1.3	Control mechanisms.....	5
2.1.3.1	Pitch control .....	5
2.1.3.2	Power control .....	5
2.2	Overview of wind turbine systems.....	6
2.2.1	Fixed speed wind turbine systems .....	6
2.2.2	Limited variable speed wind turbine systems.....	7
2.2.3	Variable speed wind turbines systems.....	7
2.2.4	Comparison of wind turbine systems.....	9
2.3	Connection topologies .....	11
2.3.1	Different wind park concepts.....	11
2.3.1.1	AC-AC concept.....	11
2.3.1.2	AC-DC concept.....	12
2.3.1.3	DC-DC concepts .....	12
2.3.2	Comparison of connection topologies .....	14
2.4	AC-DC-converters .....	15
2.4.1	Boost converter .....	15
2.4.2	Buck-boost converter .....	16
2.4.3	Buck-Boost converter with high frequency transformer .....	18
2.4.4	Cúk converter .....	18
2.4.5	Cúk converter with high frequency transformer.....	20
2.4.6	Full-bridge converter .....	20
2.4.7	Active three phase rectifier .....	21
2.5	Comparison of AC-DC-converters.....	22
2.6	Summary.....	23
<b>3</b>	<b>Specifications of the wind turbine system.....</b>	<b>24</b>
3.1	Wind turbine .....	24

3.2	Gear box and generator .....	24
3.3	HVDC connection.....	25
<b>4</b>	<b>Wind turbine system modeling.....</b>	<b>26</b>
4.1	Wind .....	26
4.2	Rotor.....	26
4.3	Gear box .....	28
4.4	Generator .....	29
4.5	DC-DC connection.....	32
4.6	AC-DC converters .....	33
4.6.1	Three phase rectifier .....	33
4.6.2	Buck-boost converter with a high frequency transformer.....	35
4.6.2.1	Configuration and design of the Buck-boost converter .....	35
4.6.2.2	Simulation of the ideal Buck-boost converter.....	38
4.6.2.3	Modeling the Buck-boost converter.....	39
4.6.3	Cúk converter with a high frequency transformer.....	50
4.6.3.1	Configuration and design of the Cúk converter .....	50
4.6.3.2	Simulation of the ideal Cúk converter.....	54
4.6.3.3	Modeling the Cúk converter.....	55
4.6.4	Summary.....	67
<b>5</b>	<b>Simulation and evaluation of the results.....</b>	<b>68</b>
5.1	Simulation.....	68
5.1.1	Iteration of the duty ratio D .....	68
5.1.1.1	Calculation of the real duty ratio in a Buck-boost converter .....	68
5.1.1.2	Calculation of the real duty ratio in a Cúk converter .....	69
5.1.2	Iteration of the power factor $c_p$ .....	69
5.1.3	Algorithm behind the simulation .....	69
5.2	Performance factors and evaluation.....	71
5.2.1	Efficiency .....	71
5.2.2	Annual energy production.....	73
<b>6</b>	<b>Conclusion .....</b>	<b>76</b>
6.1	Further work.....	76
	<b>References .....</b>	<b>77</b>
	<b>List of figures.....</b>	<b>79</b>
	<b>Appendix .....</b>	<b>a</b>

# **1 Introduction**

## **1.1 Abstract**

This master thesis is initiated by a project proposal from Vestas Wind Systems A/S which is one of the leading manufacturers of wind turbine systems in the world. The proposal deals with DC-DC connected offshore wind farms with a HVDC-link to the shore line. This is a promising technical solution regarding the increasing demand of electrical power and the long distances between on- and offshore sites. The main goal is the development of steady state models of an entire wind turbine system with selected AC-DC converters between the generator output and DC-DC connection of the wind turbines. The Buck-boost and the Cúk converter both in combination with a high frequency transformer and a three phase rectifier are selected for modeling in this thesis. The models are used as a basis for the simulations of the two different wind turbine systems with a wind speed ramp as input. Relying on these simulations two performance factors are investigated, efficiency and annual energy production.

## **1.2 Importance of wind power**

Sustainable energies become more and more important as part of the global electrical energy consumption. The demand of electrical energy is rising globally. Usual sources like coal fired power plants or nuclear power stations cause environmental problems today and even more in the near future. The greenhouse effect and the still not solved problem of a safe disposal of radioactive waste are merely two keywords which should be mentioned here.

One way out of the dilemma explained above is wind power as a source for electrical power. There are countries like Denmark or Germany which follow ambitious aims in increasing their capacity of wind power up to 20 % of the national electrical energy consumption. But wind power, which is the most important source among renewable energies, is also an answer to the continuously rising demand of electrical energy in countries like India or China.

## **1.3 Background**

Previously, wind turbines were sited individually or in small concentrations which made it most economical to operate each turbine as a single unit. Today and in the future, wind turbines will be located in remote areas (especially offshore) and in large concentrations counting up to several hundreds of MW installed power. This opens new technical opportunities for designing and controlling the wind turbines. But at the same time, demands to reliability and availability increase.

## **1.4 Objectives of the master thesis**

In this thesis entire wind power systems as described in the abstract are modeled. The main focus is set on the development of AC-DC-converter models in the steady state theory as needed in these wind turbine systems. Next to the modeling, the simulation of the entire wind turbine system is another important aspect. In the end, two wind power systems which differ in the used AC-DC converters are compared according to the selected performance factors efficiency and annual energy production.

## **1.5 Problem statement**

Development of a simulation tool for selected AC-DC converters as part of a variable speed wind turbine system equipped with a synchronous generator to compare these AC-DC converters.

## **1.6 Outline of the following report**

After a brief comparison of the commonly used turbine and generator concepts the most suitable solution is chosen. It is a permanent magnet synchronous generator with a gearbox. In a next step, connection topologies of the wind turbine systems to the grid are considered and an applicable version is selected for further investigation. In this case, a DC-DC connected wind farm with a HVDC-link to the shore line is chosen. The two interfaces, the turbine-generator concept and the HVDC connection, build a frame for the comparison of AC-DC-converters between the generator and the HVDC transmission. Different types of AC-DC converters are introduced and compared. The two most promising applications are the Buck-boost and the Cúk converter (chapter 2).

The specifications of the wind turbine system are stated in chapter 3. The data describing the wind turbine, the gear box, the generator and the HVDC connection are presented here.

All selected parts of wind turbine system for DC-DC connected offshore wind farms with a HVDC-link to the shore line are modeled in Matlab in the steady state theory. Before the AC-DC converters are modeled their circuits are configured. This means values for electrical devices like inductors and capacitors are computed depending on the needed performance of the converters. In order to prove the functionality, both converters are simulated in the real time circuit simulation software PSIM. This software is also used to verify the modeling of the converters (chapter 4).

Based on the models developed in chapter 4 both wind turbine systems depending on the different converters are simulated. The simulation algorithm is explained in detail. The wind turbine systems are discussed regarding the performance factors efficiency and annual energy production (chapter 5).

The conclusion of the work done during this master thesis is stated in chapter 6.

## 2 Background information and basics

This chapter discusses background information and basics about wind power systems regarding the proposal. It gives a brief overview about the topic and explains which wind turbine system concepts, connection topologies and converter types are selected in this thesis.

### 2.1 Conversion of wind power to electrical power

In this section is explained how the power of the wind is extracted by a wind turbine and converted to electrical power. At first, the energy content of the wind is calculated. Later on is described which part of the wind power can be converted to mechanical power which is depending on the efficiency related to the electrical power.

#### 2.1.1 The energy content of the wind

The energy of a moving medium is:

$$E = \frac{1}{2}mv^2 \quad 2-1$$

*E: energy*

*m: mass of the medium (in this case air)*

*v: velocity of the medium (in this case wind speed)*

The power of the wind can be calculated by derivation of the wind energy (2-2). The wind speed  $v$  is assumed to be constant.

$$\frac{dE}{dt} = P = \frac{1}{2} \frac{dm}{dt} v^2 \quad 2-2$$

With (2-3)

$$\frac{dm}{dt} = \rho \frac{dV}{dt} = \rho A \frac{ds}{dt} = \rho Av \quad 2-3$$

*$\rho$ : density of air (is estimated to be constant)*

*V: volume*

the power of the wind is expressed in the following equation:

$$P = \frac{1}{2} \rho Av^3 \quad 2-4$$

*A: swept area*

The swept area depends on the length of the rotor blades  $r_b$ , so the power of the wind can finally be written as:

$$P = \frac{1}{2} \rho r_b^2 \pi v^3 \quad 2-5$$

The density of air is  $\rho = 1,225 \text{ kg/m}^3$  at  $p = 1013 \text{ hPa}$  and  $T = 288\text{K}$  or  $15^\circ\text{C}$ . This density value will be used in the following report [1] [2].

### 2.1.2 The amount of power harnessed from the wind

A German physicist<sup>1</sup> calculated the maximum value of power which could be extracted from the wind. This border is called Betz limit and says that not more than 59,3 % of wind power can be transformed into mechanical power. The Betz limit is merely an ideal value. It is based on physical laws and mathematical equations and does not depend on the design of the wind turbine. Real wind turbines have a power coefficient  $c_p$  which is lower than the Betz limit. But similar to the Betz limit the power coefficient says which percentage of the wind power can be converted to mechanical power and additionally depending on the efficiency to electrical power [2].

$$P = \frac{1}{2} c_p \rho r_b^2 \pi v^3 \quad 2-6$$

The power coefficient  $c_p$  is a function of the tip speed ratio  $\lambda$  and the pitch angle  $\theta$ , which can be seen in figure 2.1. The pitch angle  $\theta$  is the angle between the plane of rotation and the blade cross section chord. Its value is zero at the maximum power extraction from wind.

The tip speed ratio is defined in the following equation [1]:

$$\lambda = \frac{v_{rotor}}{v_{wind}} = \frac{r_b \omega}{v_{wind}} \quad 2-7$$

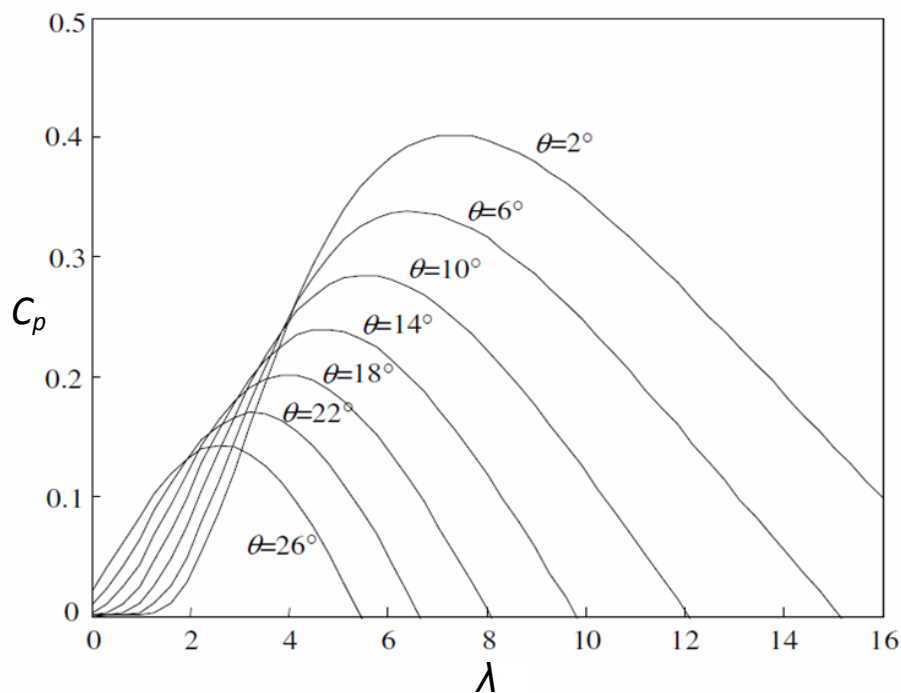


Figure 2.1 Power coefficient  $C_p$  as a function of the tip speed ratio  $\lambda$  and the pitch angle  $\theta$  [3]

<sup>1</sup> Albert Betz 1885-1965

### 2.1.3 Control mechanisms

Wind turbines must be controlled depending on the available wind power and the required power output. There are two control strategies, stall and pitch control. The stall control mechanism is a passive regulation of the wind turbine. Its main duty is to reduce the power extraction from the wind at too high wind speeds, which are dangerous for the wind turbine. It is used in fixed speed wind turbines (→ 2.2.1). Nowadays a pitch control is used in variable speed turbines [1].

#### 2.1.3.1 Pitch control

In contrast to the stall control, the pitch control mechanism is an active regulation of the power extracted from the wind. It changes the pitch angle by turning the blades. The pitch angle is zero at maximum power extraction. It is increased at too high wind speeds or if the demand of power is less than the possible extracted power. Both is done in order to decrease the output power and to reduce the rotational speed of the wind turbine. But in this thesis the main focus is on the maximum power extraction of the wind. So the pitch control is only used to avoid too high rotational speeds at wind speeds above nominal speed [1].

#### 2.1.3.2 Power control

The power harnessed from the wind by the turbine is converted in electrical power by the generator. As mentioned above a maximum power extraction of the wind is considered in this report. Figure 2.2 shows the output power of the generator as function of the wind speed  $v$ . At cut-in speed of the wind the turbine starts working. The power coefficient  $c_p$  is kept constant at its maximum value. When reaching rated speed, the tip speed is at its maximum. If the wind speed is still increasing the tip speed has to be constrained in order to avoid damage of the wind turbine. Keeping the tip speed constant, means decreasing the power coefficient and so the output power of the generator is kept constant at its maximum. At cut-out speed of the wind the wind turbine is shut down to prevent damage to rotor and generator [4].

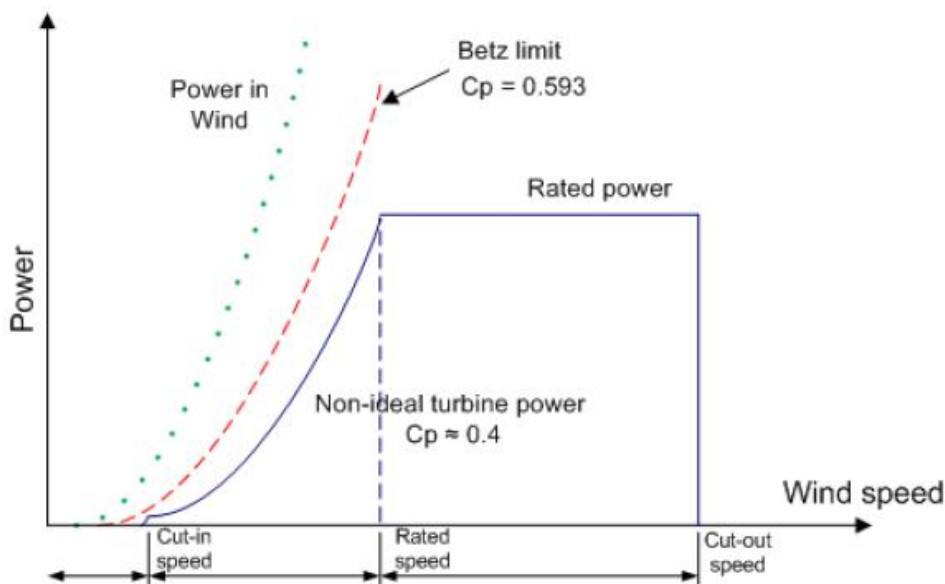


Figure 2.2 Power versus wind speed [4]

## 2.2 Overview of wind turbine systems

Wind turbine systems can mainly be divided in fixed, limited variable and variable speed concepts.

### 2.2.1 Fixed speed wind turbine systems

These turbine systems (figure 2.3) were developed more than 25 years ago and do not contain power electronics. They are directly connected to the grid. The active power is limited aerodynamically by stall (I) , active stall (II) or pitch (III) control. The aerodynamical control is not able to operate very fast, only within a few seconds. Systems based on this solution cause negative impacts on the grid. The induction generator with its demand of reactive power makes a reactive power compensator necessary. The large inrush current while the wind turbine system starts operating causes the need of soft starter. Otherwise the high current value creates flicker problems [5]. This configuration relying on an induction generator with a direct grid coupling is known as the 'Danish concept'. It was introduced and commonly built in the 1980s [1] [6].

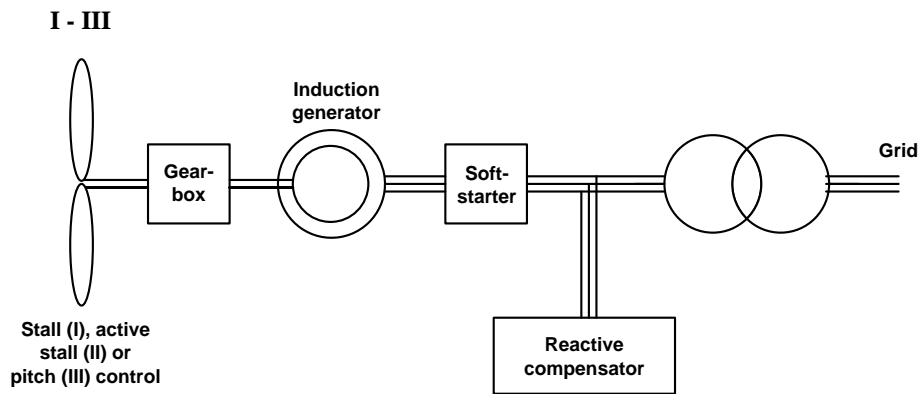


Figure 2.3 Fixed speed wind power system with different control mechanisms [5]

Another type of this concept (IV) which allows a very limited variability of speed is explained in figure 2.4. It consists of an induction generator with a wound rotor. Power electronics controls a resistance which is connected to the rotor via slip-rings. A speed range of 2 – 5 % around synchronous speed is possible with this dynamic slip controller. This solution of a wind turbine system still needs a reactive power compensator and a soft starter in order to avoid negative impacts on the grid. Compared to systems mentioned above a better control bandwidth can be achieved. The small speed range is the reason why it is added to the fixed speed wind power concepts [5].

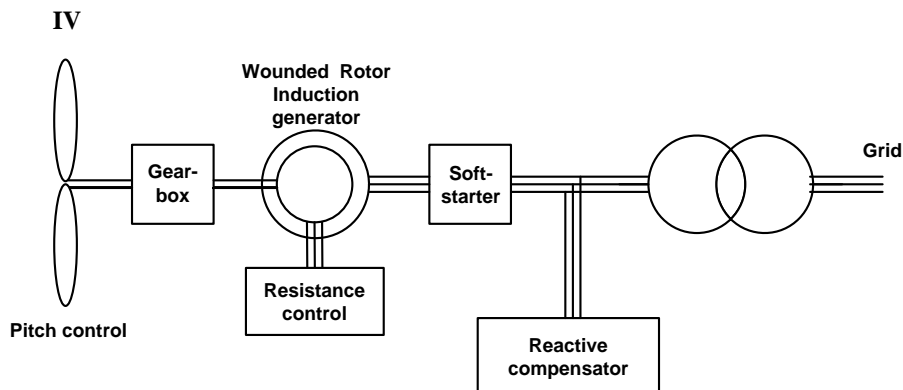


Figure 2.4 Wind turbine with a wounded rotor induction generator and resistance control [5]

### 2.2.2 Limited variable speed wind turbine systems

Systems relying on this concept (V) are the next generation of wind turbines. A higher performance and a better controllability of the active power can be achieved by the usage of power electronics.

The type of a limited speed wind turbine mentioned here consists mainly of a double-fed induction generator. It uses a medium scale power converter to rule the wounded rotor induction machine. The power converter controls the current in the rotor and allows so a speed range of +/- 30 % around synchronous speed. The medium scale converter must be created for merely 30 % of the generated power, which makes this solution cost effective [5]. This application is able to control active and reactive power provided for the grid and the medium scale converter performs the reactive power compensation and a smooth grid connection [6].

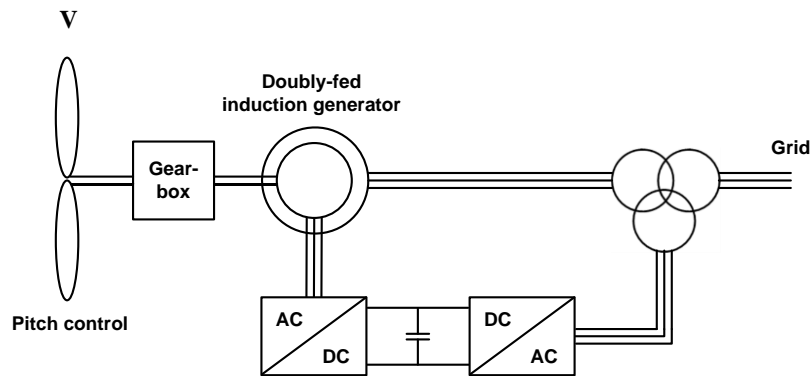


Figure 2.5 Limited speed wind power system with a doubly-fed induction generator [5]

### 2.2.3 Variable speed wind turbines systems

These turbines are systems with a full scale power converter between the generator and the grid. In this solution the generator works absolutely independently because the DC-Link uncouples the generator from the grid. Hence, these wind turbine systems offer the best dynamic system behavior; they are the ultimate technical solutions. However, the generated power must pass the power converter and as a result there are higher losses compared to the concept containing a double fed induction machine. But a higher performance can be achieved. So reactive and active power is controlled and reactive power can be provided even if there is no wind [6] [5].

Solutions VI to IIX (figure 2.6, 2.7 and 2.8) show variable speed wind turbines equipped with an asynchronous and in the last two cases with synchronous machines. All applications need a gear box [5]. Comparing the solutions with a synchronous generator, concept VII needs a medium scale converter for field excitation while application IIX uses permanent magnets instead.

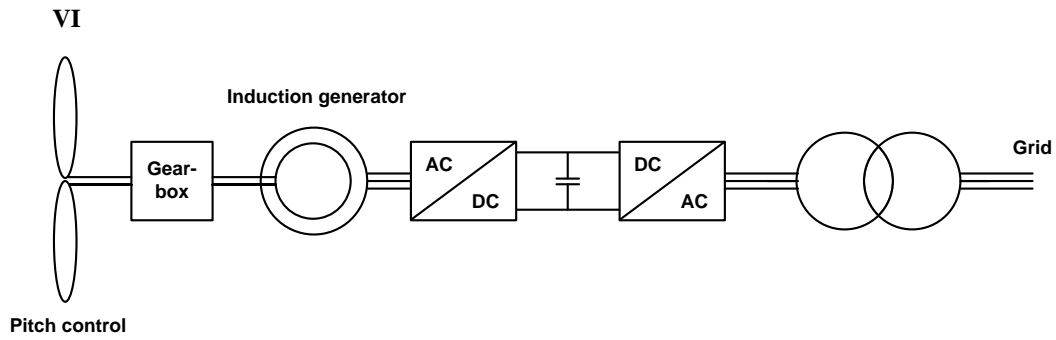


Figure 2.6 Variable speed wind power system with a squirrel cage induction generator [5]

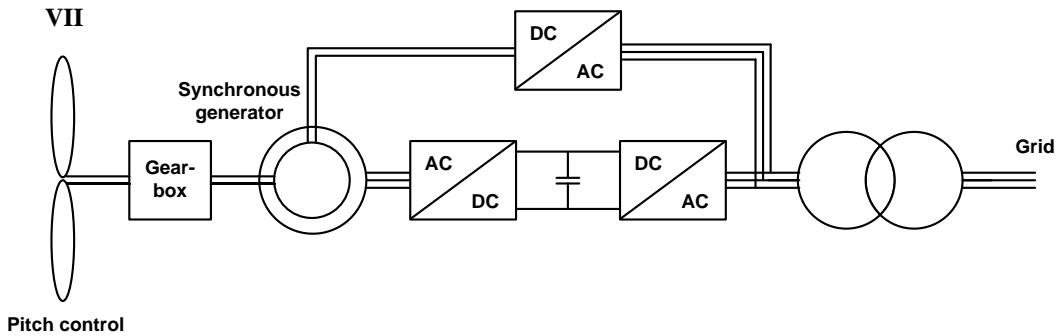


Figure 2.7 Variable speed wind power system with a synchronous generator [5]

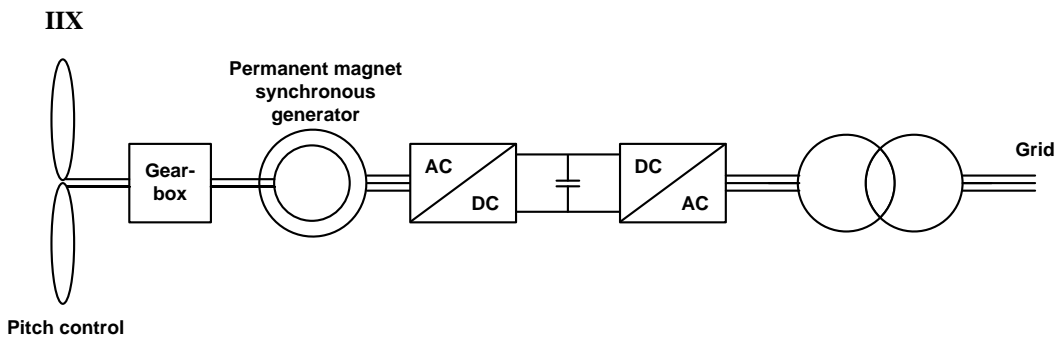


Figure 2.8 Variable speed wind power system with a permanent magnet synchronous generator

The wind turbine systems shown in the figure 2.9 and 2.10 do not need a gear box because Multi-pole synchronous generators are used here. The application X is equipped with permanent magnets and does not need a medium scale converter for field excitation like solution IIX does [5].

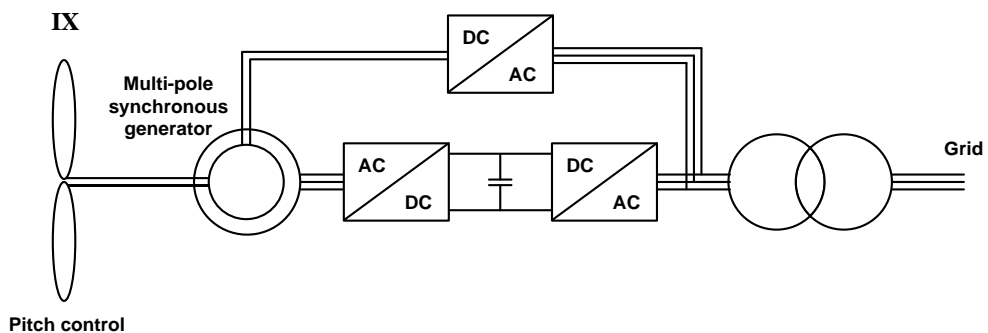


Figure 2.9 Variable speed wind power system with a Multi-pole synchronous generator [5]

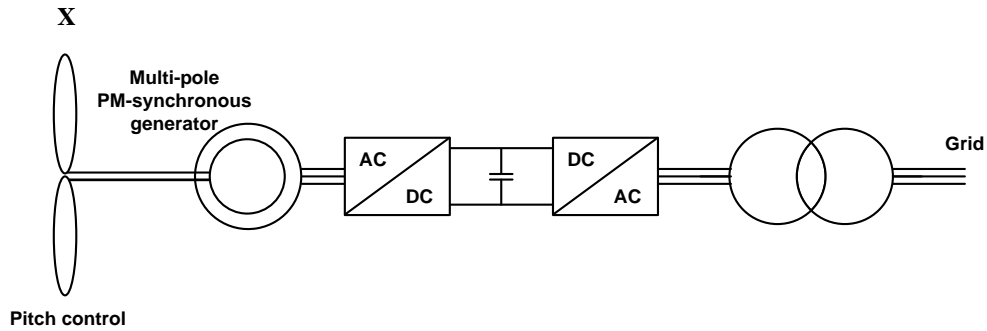


Figure 2.10 Variable speed wind power system with a Multi-pole PM-synchronous generator [5]

### 2.2.4 Comparison of wind turbine systems

System comparison of wind turbines [5]										
System	I	II	III	IV	V	VI	VII	IIX	IX	X
Variable speed	No	No	No	No	limited	Yes	Yes	Yes	Yes	Yes
Control active power	limited	No	limited	limited	Yes	Yes	Yes	Yes	Yes	Yes
Control reactive power	No	No	No	No	Yes	Yes	Yes	Yes	Yes	Yes
Short circuit (fault-active)	No	No	No	No	No /Yes	Yes	Yes	Yes	Yes	Yes
Control bandwidth	1-10s	1-10s	1-10s	100ms	1ms	0,5-1ms	0,5-1ms	0,5-1ms	0,5-1ms	0,5-1ms
Flicker	Yes	Yes	Yes	Yes	No	No	No	No	No	No
Softstarter needed	Yes	Yes	Yes	Yes	No	No	No	No	No	No
Reactive power compensator	Yes	Yes	Yes	Yes	No	No	No	No	No	No
Investment	++	++	++	++	+	0	0	0	0	0
Maintenance	++	++	++	++	0	+	+	+	+	+

Table 2.1 Comparison of wind turbine systems

This table shows all different wind turbine concepts in direct comparison. The three mentioned groups of wind turbine systems are colored differently.

The fixed speed solutions (*dark grey*) show a not dynamic behavior as part of the grid. The control of active power is slow and limited. These applications do not provide a reactive power control. In case of a short circuit the generator is disconnected and cannot be used to build grid voltage up again [6]. But the investments for these systems and the costs for maintenance are low [5].

The wind turbine with a limited speed concept (*grey*) has a better dynamic behavior according to active and reactive power control and the control bandwidth. On the other hand investment and maintenance costs increase [5].

## **2. Background information and basics**

Variable wind speed turbines (*white*) show the best dynamic behavior with a positive impact on the grid regarding reactive power. These types of turbines are able to stay connected to the grid during and after a fault if they are equipped with power converter protection, so they can improve the stability of the grid [6]. Nevertheless the investment and maintenance costs have the highest value of all WPSs mentioned here [1].

Power generation in general will contain more wind power in the near future. Wind turbines must be reliable and dynamically controllable depending on the demand of active and reactive power. Another important aspect is the negative impact on the grid; it should be as less as possible. Wind turbines relying on fixed or limited fixed speed concepts are developments of a time in which semiconductors with a high performance were not available or too cost intensive. These concepts are not able to fulfill the mentioned requirements. Only variable speed wind turbines are able to fulfill these requirements. That is the reason why only concepts based on variable speed will be investigated in this thesis.

## 2.3 Connection topologies

In this part of the chapter the commonly discussed connection topologies in wind farms situated offshore are introduced. The demand of electrical power generated by the wind will increase in the near future. Offshore wind energy is an important way to cover this demand and so a keystone of the policy of many European countries. The electrical power generated by the wind turbine and harnessed from the wind has to be transferred from the offshore wind farm to the grid [7].

Figure 2.11 shows the general topology of an offshore wind farm. A number of wind turbines (WT), it differs from less than ten to a multiple of ten, are connected parallel to radials at the collecting point depending on the topology [8]. Each wind turbine can have its own voltage adjuster (VA) which offers an individual control of the wind turbine (string a)). But it is also possible to group a number of wind turbines parallel with merely one voltage adjuster (string b)). In this case all turbines within a group operate at the same speed, which may not be the optimum for each single unit. Losses in efficiency are the result and so the individual control with one voltage adjuster per turbine unit is preferred in this thesis [9]. In all following drawings the voltage adjuster (VA) is part of the wind turbine (WT) and is not shown separately. The wind turbine strings transfer the power to the collecting point in parallel connection, where the voltage is increased to a suitable level for transmission. The energy is transferred via the transmission system at a high voltage level from the collecting point to the wind farm grid interface. Here the voltage, frequency and reactive power of the transmission system are adjusted to the values required by the grid in the PCC (point of common connection) [10].

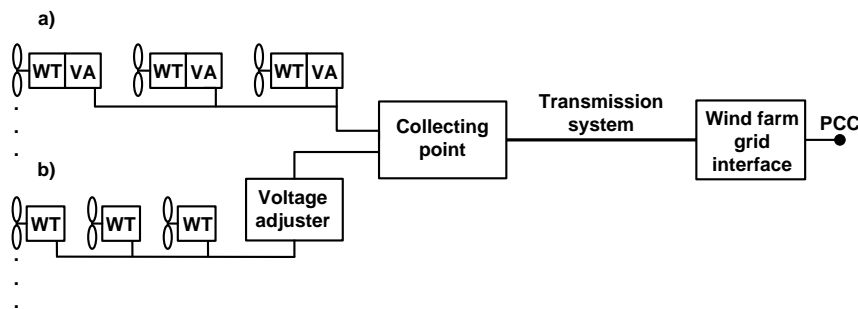


Figure 2.11 General topology of an off shore wind farm

### 2.3.1 Different wind park concepts

In the following more detailed solutions for wind farm topologies are discussed. The main focus is set on large wind farms with up to several 100 MW of output power, so concepts of small wind parks are not explained here

#### 2.3.1.1 AC-AC concept

This concept (figure 2.12) is based on a local wind park grid at a lower voltage level at a multiple of 10 kV. A number of wind turbines are connected parallel to a string and these join parallel at the collection point on an offshore platform. The medium voltage is increased by a transformer to a high voltage level. The transmission system is a HVAC-connection in this case. There were wind parks built relying on this concept like Horns Rev (Esbjerg, Denmark) or Nysted, (Lolland, Denmark) [10] [11]. The main disadvantages of this concept are that the losses increase with the transmission distance ( $\rightarrow$  2.3.2) and a lower redundancy as a result of the string connection. In case of a failure in one string connection to the PCC, all wind turbines belonging to this string are affected.

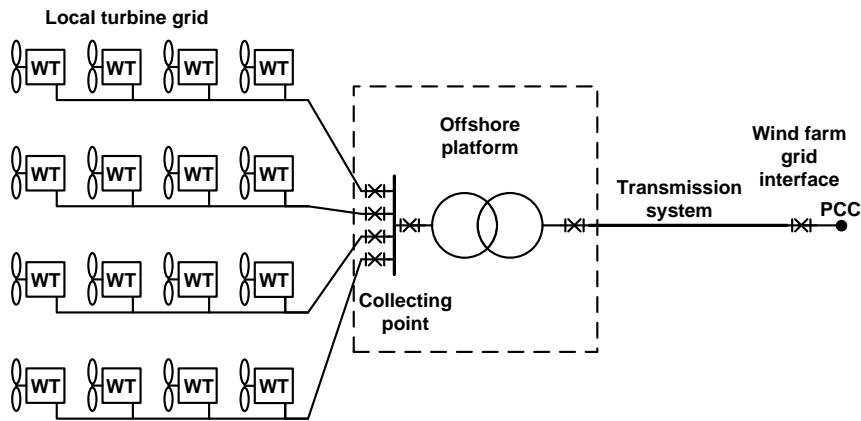


Figure 2.12 Offshore wind farm based on an AC-AC concept [10]

### 2.3.1.2 AC-DC concept

Comparing figure 2.12 to figure 2.13 the transformer is replaced by an AC-DC converter and the transmission system is a HVDC connection. The local wind turbine grid is an independent AC system where voltage and frequency are controlled by the offshore converter. Although this concept does not exist today it offers advantages regarding longer distances between offshore site and PCC [10]. The drawback of this concept is less redundancy because the string connection remains.

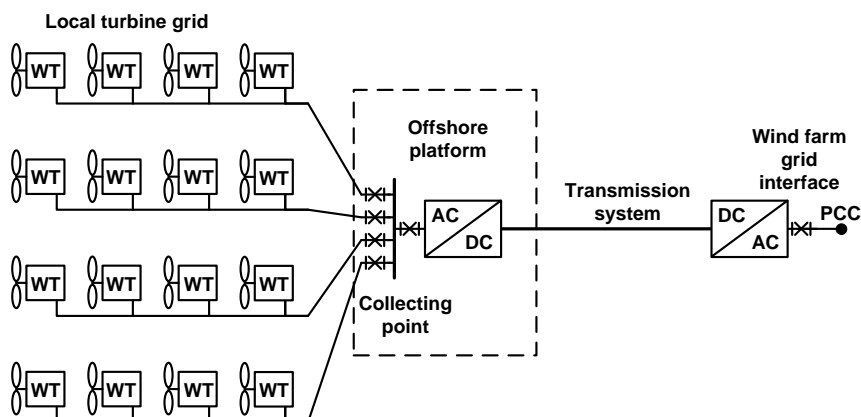


Figure 2.13 Offshore wind farm based on an AC-DC concept [10]

### 2.3.1.3 DC-DC concepts

In these concepts the wind turbines (WT) have a voltage adjuster (VA) with a DC output voltage. The electrical system of a large DC wind farm shown in figure 2.14 requires one or two converter steps to reach the high voltage level applicable for transmission. Depending on the output voltage of the wind turbines one step for output voltages of 20 to 40 kV and two converter steps for lower voltages of a few kV are needed. If two steps for conversion of the voltage are required the wind turbines are separated into smaller groups called clusters which are connected to the first conversion step parallel. The converters in the first step transfer the energy to a second converter in parallel connection. Here the voltage is built up to a level suitable for HVDC transmission. In this solution one offshore platform per cluster and one at the collection point are necessary. But if there is only one conversion step needed the wind turbines are connected radial to the converter at the collection point and merely one offshore platform must be installed [10].

## 2. Background information and basics

The concept explained above is a very complex system. The parallel connection needs many different cable routs and in case of a two step boosted voltage several offshore platforms are necessary. On the other hand it offers high redundancy in case of a failure and each turbine only has to be insulated against its own low or medium level voltage.

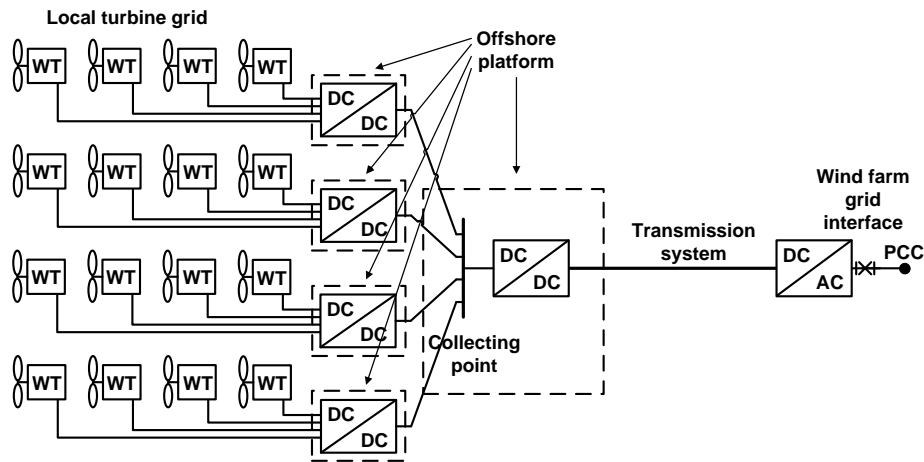


Figure 2.14 Offshore wind farm based on a DC-DC concept with parallel connection [10]

Figure 2.15 shows a DC system with a serial connection of the wind turbines which assures a high voltage level applicable for transmission. Wind farms relying on this solution can reach large sizes and do not need extra DC converters and offshore platforms, so this kind of a DC-DC concept needs fewer components than the one explained in figure 2.14 [10]. But each wind turbine has to be insulated against the high voltage of the HVDC link and the redundancy is lower compared to the other DC-DC concept above.

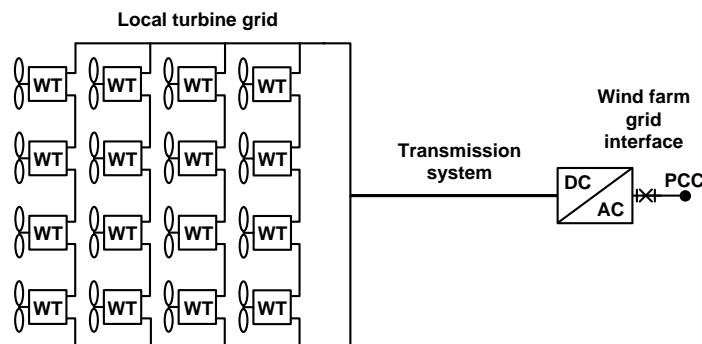


Figure 2.15 Offshore wind farm based on a DC-DC concept with serial connection [10]

### 2.3.2 Comparison of connection topologies

In the future, wind farms will be situated at large distances from the coastline, approaching 100 to 150 km. The reasons for building wind farms far away from the shore are environmental and social aspects, but also the increased energy yield [12].

Up to a distance of 60 km between offshore and on side an AC or DC link is theoretically possible. But at greater distances merely DC connections are suitable. The main advantages of DC transmission compared to an AC link between offshore wind farm and the onshore connection to the grid are stated here [13] [12]:

- At the same power level, DC cables are smaller, have lower losses and their length is not limited beyond practical constraints of cable manufacturing and cable laying [9] [14].
- The demand of reactive power is much lower compared to AC-cables, where a reactive power compensator is needed [14].
- The DC link provides fast control of active and reactive power, whereas the AC link provides no or slow control [7].
- There is no resonance between the cables and other AC devices [7].
- A high voltage direct current (HVDC) linked to the grid meets all interconnection voltage/frequency requirements. A larger AC cable installation will need an additional converter system onshore to reduce losses, assure stability and meet the interconnection voltage/frequency requirements [9].

This report focuses on wind farms located offshore where distances beyond 60 km are usual and so a HVDC link is the most applicable interconnection of wind farm and grid.

The different wind farm concepts based on a HVDC interconnection which are mentioned before, are compared in the following table.

Performance factor	AC-DC concept	DC-DC concept parallel connected	DC-DC concept serial connected
<i>Number of offshore platforms</i>	1	≥ 1	0
<i>Simplicity</i>	-	--	++
<i>Redundancy</i>	-	++	-

“-”: negative performance; “0”: in the middle; “+”: positive performance

**Table 2.2 Comparison of connection topologies**

The comparison in table 2.2 shows that the DC-DC concept with a serial connection of the wind turbine is most suitable especially regarding simplicity. It is also stated in [10] that the energy production costs for the series DC wind park are the lowest for all investigated wind park concepts explained in chapter 2. Hence the DC-DC park layout with serial connected wind turbines is the most promising solution and so chosen in this report.

## 2.4 AC-DC-converters

In section 2.3 a serial DC-DC connection topology is chosen as the most suitable park layout. This topology makes voltage adjusters between wind turbine and DC connection necessary which from now on are called AC-DC converters. A number of AC-DC converters which are commonly used as part of a wind power system are introduced here. They regulate the power flow from the generator to the main converter and so assure the maximum power output of the generator.

The first six converters have a DC-input and output voltage. The output AC-voltage of the generator is rectified by a three phase diode bridge in these applications and is assumed to be constant.

### 2.4.1 Boost converter

This converter is also called step-up converter (Figure 2.16) and as the name says its output voltage is greater than its input voltage. During the time the switch is on (Figure 2.17 a) the diode is reversed biased and the input energy is stored in the inductor. When the switch is turned off (Figure 2.17 b) the load receives energy from the input voltage as well as from the inductor, which is working as a source in this state. The current of the inductor, which is equal to the input current, rises during the on-state and decreases while the switch is turned off [15] [16].

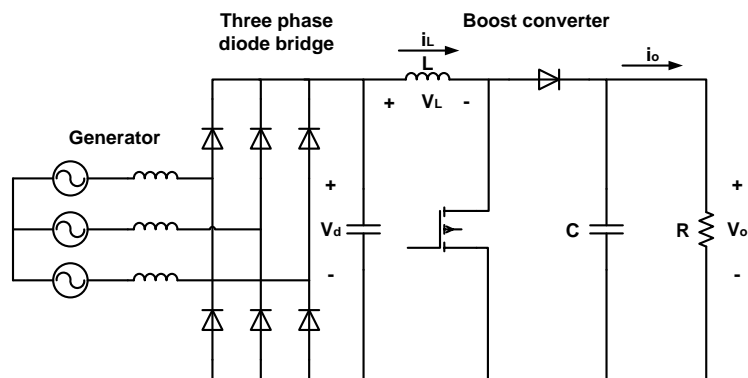


Figure 2.16: Boost converter

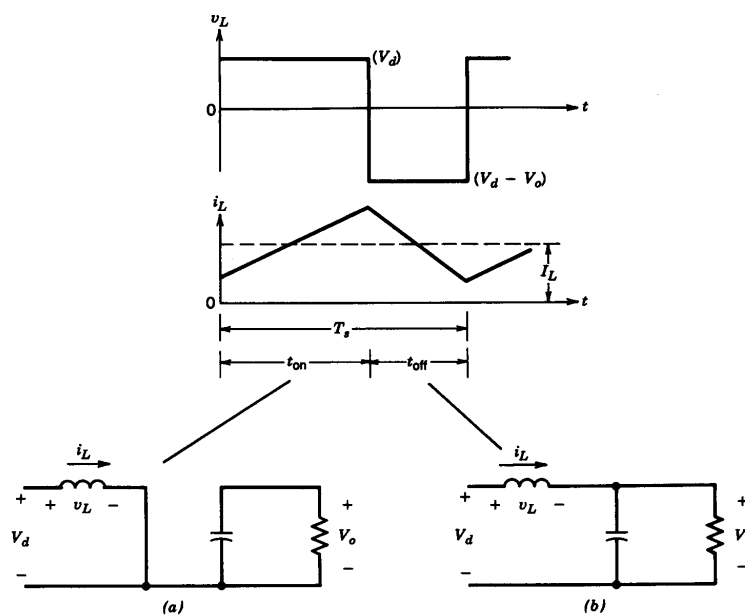


Figure 2.17: Off and on state of the boost converter [15]

The mathematical equation of the input and output voltage yields:

$$\frac{V_o}{V_d} = \frac{1}{1 - D} \quad 2-8$$

D is the duty ratio and defined by the ratio of the time when the switch is turned on and switching period.

Assuming a lossless converter, the equation for the currents follows:

$$\frac{I_o}{I_d} = 1 - D \quad 2-9$$

One of the drawbacks of this circuit is the great output capacitor needed to reduce the ripple of the output voltage. Another drawback is the losses at high duty cycles. They are caused by the copper resistance of the inductor.

### 2.4.2 Buck-boost converter

The Buck-boost converter is a cascade of a buck (step down) and a boost (step up) converter (Figure 2.18). It can have a higher or lower output voltage compared with the input voltage depending on the duty ratio. But the voltage at its output has a negative polarity. During the on state of the switch the inductor receives energy from the input voltage and the diode is reversed biased. When the switch is turned off the stored energy in the inductor is transferred to the output. The input voltage is disconnected and so does not transfer energy to circuit. The current of the inductor rises during the on-state and decreases while the switch is turned off (Figure 2.19).

Input and output voltages depend on each other as shown in the following equation:

$$\frac{V_o}{V_d} = \frac{D}{1 - D} \quad 2-10$$

Assuming a lossless circuit, the equation for the currents yields:

$$\frac{I_o}{I_d} = \frac{1 - D}{D} \quad 2-11$$

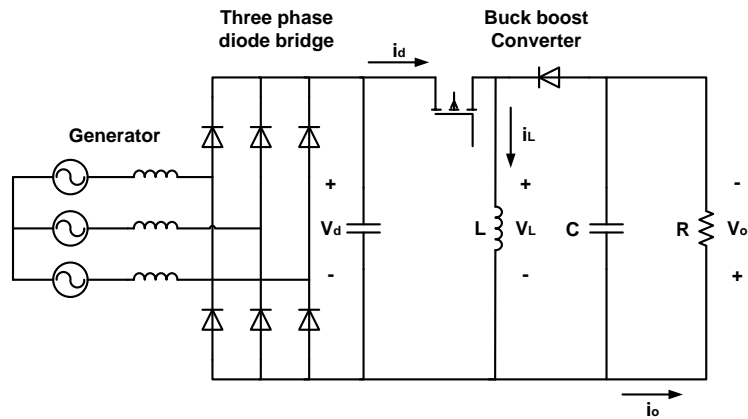


Figure 2.18: Buck boost converter

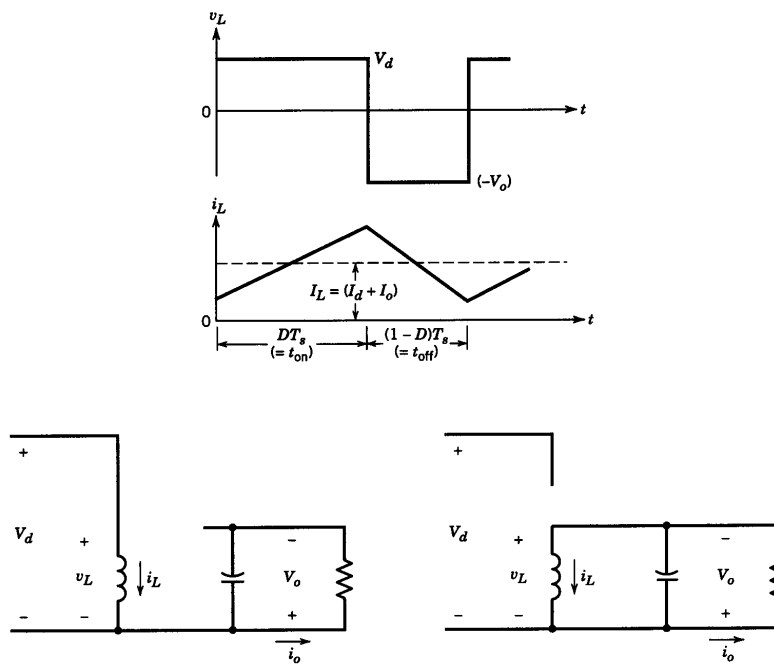


Figure 2.19: Off and on state of the buck boost converter [15]

The drawbacks of this converter version are the great ripple of the input current, the need of a large capacitor to stabilize the output voltage and a low efficiency at high duty ratios. The ripple of the input is a result of the off-state of the circuit. The input current is zero during this time and while the switch is on the input and inductor current are equal. Similar to the Boost-converter a large capacitor is required to reduce the voltage ripple at the output. When reaching high duty ratios and assuming a not lossless circuit the efficiency of the converter decreases. A higher duty ratio means a higher amount of energy is stored in the inductivity. When there is more energy stored there are higher losses at the copper resistance of the inductor [15].

### 2.4.3 Buck-Boost converter with high frequency transformer

An interesting application of the buck-boost converter is shown in figure 2.20. The inductor is replaced with a high frequency transformer. A higher output voltage can be reached which makes this converter more suitable for HVDC systems. A positive polarity of the output voltage is achieved by changing the rotation direction of the windings. The disadvantages explained above remain, except the low efficiency at high duty ratios. If a high voltage output is required it can be implemented by the winding ratio of the transformer instead of increasing the duty ratio [17].

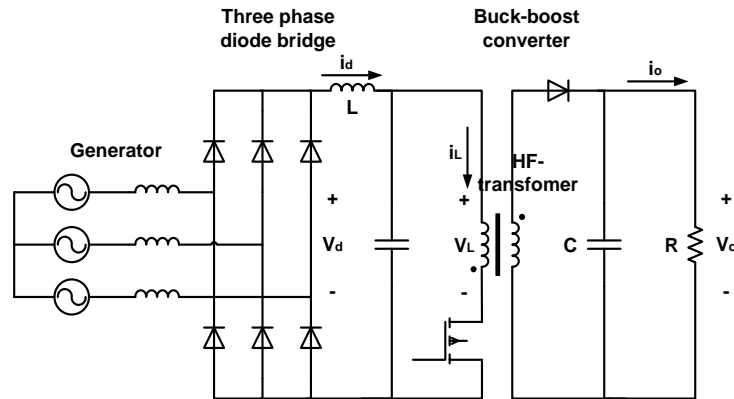


Figure 2.20 Buck boost converter with a HF transformer

### 2.4.4 Cúk converter

The output voltage of this converter (Figure 2.21) is negative and can have a lower or a higher value compared to the input voltage. During the off-state both inductor currents flow through the diode. The capacitor is charged by the input source and the inductor on the input side. Energy from the input source is stored in the capacitor. The inductor currents decrease during that time. When the switch is turned on the diode is reversed biased and the inductor currents flow through the switch. The capacitor is discharged and transfers energy to the output. The two inductor currents increase during this time (Figure 2.22).

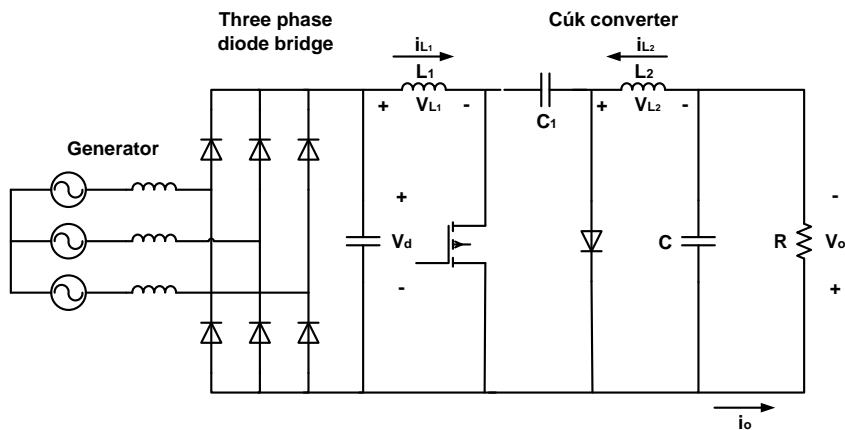


Figure 2.21 Cúk converter

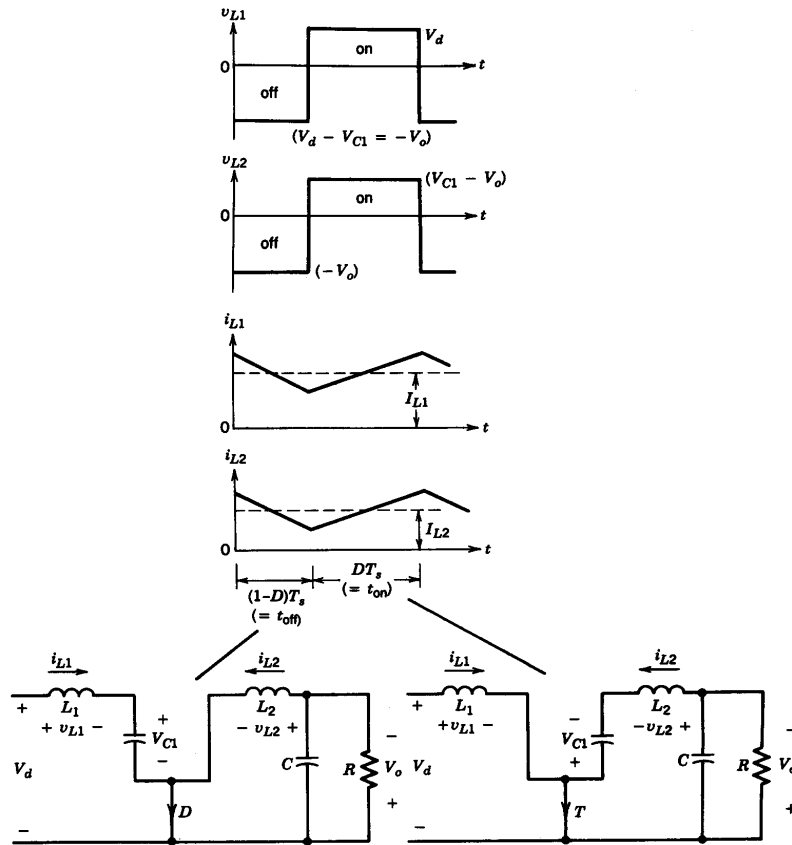


Figure 2.22 Off and on state of the Cúk converter [15]

The functions showing the relationship between input and output voltage and current are the same as the ones of the Buck-boost converter:

$$\frac{V_o}{V_d} = \frac{D}{1 - D} \quad 2-12$$

$$\frac{I_o}{I_d} = 1 - D \quad 2-13$$

The disadvantages of the converter above are the need of a large capacitor to stabilize the output current and a low efficiency at high duty ratio similar to the converters already mentioned [15].

### 2.4.5 Cúk converter with high frequency transformer

Similar to the buck-boost converter there is also a solution of the Cúk converter with a high voltage output. The high frequency transformer is added between two capacitors as shown in figure 2.23. Comparing this circuit with the original Cúk converter in figure 2.21, the capacitor is divided in two, one at the primary and one at secondary side of the transformer [17]. The high voltage output makes again a usage in HVDC applications possible. A higher efficiency can be obtained by a certain winding ratio instead of high duty ratios. But the other drawbacks already mentioned remain.

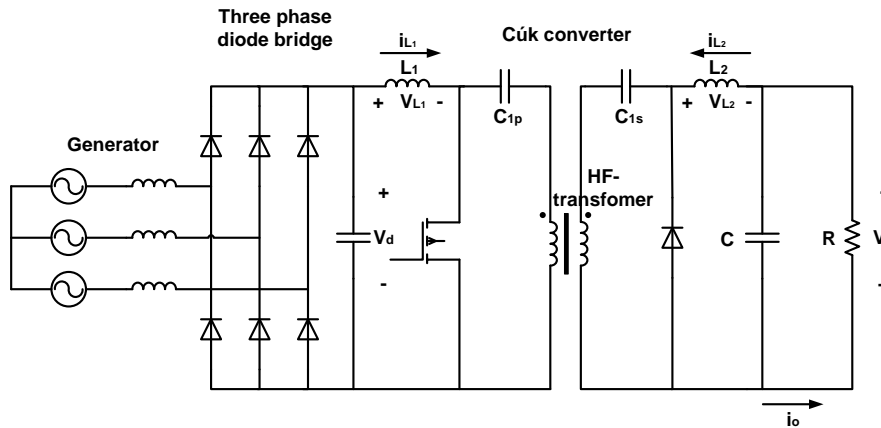


Figure 2.23 Cúk converter with high frequency transformer [17]

### 2.4.6 Full-bridge converter

The Full-bridge converter (figure 2.24) follows a different concept compared with the converters described above. It is not a pure DC-DC converter; it has an AC step between the DC in- and output. The input bridge generates a high frequency square wave at the transformer. It transforms the voltage to a higher level depending on the winding ratio. This high voltage is rectified by a diode bridge at the output. The ripple of the output voltage is reduced by a two level filter [18].

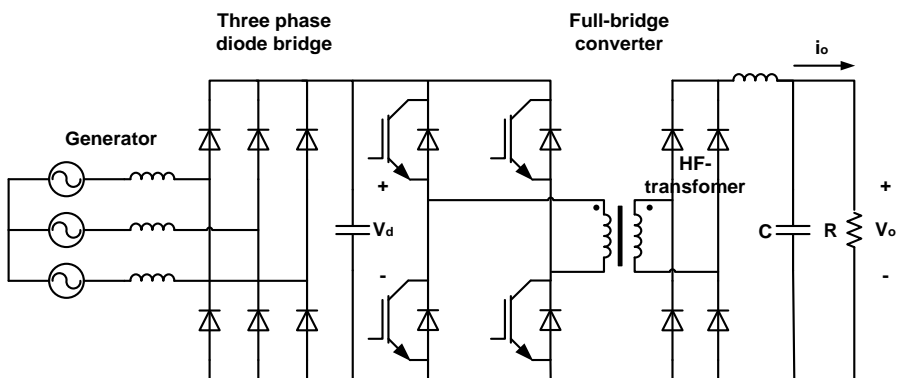


Figure 2.24 Full-bridge converter

The drawbacks of this converter concept are the complexity and the need of an output filter to reduce the ripple of the output voltage. There are four switches needed instead of only one compared with the converter types mentioned above. In addition to this a high frequency transformer and a second one phase diode bridge are part of the converter.

### 2.4.7 Active three phase rectifier

The active three phase rectifier (ATR) (figure 2.25) is the only converter shown in this thesis which does not need a three phase diode rectifier. It converts the three phase AC voltage directly to a DC-output voltage and it is able to operate in all four quadrants. The circuit is bidirectional and active and reactive power flow can be controlled independently. That is the reason why this type of converter is the only one among the discussed here which can be combined with an asynchronous generator because it demands reactive power for magnetization. The six switches are steered by PWM signals. The controlling algorithm will not be explained here in detail [19].

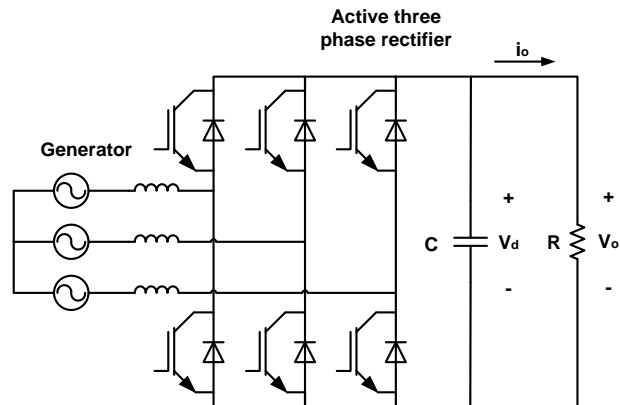


Figure 2.25 Active three phase rectifier

Depending on the inductors at the input side and the current the output DC-voltage can be higher than the AC-input voltage.

In order to assure a proper functionality of the circuit the DC-voltage  $V_d$  must be greater than the peak of the input AC voltage:

$$V_d > \sqrt{2}V_s$$

2-13

The drawbacks of the ATR are the need of six switches and the great harmonics in the output current which make a filter or at least a large capacitor necessary [15].

## 2.5 Comparison of AC-DC-converters

In chapter 2.4 seven different AC-DC converters are described. They change the AC output voltage of the generator to a higher DC voltage while controlling the power flow of generator to the DC-link. The maximum power output of the generator is assured this way. A high output voltage of the converter is an advantage regarding the HVDC transmission. That is why the improved Cúk- and Buck-boost converters with a high frequency transformer are compared to the other applications mentioned in the foregoing section. The original versions of both converters are not used. The comparison depending on certain performance factors is shown in table 2.3.

Performance factor	Boost converter	Buck-boost converter with HF-transformer	Cúk-converter with HF-transformer	Full-bridge converter	Active three phase rectifier
<i>Input current ripple</i>	0	-	0	0	0
<i>Galvanic separation</i>	No	Yes	Yes	Yes	No
<i>Output voltage amplitude</i>	0	++	++	++	0
<i>Component loading</i>	0	0	-	0	0
<i>Simplicity</i>	++	+	+	--	+

"-": negative performance; "0": in the middle; "+": positive performance

**Table 2.3 Comparison of AC-DC converters**

### *Input current ripple*

All described converter types create input current harmonics. But the boost-buck converter with a HF-transformer causes the highest current ripple as explained in 2.3.2. So the capacitor in parallel connection to the input has to be larger compared with the other converter types.

### *Galvanic separation*

A galvanic separation is a great advantage for converters used as part of HVDC transmission. It is implemented by the usage of a transformer. Only the secondary side has to be insulated against high voltage. The primary side including its converter part and the generator must merely be insulated against a lower voltage level. Without galvanic separation the entire system must have high voltage insulation. This causes a high effort in insulation which makes the wind power system more expensive.

### *Output voltage amplitude*

If a high voltage output can be achieved by the converter, a smaller number of turbine units have to be connected in serial to reach HVDC level. A smaller amount of turbine units in serial connection is a less complex system and can provide a higher redundancy in case of a failure. If there is a break in the connection, all serial connected turbines do not provide electrical energy to the grid.

### *Component loading*

If a part of a circuit is stressed heavily during operation the lifetime of this component decreases. Especially the two capacitors at the input and the output of the transformer of the Cúk converter with HF-transformer are loaded heavily. These two components must assure the entire power flow from the generator to the grid. Hence, more effort must be put in these components, which causes higher costs.

### *Simplicity*

A simple solution for a converter means that there are few parts used to build it. A full-bridge converter, for instance, consists of 18 semiconductors whereas a buck boost converter only needs eight. So simplicity is also a question of investment and maintenance costs.

All converter concepts have advantages and drawbacks as stated above and in chapter 2. But the Buck-boost and Cúk converter concepts based on a high frequency transformer show more advantages than disadvantages in this technical context. The most important benefits these solutions provide are a galvanic separation, a high output voltage and a simple circuit. Hence, these two converters, Buck-boost and Cúk converter are used for further investigation in this report.

## **2.6 Summary**

In this chapter different wind turbine systems, possible connection topologies and a number of converter concepts are introduced. They are compared regarding their drawbacks and advantages.

The following devices are chosen for further investigation:

A variable speed wind turbine is selected. The DC-DC concept, with a parallel connection of the wind turbines, is the connection topology for an offshore wind farm of interest. Both concepts are interfaces for the two selected converter types and build a frame for investigating them. These two types are the Buck-boost converter and the Cúk-converter both equipped with a high frequency transformer.

### 3 Specifications of the wind turbine system

In this chapter the specifications of all parts used in the wind turbine are presented. An appropriate generator is selected. The choice must be seen in the technical context of all parts of an offshore wind farm because they all depend on each other. Further on, data of the HVDC connection for the chosen topology in chapter 2.3 is introduced.

#### 3.1 Wind turbine

The wind turbine is based on a standard three blade concept. The data of the wind turbine used in this thesis are shown in table.

Parameters	Value
Rotor diameter	80 m
Nominal revolutions	16,7 rpm
Operational interval	9-19 rpm
Cut-in wind speed	4 m/s
Rated wind speed	12 m/s
Cut-out wind speed	25 m/s
Amount	100

Table 3.1 Wind turbine data

#### 3.2 Gear box and generator

The selected AC-DC converters in chapter 2 are unidirectional which means the power can only flow in one direction, from the wind turbine to the DC-link. These converter types are not able to provide reactive power to the generator. Induction machines have a need of reactive power for magnetization. That is why merely synchronous generators which do not need reactive power are chosen in this report. As known from chapter 2 there are three different synchronous generator types possible:

- A synchronous generator with a medium scale converter for field excitation and a gearbox (→ solution VII in chapter 2.2.3)
- A Multi-pole synchronous generator with a medium scale converter for field excitation (→ solution VIII in chapter 2.2.3)
- A Multi-pole synchronous generator equipped with permanent magnets (→ solution IX in chapter 2.2.3)

The most important advantage of generators with a variable field excitation is the controllability of the output voltage of the generator especially at low rotational speeds. A constant field excitation causes more amplitude variations in the voltage. The AC-DC converter has to deal with a higher input voltage range to ensure a certain high voltage at the DC link. When using generators with a variable field excitation the control of the AC-DC converters becomes less complex.

But the additional medium scale converter makes these concepts more complicated especially when it is not a back to back application as it is in this case. The converter has to be supplied with power from the DC-link which has a higher voltage level. Hence, synchronous generator concepts relying on a medium scale converter are not applicable for further investigation. They do not fit in the required context of a unidirectional AC-DC converter and a HVDC transmission. A permanent magnet synchronous generator is the most suitable solution and chosen in this report. The parameters of the selected generator are shown in table 3.2. A Multi-pole permanent would also be possible but the data needed for this generator concept was not available.

### 3. Specifications of the wind turbine system

Parameters	Value
Nominal power	2 MW
Number of pole pairs	4
Resistance of the stator	2 m $\Omega$
Inductivity of the stator in d-axes	110 $\mu$ H
Inductivity of the stator in q-axes	110 $\mu$ H
Nominal voltage	650 V
Machine constant	0,6 Vs/RAD

Table 3.2 Generator data

### 3.3 HVDC connection

The parameters of the HVDC link between offshore wind park and grid connection onshore are shown in table 3.3.

Parameters	Value
Voltage level	170 kV
Power	200 MW
Distance	150 km

Table 3.3 HVDC connection data

## 4 Wind turbine system modeling

In this chapter all parts of a wind turbine system are described by mathematical equations. Based on these, models for each part are developed. The modeling is done in the steady state theory, so it is assumed that there are no changes in time and the system operates in stable conditions. The wind turbine system is treated to be well controlled by controlling mechanisms which are not part of this thesis. These assumptions can be made due to the investigation of the performance factors efficiency and annual energy production do not need a dynamic model. Both performance factors are usually calculated while the wind turbine system is operating stably. The dynamic behavior of the system is not part of the investigation of the two factors.

Annual energy production and efficiency are related to the losses of the wind turbine system such as friction or ohmic losses due to parasitic elements in circuits. Hence the power losses in total must be estimated and are an important part of the modeling.

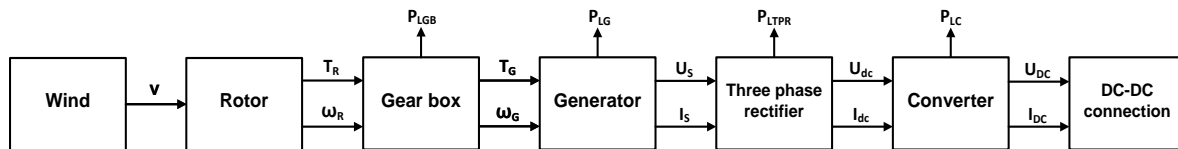


Figure 4.1 Overview of the entire model

Figure 4.1 illustrates a model overview. All parts of a wind turbine system are represented by a block, with its input and output variables. Each single block is explained in detail in the next sections of this chapter.

### 4.1 Wind

The wind is defined by the wind speed  $v$ . Sudden changes of the wind speed are neglected. Their investigation is not necessary in a steady state model. Hence it is assumed to have a 10 minutes average value of the wind speed. During the simulation, which is done later, wind speed ramp is used as input for the model of the wind turbine system. The block diagram of the wind is shown in figure 4.2.

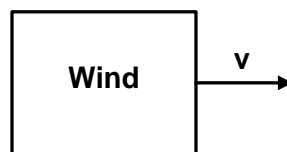


Figure 4.2 Block diagram of the wind

### 4.2 Rotor

The rotor converts the power of the wind into mechanical power. As explained in chapter 2, the wind power harnessed from the wind by the rotor is expressed by the following equation:

$$P = \frac{1}{2} c_p \rho r_b^2 \pi v^3 \quad 4-1$$

The power coefficient  $c_p$  is delivered by a look up table (Appendix) which shows the relationship between a certain wind speed  $v$  and the actual power coefficient  $c_p$ . (figure 4.3)

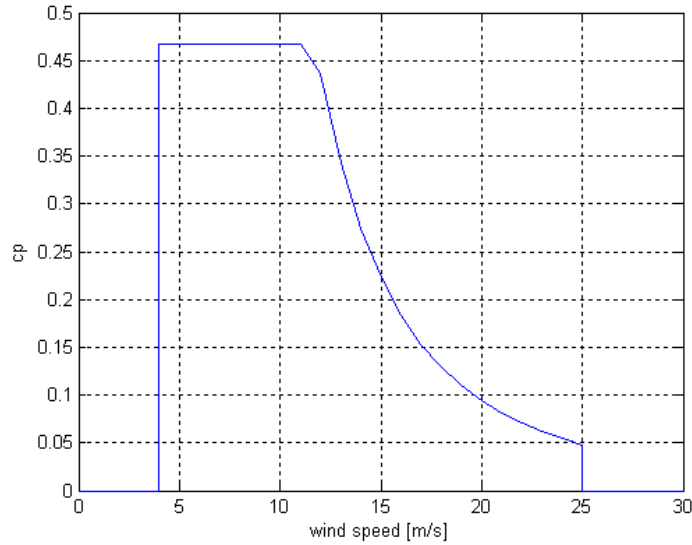


Figure 4.3 Power coefficient  $c_p$  as function of the wind speed  $v$

The rotational speed of the rotor  $\omega_R$  is also given by a look up table (Appendix). Figure 4.4 shows  $\omega_R$  as a function of the wind speed  $v$ .

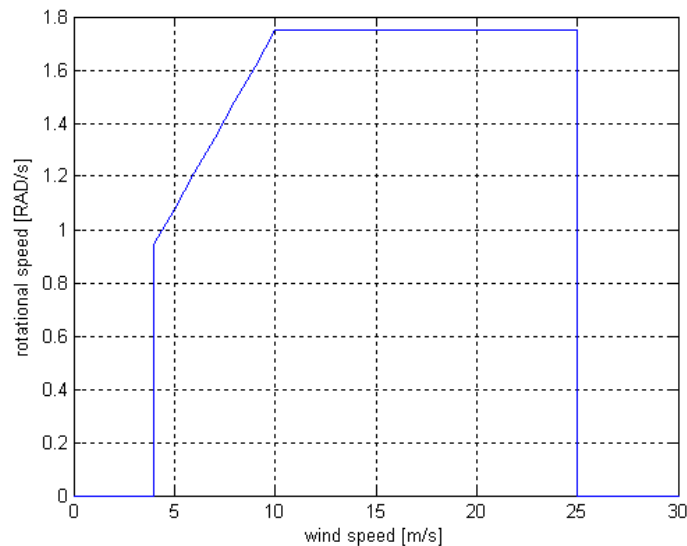


Figure 4.4 Rotational speed of the rotor  $\omega_R$  as function of the wind speed  $v$

Dividing the power (4-1) by the rotational speed of the rotor  $\omega_R$ , the equation for the rotor torque  $T_R$  yields:

$$T_R = \frac{1}{2} \frac{c_p \rho r_b^2 \pi v^3}{\omega_R} \quad 4-2$$

Figure 4.5 shows the block diagram of the rotor model, with the wind speed  $v$  as input and the rotor torque  $T_R$  and the rotational speed of the rotor  $\omega_R$  as outputs. The relationship between rotor torque  $T_R$  and wind speed  $v$  is described in figure 4.6.



Figure 4.5 Block diagram of the rotor

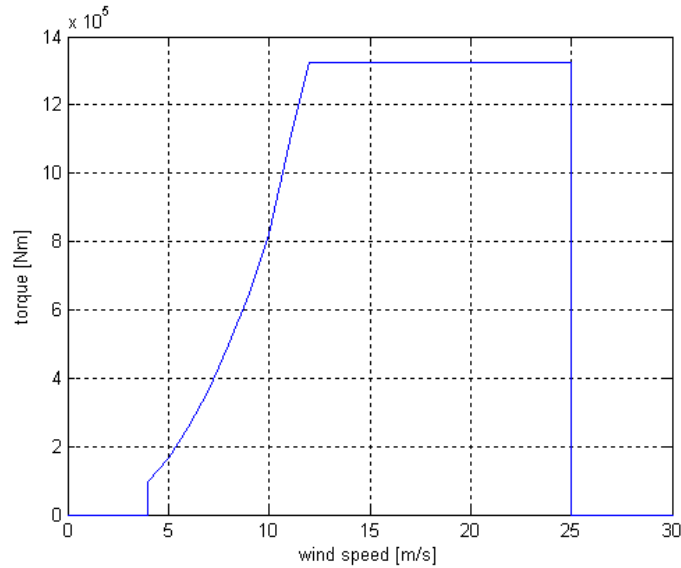


Figure 4.6 Rotor torque  $T_R$  as function of the wind speed  $v$

### 4.3 Gear box

The rotor torque  $T_R$  and the rotational speed of the rotor  $\omega_R$  are the inputs of the gear box which is the mechanical connection of the rotor shaft and the generator. The torque on the generator side  $T_G$ , the rotational speed of the generator  $\omega_G$  and the losses of the gearbox  $P_{LGB}$  are the outputs of this model (figure 4.7).

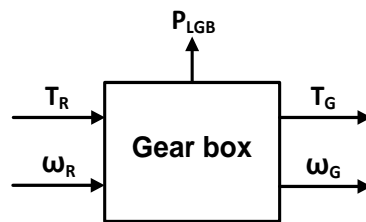


Figure 4.7 Block diagram of the gear box

Depending on the gear ratio  $n$  and the efficiency of the gearbox  $\eta_{GB}$ , the relationship between input and output values are explained in the following equations (4-3 and 4-4):

$$T_G = \frac{T_R}{n} \eta_{GB} \quad 4-3$$

$$\omega_G = \omega_R n \quad 4-4$$

The efficiency of the gearbox  $\eta_{GB}$  is estimated to be 90 %. Relying on this parameter the losses of the gearbox  $P_{LGB}$  are computed. The gear ratio is calculated (4-5) by the ratio of the nominal rotational speed of the generator and the nominal rotational speed of the rotor:

$$n = \frac{\omega_{Gnominal}}{\omega_{Rnominal}} \approx 90 \quad 4-5$$

With:

$$\omega_{Gnominal} = \frac{f_{enominal} 2 \pi}{p}$$

$$\omega_{Rnominal} = \frac{r_{nominal} 2 \pi}{60s}$$

$f_{enominal}$ : electrical frequency of the generator at nominal wind speed (*here: 100 Hz*)

$p$ : number of pole pairs (*here: 4*)

$r_{nominal}$ : nominal revolutions of the wind turbine (*here: 16,7 RPM*)

#### 4.4 Generator

The permanent magnet synchronous generator can be characterized by a one phase circuit shown in figure 4.8 [20] [21].  $E$  represents the induced electromotive force.  $R_s$  is the winding resistance and  $L_s$  is the inductance of one phase. The output values are the voltage  $U_s$  and the current  $I_s$ .

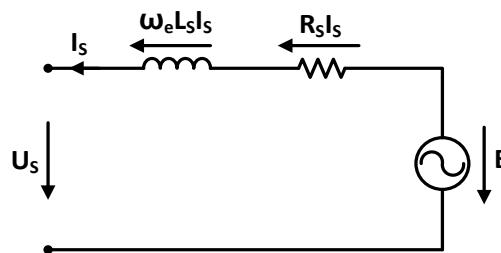


Figure 4.8 One phase circuit of a synchronous generator

The relationship of the voltages and the current is explained in a space vector diagram (figure 4.9) [22]. The output power of the generator must be active only due to the used converter concepts are not able to work with reactive power. Hence, the generator operates at unity power factor and the output voltage  $U_s$  and current  $I_s$  are in phase. This causes a voltage drop along the resistor  $R_s$  which is parallel to  $U_s$ . The voltage drop along the inductance  $L_s$  is perpendicular to the output voltage  $U_s$  and current  $I_s$ .

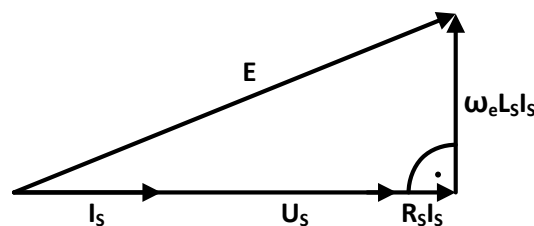


Figure 4.9 Space vector diagram of the synchronous generator

The induced electromotive force E can be calculated like the following [21]:

$$E = \omega_e K_\Phi \quad 4-6$$

$K_\Phi$ : machine constant of the synchronous generator  
 $\omega_e$ : electric rotational speed

The model of the generator has the torque  $T_G$  and rotational speed  $\omega_G$  as inputs. The voltage  $U_S$ , the current  $I_S$  and the losses  $P_{LG}$  are outputs of the generator (figure 4.10).

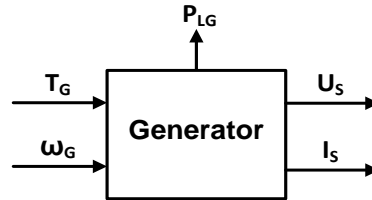


Figure 4.10 Block diagram of the synchronous generator

The equation describing input and output power yields:

$$P_{input} = P_{output} + P_{LG} \quad 4-7$$

The losses of the generator  $P_{LG}$  are generally divided in stator resistance  $P_{LSr}$ , friction  $P_{Lf}$  and iron losses  $P_{Li}$  which are stated in the following:

$$P_{LG} = P_{LSr} + P_{Lf} + P_{Li} \quad 4-8$$

$$P_{LSr} = 3R_S I_S^2$$

$$P_{Lf} = \left[ 2 \frac{f_e}{f_{e \text{ nominal}}} + \left( \frac{f_e}{f_{e \text{ nominal}}} \right)^2 \right] \frac{P_{Lf \text{ nominal}}}{3} \quad [4]$$

$$P_{Li} = B^2 (c_1 f_e + c_2 f_e^2) \quad [5]$$

The friction  $P_{Lf}$  and iron losses  $P_{Li}$  do not affect the circuit illustrated in figure 4.8 and are not investigated in detail in further calculations. Finally, the equation describing in- and output power yields:

$$T_e \omega_e = 3U_S I_S + 3R_S I_S^2 + P_{Lf} + P_{Li} \quad 4-9$$

With:

$$\omega_e = \omega_G p$$

$$T_G = \frac{T_e}{p}$$

$p$ : number of pole pairs (here: 4)  
 $P_{Lf \text{ nominal}}$ : friction losses at nominal wind speed (here: 6 kW)  
 $B$ : flux density of the permanent magnets (here: 1T)  
 $c_1$ : constant (here: 70 m<sup>4</sup>A/Vs)  
 $c_2$ : constant (here: 7 m<sup>4</sup>A/V)

The output power of the generator contains only active power due to merely active power can be transferred by a DC-DC connection. Hence the output voltage  $U_s$  and current  $I_s$  are in phase. This is the reason why the space vector diagram is always a triangle with a right angle. The Pythagorean Theorem can be used to describe the relationship of the different voltages (4-10):

$$E^2 = (U_s + R_S I_s)^2 + (\omega_e L_S I_s)^2 \quad 4-10$$

Combining equation 4-9 and 4-10 and solving them for  $I_s$  and  $U_s$ , the following results for the output variables are achieved:

$$I_s = \sqrt{\frac{E^2 - \sqrt{E^4 - \frac{4}{9} \omega_e^2 L_S^2 (T_e \omega_e - P_{Lf} - P_{Li})^2}}{2 \omega_e^2 L_S^2}} \quad 4-11$$

$$U_s = \frac{T_e \omega_e - 3 R_S I_s^2 - P_{Lf} - P_{Li}}{3 I_s} \quad 4-12$$

$$U_s = \frac{T_e \omega_e - 3 R_S \frac{E^2 - \sqrt{E^4 - \frac{4}{9} \omega_e^2 L_S^2 (T_e \omega_e - P_{Lf} - P_{Li})^2}}{2 \omega_e^2 L_S^2} - P_{Lf} - P_{Li}}{3 \sqrt{\frac{E^2 - \sqrt{E^4 - \frac{4}{9} \omega_e^2 L_S^2 (T_e \omega_e - P_{Lf} - P_{Li})^2}}{2 \omega_e^2 L_S^2}}}$$

The relationship between both output voltage  $U_s$  and current  $I_s$  and the wind speed are shown in figure 4.11. When reaching nominal wind speed of 10 m/s the output voltage  $U_s$  decreases until the output power is limited (figure 4.11). This behavior of the voltage is the result of the increasing voltage drops across the winding resistance  $R_S$  and the winding inductance  $L_S$  due to the also rising current  $I_s$ . At nominal wind speed the electric rotational speed  $\omega_e$  is constant and so the induced electromotive force  $E$  is constant too. Under these conditions the voltage  $U_s$  declines (see figure 4.9).

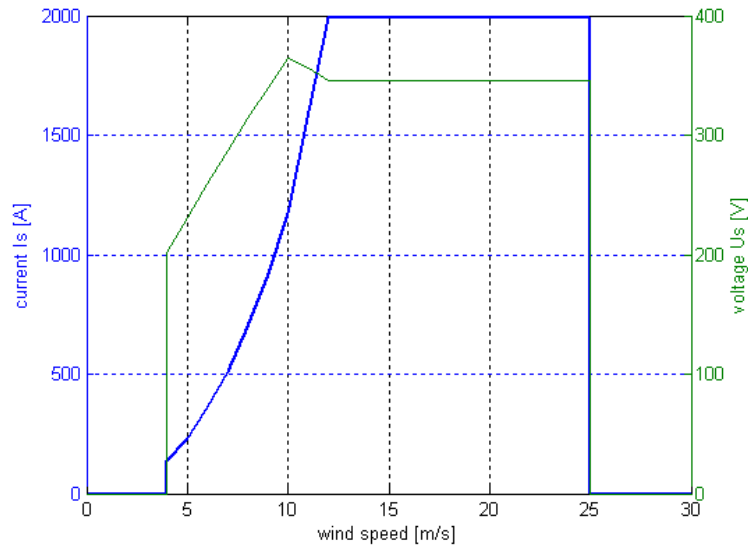


Figure 4.11 Output voltage  $U_s$  and  $I_s$  as function of the wind speed  $v$

#### 4.5 DC-DC connection

The HVDC connection of offshore and onshore is as its name says at high constant voltage level. This constant voltage level is controlled by the converter on the grid side onshore. Hence, the DC-DC connection can be modeled by a constant voltage source at the output of each single turbine unit. Figure 4.12 shows the source with the constant voltage  $U_{DC}$ . The value of the voltage depends on the number of turbines in serial connection. In this thesis a number of 10 turbines connected serial is assumed. With a voltage of 170kV for HVDC transmission a source voltage of 17kV is obtained.  $U_{DC}$  is used as a constant input in the converter models due to its value is known.

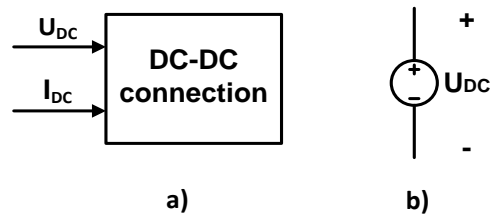


Figure 4.12 Model of the DC-DC connection as block a) and as circuit b)

The model of the DC-DC connection and the generator are the interfaces for the converter models explained in the next sections. The generator provides power and the DC-DC connection acts as a power sink.

## 4.6 AC-DC converters

In this part of the chapter the two selected converter types introduced in chapter 2 are modeled. In a first step the converters are treated to be ideal without any losses. The values for inductors and capacitors are calculated. Depending on these results real electrical devices are chosen. Here the converters must assure that the input power provided by the generator is equal to the sum of output power and losses of the converter. Hence, the turbine is always operating at its maximum power output. The block-diagram 4.13 shows this relationship. The functionality of the configured converters is proved by a simulation in PSIM, which is a real time circuit simulation program.

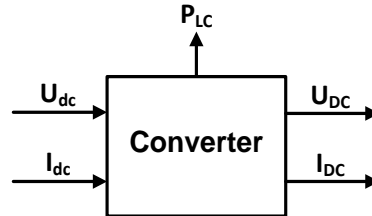


Figure 4.13 Block diagram of the synchronous generator

In a second step, the converters are modeled including the parasitic elements of the devices chosen during the first step. These parasitic elements which are modeled as resistors are responsible for power losses. Appropriate semiconductors such as diodes and switches are also selected.

All converters include a three phase rectifier. That is why the three phase rectifier is seen as an individual part and modeled as an independent block.

### 4.6.1 Three phase rectifier

This part of the circuit rectifies the three phases of the generator and converts them to a DC voltage  $U_{dc}$  and a DC current  $I_{dc}$ . Sinusoidal input variables ( $U_s$  and  $I_s$ ) are estimated here. The relationship between input and output power is stated in the following equation:

$$P_{input} = P_{output} + P_{ITPR} \quad 4-13$$

$$3U_S I_S = U_{dc} I_{dc} + P_{ITPR}$$

The losses  $P_{ITPR}$  are divided in conduction  $P_{IDcon}$  and in switching losses  $P_{IDsw}$ . The conduction and switching losses for one diode are stated in equation 4-14 and 4-15. The blocking or leakage losses are neglected [23]

$$P_{IDcon} = V_{(TO)} I_{Fav} + r_T I_{FRMS}^2 \quad 4-14$$

$$P_{IDsw} = E_{rr} \frac{I_F}{I_{FM}} f_e \quad 4-15$$

With:

- $V_{(TO)}$ : threshold voltage
- $r_T$ : slope resistance
- $I_{Fav}$ : average forward current
- $I_{FRMS}$ : RMS forward current
- $I_{FM}$ : repetitive turn-on current
- $E_{rr}$ : reverse recovery energy
- $f_e$ : electrical frequency of the generator

The conduction losses  $P_{IDcon}$  in a three phase rectifier which consists of six diodes are shown in equation 4-16. The average forward current per diode  $I_{Fav}$  is equal to one third of the rectifier output current  $I_{dc}$  (three diodes are conducting at the same time). The RMS value of the diode current  $I_{FRMS}$  is equal to the output current  $I_{dc}$  divided by  $\sqrt{3}$ .

$$P_{IDcon} = 6(V_{(TO)} \frac{I_{dc}}{3} + r_T \frac{I_{dc}^2}{3}) = 2(V_{(TO)}I_{dc} + r_T I_{dc}^2) \quad 4-16$$

The repetitive turn-on current of one diode in this technical context equals the output current of the three phase rectifier  $I_{dc}$ . The switching losses of all six diodes  $P_{IDsw}$  yield:

$$P_{IDsw} = 6 \left( E_{rr} \frac{I_{dc}}{I_{FM}} f_e \right) \quad 4-17$$

In equation 4-18 is stated how  $I_S$  and  $I_{dc}$  depend on each other [24]:

$$I_{dc} = \sqrt{\frac{3}{2}} I_S \quad 4-18$$

Solving equation 4-13, 4-16, 4-17 and 4-18 for  $U_{dc}$  the result yields:

$$U_{dc} = \frac{3U_S I_S - P_{LTPR}}{\sqrt{\frac{3}{2}} I_S} \quad 4-19$$

$$= \frac{3U_S I_S - 2(V_{(TO)} \sqrt{\frac{3}{2}} I_S + r_T \frac{3}{2} I_S^2) - 6 \left( E_{rr} \frac{U_{dc}}{V_{CA}} f_e \right)}{\sqrt{\frac{3}{2}} I_S}$$

The block diagram of the three phase rectifier with the input and output variables is represented in figure 4.14.

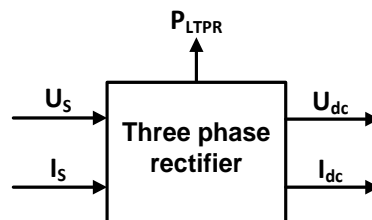


Figure 4.14 Block diagram of the three phase rectifier

The parameter values of suitable diodes are shown in table 4.1. The data is an example of a diode for the usage in such a three phase rectifier and do not belong to a certain device.

Parameter	Value
$I_{FM}$	3000 A
$V_{(TO)}$	0,7 V
$r_T$	0,7 mΩ
$E_{rr}$	0,2 mJ

Table 4.1 Values of the diode parameters

### 4.6.2 Buck-boost converter with a high frequency transformer

The output voltage  $U_{DC}$  and current  $I_{DC}$  of a Buck-boost converter with a high frequency transformer are characterized by equations 4-20 and 4-21. They are similar to the ones stated in chapter 2 according to the buck-bust converter. Here the winding ratio of the high frequency transformer  $n$  is added. It must be mentioned that in this part of the chapter all losses of the parts used in the converter are neglected.

$$U_{DC} = U_{dc} \frac{D}{1-D} n \quad 4-20$$

$$I_{DC} = I_{dc} \frac{(1-D)}{Dn} \quad 4-21$$

The converter has to make sure that the input power is transferred to the output, so the equation regarding this relationship yields:

$$P_{input} = P_{output} \quad 4-22$$

$$U_{dc} I_{dc} = U_{DC} I_{DC}$$

Solving equation 4-20 for the duty ratio  $D$  the stated result is obtained:

$$D = \frac{U_{DC}}{nU_{dc} + U_{DC}} \quad 4-23$$

#### 4.6.2.1 Configuration and design of the Buck-boost converter

In this converter as shown in picture 4.15 the L-C input filter, the inductance  $L$  of the transformer and the output capacitor  $C$  need to be configured.

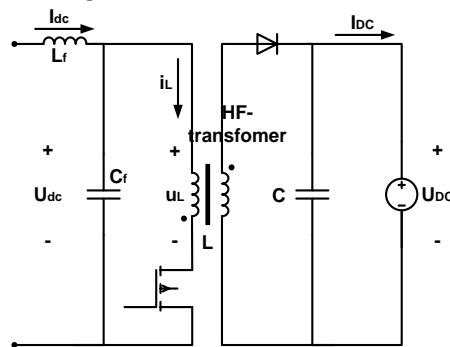


Figure 4.15 Circuit of the Buck-boost converter

#### Inductor L

In a first step the inductance  $L$  is calculated. During the time the switch is turned on, the voltage  $u_L$  across the inductor is equal to the input voltage (see chapter 2, figure 2.16) [25]:

$$u_L = U_{dc} \quad 4-24$$

The relationship of the inductor current  $i_L$  and the input voltage  $U_{dc}$  yields [25]:

$$\frac{di_L}{dt} = \frac{u_L}{L} = \frac{U_{dc}}{L} \quad 4-25$$

The ripple magnitude of the inductor current can be calculated due to the slope of the inductor current during the first switching state and its length is known. With  $\Delta i_L$  as ripple to peak value and two times  $\Delta i_L$  as peak to peak value, it is given by:

$$2\Delta i_L = \frac{U_{dc}}{L} DT_S \quad 4-26$$

As stated in [25] the current ripple can be estimated to be 10% of the value  $i_L$ . In steady state  $\Delta i_L$  can be expressed during the on-state as the following with:

$$i_L = I_{dc} \quad 4-27$$

$$\Delta i_L = 0,1i_L = 0,1I_{dc}$$

The inductance L is obtained in the next equation relying on 4-26 and 4-27.

$$L = \frac{1}{2 \cdot 0,1} \frac{U_{dcnominal}}{I_{dcnominal}} DT_S \quad 4-28$$

The input voltage and current have their nominal values which are:

$$U_{dcnominal} = 817,15V \quad 4-29$$

$$I_{dcnominal} = 2287,62A$$

The winding ratio of the transformer n is the ratio of the output voltage  $U_{DC}$  and the input voltage of the converter at cut-in wind speed  $U_{dcut-in}$ . The following value for the winding ratio is calculated:

$$n = \frac{U_{DC}}{U_{dcut-in}} = \frac{17kV}{473,24V} \approx 36 \quad 4-30$$

At higher wind speeds the converter always works at duty ratios lower than 0,5 (equation 4-23) which leads to lower losses especially at partial load [25]. The ripple current in the inductance of the transformer is proportional to the duty ratio D. Assuming the worst case, the maximum value of the duty ratio is taken, which is 0,5 as explained before. The switching frequency is 1kHz and so the switching period is 1ms. It is stated in [18] that at this frequency a good compromise between weight and losses of the transformer can be achieved. Finally a value for the inductance L is calculated:

$$L = 0,89 \text{ mH} \quad 4-31$$

#### Capacitor C

The value for the capacitor C at the output of the converter can be obtained in similar way. It is assumed that the output voltage of the converter  $U_{DC}$  has a small ripple  $u_{DCripple}$ . The capacitor C has to assure a maximum ripple of the output voltage of 1%. This ripple voltage  $u_{DCripple}$  is a result of charging and discharging the capacitor C while the converter is operating in its two different states. During the on-state of the switch the voltage ripple and the capacitor current depend on each other as shown in the following equation (see chapter 2 figure 2.19) [25]:

$$\frac{du_{DCripple}}{dt} = -\frac{I_{DC}}{C} \quad 4-32$$

The ripple magnitude of the output voltage can be calculated due to the slope of the output voltage during the first switching state and its length is known. With  $\Delta u_{DCripple}$  as ripple to peak value and two times  $\Delta u_{DCripple}$  as peak to peak value, it is given by [25]:

$$2\Delta u_{DCripple} = \frac{I_{DC}}{C} DT_S \quad 4-33$$

An equation and a certain value for the capacitor C can be obtained with 4-21 and the mentioned relationship between  $u_{DCripple}$  and  $U_{DC}$ :

$$C = \frac{1}{2 \cdot 0,01} \frac{I_{dcnominal} (1 - D)}{U_{DC}} T_S = 96,1 \mu F \quad 4-34$$

#### L-C filter

The main task of the L-C filter is to avoid a ripple in the input current  $I_{dc}$  of the converter. The current ripple  $i_{dcripple}$  occurs due to the two switching states. But an input current ripple  $i_{dcripple}$  with a high value affects the torque of the generator  $T_G$ ; the generator torque  $T_G$  and the input current  $I_{dc}$  are proportional to each other. In order to prevent physical stresses of the wind turbine as a result of a torque ripple, the input current ripple  $i_{dcripple}$  is assumed to be 0,1 % of the input current.

The filter inductor  $L_f$  relies on the following equation:

$$U_{L_f} = L_f \frac{di_{L_f}}{dt} \quad 4-35$$

$U_{L_f}$  is the voltage drop across the inductor  $L_f$  and  $i_{L_f}$  is the current ripple of the input current  $I_{dc}$ . The ripple magnitude of the input current ripple can be calculated due to the slope of the input current during the second switching state and its length is known. With  $\Delta i_{dcripple}$  as ripple to peak value and two times  $\Delta i_{dcripple}$  as peak to peak value, it is given by:

$$2\Delta i_{dcripple} = \frac{U_{L_f}}{L_f} (1 - D) T_S \quad 4-36$$

Solving equation 4-36 for  $L_f$ , it is obtained:

$$L_f = \frac{U_{L_f}}{2\Delta i_{dcripple}} (1 - D) T_S \quad 4-37$$

A certain value for  $L_f$  strongly depends on the assumptions made for  $U_{L_f}$  and  $\Delta i_{dcripple}$ . As stated before an applicable input current ripple  $\Delta i_{dcripple}$  is 0,1% of the input current  $I_{dc}$ . For the voltage drop across the inductor  $U_{L_f}$  10% of the input voltage  $U_{dc}$  are considered. With these two assumptions the value for  $L_f$  yields:

$$L_f = \frac{0,1 \cdot U_{dcnominal}}{2 \cdot 0,001 I_{dcnominal}} (1 - D) T_S = 8,9 \text{ mH} \quad 4-38$$

The capacitor  $C_f$  is estimated by considering the equality of charge caused by the voltage change across the capacitor  $\Delta u_{Cf}$  and the integral of capacitor current  $i_{Cf}$  [25]. The charge generated by the voltage drop  $\Delta u_{Cf}$  is the product of the peak to peak value of this voltage and the value of the capacitor  $C_f$ .

$$q = 2\Delta u_{Cf}C_f \quad 4-39$$

The equal charge is expressed by the integral of capacitor current  $i_{Cf}$  over time. During the second switching state the current  $I_{dc}$  has to be stored in the capacitor  $C_f$  because there is no connection between input and output of the converter. The product of input current  $I_{dc}$  and the time period of the second switching state equals the charge:

$$q = \int i_{Cf} dt = I_{dcnominal}(1 - D)T_S \quad 4-40$$

The equation for filter capacitor  $C_f$  yields:

$$C_f = \frac{1 I_{dcnominal}}{2 \Delta u_{Cf}} (1 - D)T_S \quad 4-41$$

Similar to the calculation of the filter inductor  $L_f$ , the assumptions made for  $\Delta u_{Cf}$  and  $i_{Cf}$  have a great impact on the value of  $C_f$ . The capacitor current  $i_{Cf}$  equals the input current  $I_{dc}$  and  $\Delta u_{Cf}$  is considered to be 1% of the input voltage  $U_{dc}$ . The value for  $C_f$  is shown in equation 4-42:

$$C_f = \frac{1 I_{dcnominal}}{2 \cdot 0,01 \cdot U_{dcnominal}} (1 - D)T_S = 70 \text{ mF} \quad 4-42$$

#### 4.6.2.2 Simulation of the ideal Buck-boost converter

The Simulation of the ideal Buck-boost converter is done in PSIM which is a real time circuit simulation program for power electronics. The purpose of a real time simulation is to show that the converter operates with parameter values for the electrical devices calculated before. The simulation is done to prove the computed values of the electrical parts. The converter is simulated under nominal conditions. The output voltage  $U_{DC}$  and current  $I_{DC}$  are measured (see figure 4.15) and illustrated in figure 4.16. Both reach the end value in applicable time and do not start swinging.

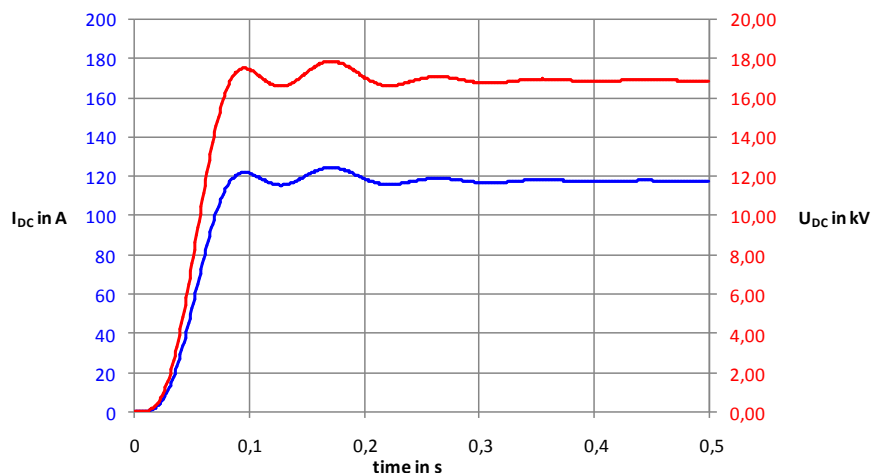


Figure 4.16 Output voltage  $U_{DC}$  and current  $I_{DC}$  of the Buck-boost converter

The input current  $I_{dc}$  before and after the L-C filter is also measured (figure 4.17). It can be seen that the input current ripple is small, so the converter does not influence the generator and the turbine due to the current is proportional to the torque.

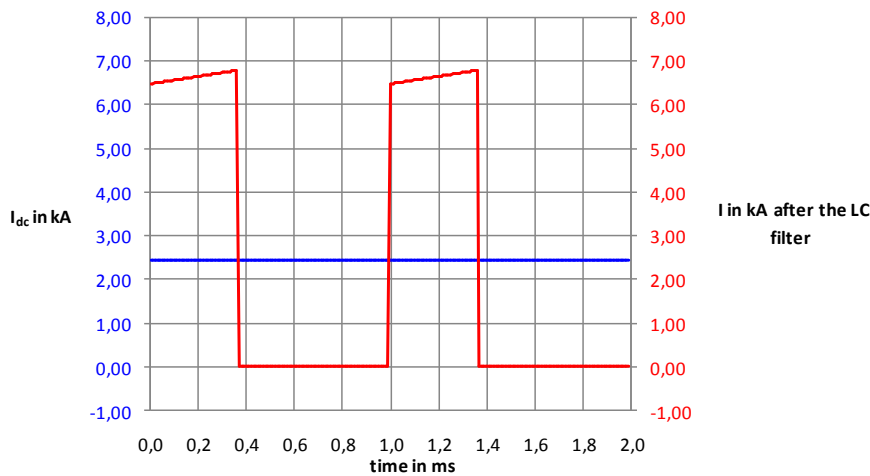


Figure 4.17 Currents before and after the L-C filter

The simulation demonstrates that the converter works with the estimated parameter values.

#### 4.6.2.3 Modeling the Buck-boost converter

In this section the losses of the parts used in the converter are not neglected. All inductors have copper losses due to the winding resistance. It is characterized by a resistor connected in series to the ideal inductor. The iron losses of the inductor are small compared with the copper losses. In [26] is stated that the ratio between copper and iron in an inductor is 1000 and so the iron losses of single inductors are neglected.

Considering transformers, iron losses are taken into account and modeled by an iron resistor which is parallel connected to the main inductance.

Capacitors have a conduction resistance which is modeled by a serial resistor.

Figure 4.18 and 4.19 show the circuit of a Buck-boost converter with the most important parasitic elements. Both switching states are illustrated in single circuits because of different currents and voltages in each state.

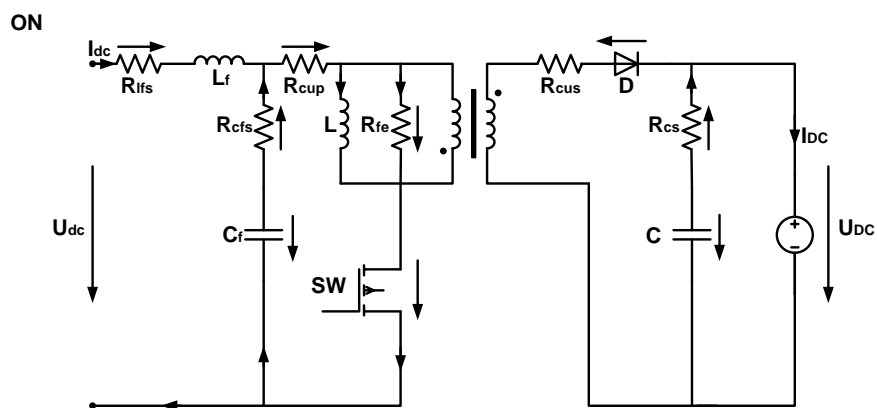


Figure 4.18 Buck-boost converter with parasitic elements during the on-state

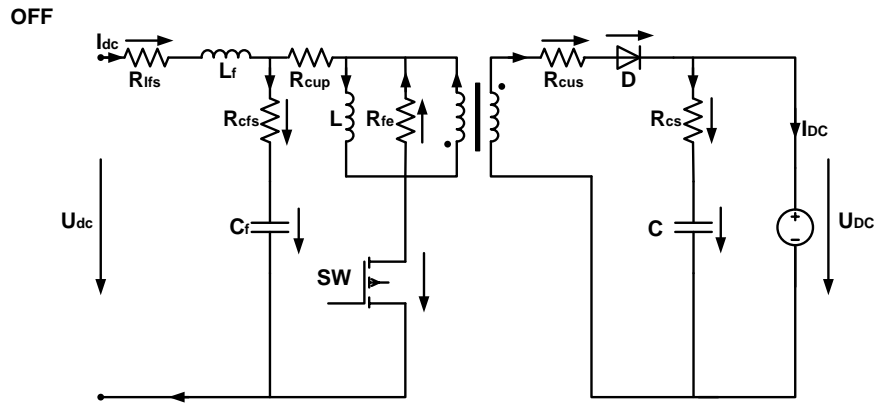


Figure 4.19 Buck-boost converter with parasitic elements during the off-state

From now on, parasitic elements, voltage drops across and currents flowing through these elements are named as follows. It is explained on the filter inductance  $L_f$ :

- The serial resistor for the copper losses is called  $R_{lfs}$ :
- The voltage drop across this resistor is named  $U_{Rlfs}$
- The current flowing through it is titled  $I_{Rlfs}$ .

In the calculation of currents and voltages merely absolute values are considered, their directions are shown in figure 4.18 and 4.19.

The calculation of the entire losses starts on the left side of the circuit with computing the copper losses of the filter inductance  $L_f$ .

*Losses of the filter inductance  $P_{lf}$*

The losses  $P_{lf}$  occur in the resistor  $R_{lfs}$  and are described in equation 4-43. The RMS value of the current  $I_{RlfsRMS}$  flowing through the resistor equals the input current  $I_{dc}$ . The voltage drop across the inductance  $L_f$  is small in comparison to the input voltage  $U_{dc}$  and is neglected in further calculations. Figure 4.20 shows both voltages gauged in a real time simulation of the Buck-boost converter made with PSIM.

$$P_{Uf} = R_{lfs} I_{RlfsRMS}^2 \tag{4-43}$$

$$P_{Uf} = R_{lfs} I_{dc}^2$$

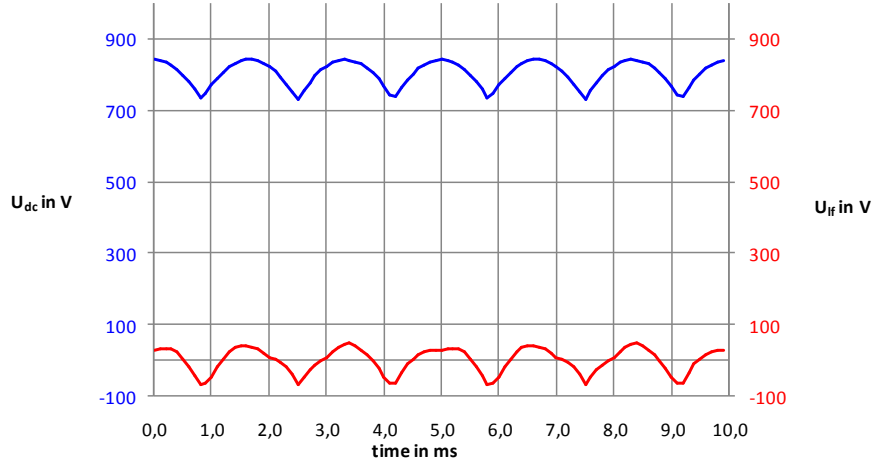


Figure 4.20 Comparison of the input voltage  $U_{dc}$  and the voltage drop  $U_{if}$  across the inductor  $L_f$

Losses of the filter capacitor  $P_{lcf}$

The resistor  $R_{cfs}$  characterizes these losses which are expressed in the next equation:

$$P_{lcf} = R_{cfs} I_{RcfsRMS}^2 \quad 4-44$$

For the calculation of the current  $I_{RcfsRMS}$  both switching states must be considered. During the off-state of the converter (figure 4.19) the current flowing through the resistor  $I_{RcfsOFF}$  is the same as the input current  $I_{dc}$ . If a constant voltage across the filter capacitor  $C_f$  is estimated the charge  $q_{OFF}$  stored during the off-state equals the charge  $q_{ON}$  which is the emitted while the switch is turned on. The following relationship is obtained:

$$q_{ON} = q_{OFF} \quad 4-45$$

$$I_{RcfsON} \cdot D \cdot T_S = I_{RcfsOFF} \cdot (1 - D) \cdot T_S$$

$$I_{RcfsON} = \frac{1 - D}{D} I_{dc}$$

Both currents during the two states are known and the RMS value  $I_{RcfsRMS}$  depending on the input current  $I_{dc}$  yields [27]:

$$I_{RcfsRMS} = \sqrt{\frac{1}{T_S} \left[ \int_0^{DT_S} (I_{RcfsON})^2 dt + \int_0^{(1-D)T_S} (I_{RcfsOFF})^2 dt \right]} \quad 4-46$$

$$I_{RcfsRMS} = \sqrt{\frac{1}{T_S} [(I_{RcfsON})^2 DT_S + (I_{RcfsOFF})^2 (1 - D) T_S]}$$

The current  $I_{Rcfs}$  is also measured in the PSIM simulation (figure 4.21). The measurement proves the calculation.

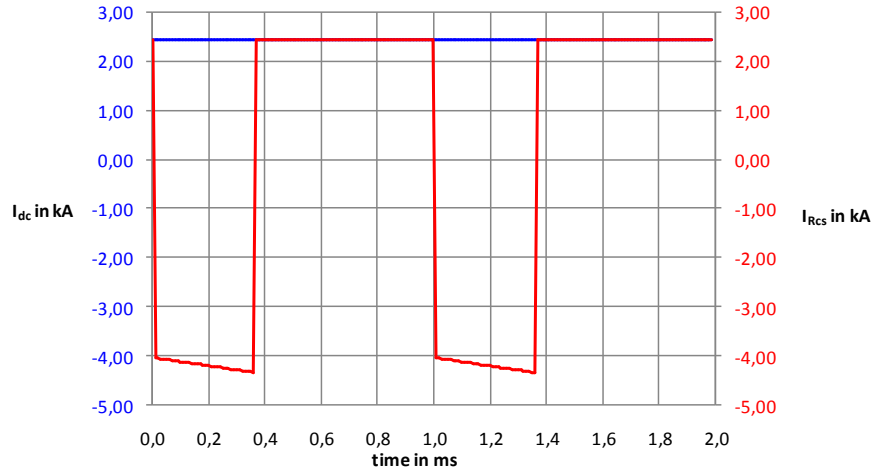


Figure 4.21 Comparison of the input current  $I_{dc}$  and the current  $I_{RCS}$

Copper losses of the transformer on the primary side  $P_{IRcup}$

Equation 4-47 describes the losses in  $R_{cup}$ :

$$P_{IRcup} = R_{cup} I_{RcupRMS}^2 \quad 4-47$$

Again the different currents relying on the switching state must be computed to calculate the current  $I_{RcupRMS}$ . The current  $I_{RcupOFF}$  is zero. During the on-state the current  $I_{RcupON}$  is the sum of the input current  $I_{dc}$  and the filter capacitor current  $I_{RcfsON}$  (equation 4-48).

$$I_{RcupOFF} = 0 \quad 4-48$$

$$I_{RcupON} = I_{dc} + I_{RcfsON}$$

The RMS value of  $I_{Rcup}$  is described in the next equation:

$$I_{RcupRMS} = \sqrt{\frac{1}{T_S} [(I_{RcupON})^2 DT_S + (I_{RcupOFF})^2 (1 - D)T_S]} \quad 4-49$$

The current  $I_{Rcup}$  is also measured in the PSIM simulation and illustrated in figure 4.22. It shows that the thoughts above regarding  $I_{Rcup}$  are correct.

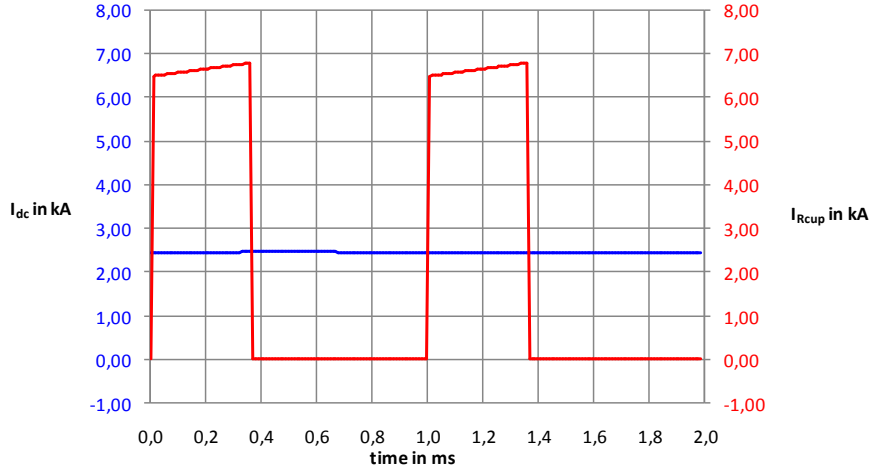


Figure 4.22 Comparison of the input current  $I_{dc}$  and the current  $I_{Rcup}$

Iron losses of the transformer  $P_{Rfe}$

These losses are calculated with the voltage drop across the main inductance  $U_{RfeRMS}$  and the resistor  $R_{fe}$ .

$$P_{LRfe} = \frac{U_{Rfe}^2}{R_{fe}} \quad 4-50$$

The voltage across  $R_{fe}$  while the switch is on  $U_{RfeON}$  is computed as stated in equation 4-51:

$$U_{RfeON} = U_{dc} - U_{RcupON} - U_{RlfsON} - U_{SWON} \quad 4-51$$

$$U_{RfeON} = U_{dc} - R_{cup}I_{RcupON} - R_{lfs}I_{RlfsON} - U_{SWON}$$

Assuming that the products of voltage across the main inductance and time are equal in both switching states the relationship between  $U_{RfeON}$  and  $U_{RfeOFF}$  yields:

$$U_{RfeON} \cdot D \cdot T_S = U_{RfeOFF} \cdot (1 - D) \cdot T_S \quad 4-52$$

$$U_{RfeOFF} = \frac{D}{1 - D} U_{RfeON}$$

In a next step the  $U_{RfeRMS}$  is calculated:

$$U_{RfeRMS} = \sqrt{\frac{1}{T_S} [(U_{RfeON})^2 D T_S + (U_{RfeOFF})^2 (1 - D) T_S]} \quad 4-53$$

The measurement of the voltage  $U_{Rfe}$  proves the equations mentioned before (figure 4.23).

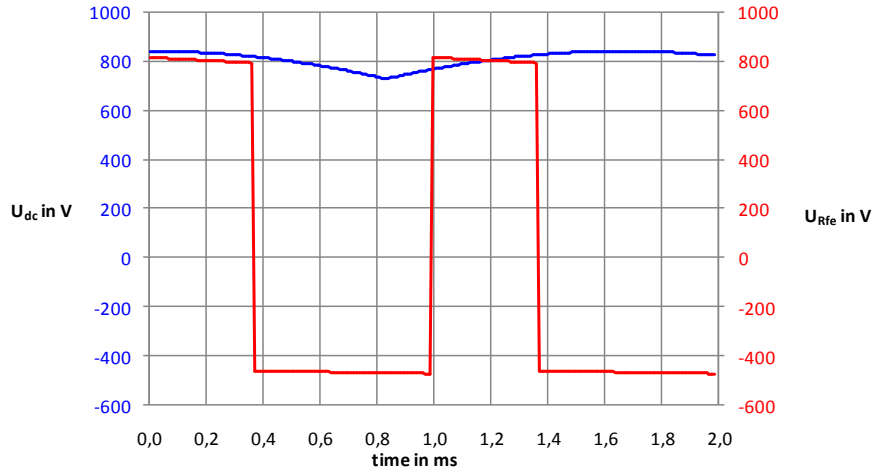


Figure 4.23 Comparison of the input voltage  $U_{dc}$  and the voltage  $U_{Rfe}$

*Losses of the Switch  $P_{ISW}$*

These losses are estimated in a similar way compared to those of the diodes used in the three phase rectifier. An IGBT is selected as a suitable switch. There are again conduction  $P_{ISWcon}$  and switching losses  $P_{ISWsw}$  [23]:

$$P_{ISW} = P_{ISWcon} + P_{ISWsw} \quad 4-54$$

$$P_{ISWcon} = V_{(TO)}I_{Fav} + r_T I_{FRMS}^2$$

$$P_{ISWsw} = (E_{on} + E_{off}) \frac{U_{CEOFF}}{V_{CE}} f_S$$

With:

- $V_{(TO)}$ : threshold voltage which is equal to  $U_{SWON}$
- $r_T$ : slope resistance
- $I_{Fav}$ : average forward current
- $I_{FRMS}$ : RMS forward current
- $E_{on}$ : turn on energy per pulse
- $E_{off}$ : turn off energy per pulse
- $V_{CE}$ : nominal collector emitter voltage
- $f_S$ : switching frequency

The conduction losses depend on the average  $I_{SWAV}$  and the RMS value  $I_{SWRMS}$  of the current flowing through the switch  $I_{SW}$ . The current  $I_{SW}$  equals  $I_{Rcup}$  and so  $I_{SWAV}$  and  $I_{SWRMS}$  yield:

$$I_{SWAV} = \frac{1}{T_S} \left( \int_0^{DT_S} I_{RcupON} dt + \int_0^{(1-D)T_S} I_{RcupOFF} dt \right) \quad 4-55$$

$$I_{SWAV} = I_{RcupON} D$$

$$I_{SWRMS} = I_{RcupRMS} \quad 4-56$$

Figure 4.22 illustrates the behavior of  $I_{SW}$  because it equals  $I_{Rcup}$ .

The reverse voltage between collector and emitter of the IGBT while it is turned off  $U_{CEOFF}$  is computed in the following way:

$$U_{CEOFF} = U_{RfeOFF} + U_{dc} - U_{RlfsOFF} \quad 4-57$$

$$U_{CEOFF} = U_{RfeOFF} + U_{dc} - R_{lfs}I_{dc}$$

The voltage  $U_{CE}$  is illustrated in figure 4.24.

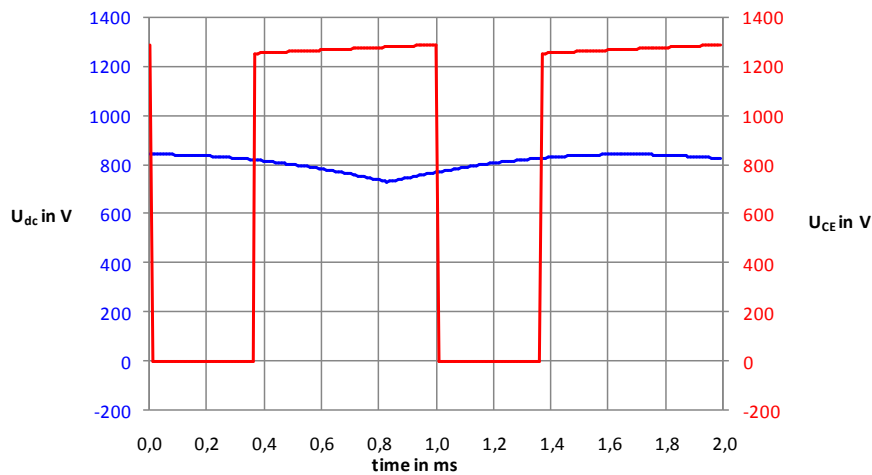


Figure 4.24 Comparison of the input voltage  $U_{dc}$  and the voltage  $U_{CE}$

The data of a suitable IGBT is shown in table 4.2. The parameters are examples of an IGBT used in this technical context and do not belong to a certain device.

Parameter	Value
$V_{CE}$	1500 V
$V_{(TO)}$	0,6 V
$r_T$	0,65 mΩ
$E_{on}$	0,7 mJ
$E_{off}$	0,8 mJ

Table 4.2 Values of the IGBT parameters

Copper losses of the transformer on the secondary side  $P_{IRcus}$

The copper losses are expressed in the next equation, similar to the copper losses on the primary side:

$$P_{IRcus} = R_{cus}I_{RcusRMS}^2 \quad 4-58$$

If a constant current in the main inductance  $I_L$  is assumed, it yields relying on current values of the on-state:

$$I_L = I_{RcupON} - I_{RfeON} \quad 4-59$$

$$I_L = I_{RcupON} - \frac{U_{RfeON}}{R_{fe}}$$

While the switch is off, the current running through the ideal side of the transformer  $I_{pOFF}$  is calculated as follows:

$$I_{pOFF} = I_L - \frac{U_{RfeOFF}}{R_{fe}} \quad 4-60$$

Finally, the current  $I_{RcusOFF}$  is described by equation 4-61:

$$I_{RcusOFF} = \frac{I_{pOFF}}{n} \quad 4-61$$

For the computation of the current  $I_{RcusRMS}$  it must be taken into account that  $I_{RcusON}$  is zero:

$$I_{RcusRMS} = \sqrt{\frac{1}{T_S} [(I_{RcusON})^2 DT_S + (I_{RcusOFF})^2 (1 - D) T_S]} \quad 4-62$$

$$I_{RcusRMS} = I_{RcusOFF} \sqrt{1 - D}$$

The measured current  $I_{Rcus}$  (figure 4.25) shows the same behavior and values as explained in the equations above.

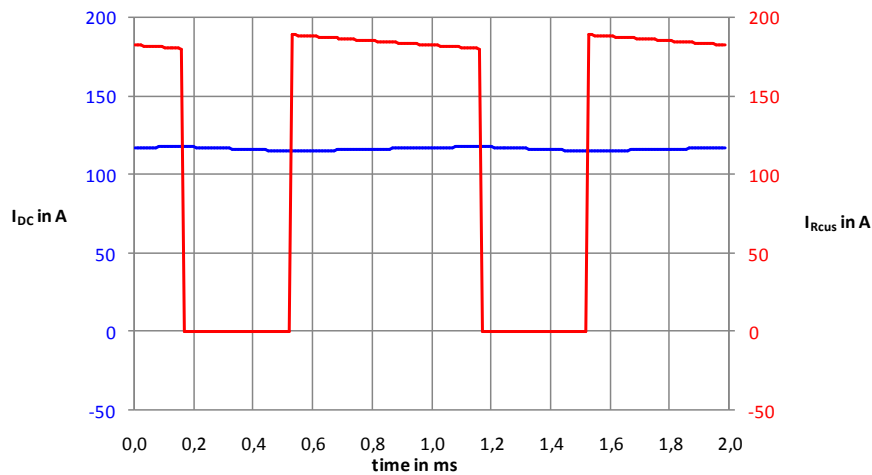


Figure 4.25 Comparison of the output current  $I_{DC}$  and the current  $I_{Rcus}$

Losses of the diode  $P_{ID}$

There are again switching  $P_{IDsw}$  and conduction losses  $P_{IDcon}$  (compare section 4.6.1):

$$P_{ID} = P_{IDcon} + P_{IDsw} \quad 4-63$$

$$P_{IDcon} = V_{(TO)} I_{Fav} + r_T I_{FRMS}^2$$

$$P_{IDsw} = E_{rr} \frac{U_{CAON}}{V_{CA}} f_S$$

With:

$V_{(TO)}$ : threshold voltage

$r_T$ : slope resistance

$I_{Fav}$ : average forward current

$I_{FRMS}$ : RMS forward current

$V_{CA}$ : nominal cathode anode voltage

$E_{rr}$ : reverse recovery energy

$f_S$ : switching frequency

The average and the RMS value of the diode current  $I_D$  are expressed in equation 4-64 and 4-65:

$$I_{DAV} = \frac{1}{T_S} \left( \int_0^{DT_S} I_{RcusON} dt + \int_0^{(1-D)T_S} I_{RcusOFF} dt \right) \quad 4-64$$

$$I_{SWAV} = I_{RcusOFF} (1 - D)$$

$$I_{SWRMS} = I_{RcusRMS} \quad 4-65$$

The behavior of  $I_D$  is illustrated in Figure 4.25 because  $I_D$  equals  $I_{Rcus}$ .

The voltage between cathode and anode of the diode during the on-state is calculated in equation 4-66:

$$U_{CAON} = U_{DC} + U_{RfeON} \cdot n \quad 4-66$$

The voltage  $U_{CA}$  is shown in figure 4.26.

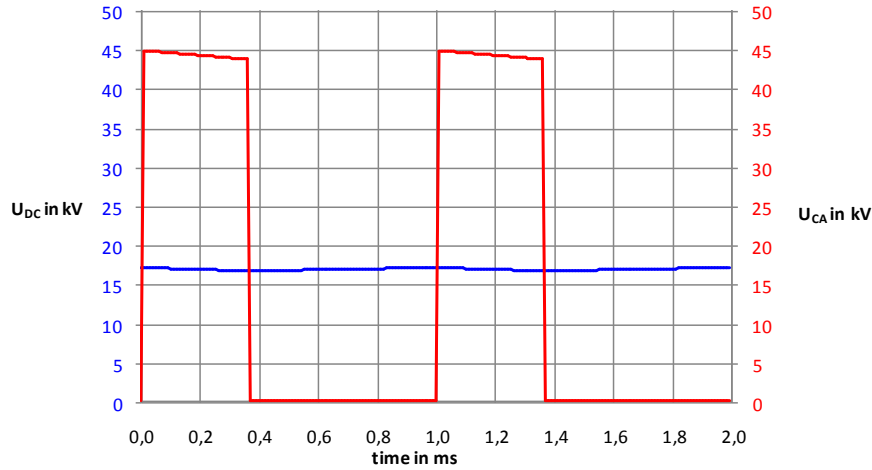


Figure 4.26 Comparison of the input voltage  $U_{DC}$  and the voltage  $U_{CA}$

The data of an applicable diode is stated in table 4.3. All parameters are examples of a diode used in this technical context and do not belong to a certain device.

Parameter	Value
$V_{CA}$	1700 V
$V_{(TO)}$	0,6 V
$r_T$	0,75 m $\Omega$
$E_{rr}$	0,2 mJ

Table 4.3 Values of the diode parameters

The maximum reverse voltage of the diode is too small in this application. A serial connection of several diodes is necessary. The number of diodes  $x$  is calculated with a 50% safety margin:

$$x = \frac{1,5 \cdot U_{CAON}}{V_{CA}} = \frac{1,5 \cdot 46kV}{1,7kV} \approx 41 \quad 4-67$$

At last, the equation for the power losses of all serial connected diodes  $P_{IDall}$  yields:

$$P_{IDall} = x \cdot P_{ID} \quad 4-68$$

Losses of the capacitor  $P_{Ic}$

For the losses of the capacitor the current  $I_{RCS}$  must be determined (equation 4-69).

$$P_{Ic} = R_{CS} I_{RCSRMS}^2 \quad 4-69$$

At first the equality of charge during on- and off-state is assumed, which leads to the relationship of  $I_{RCSON}$  and  $I_{RCSOFF}$ :

$$q_{ON} = q_{OFF} \quad 4-70$$

$$I_{RcsON} \cdot D \cdot T_S = I_{RcsOFF} \cdot (1 - D) \cdot T_S$$

$$I_{RcsOFF} = \frac{D}{1 - D} I_{RcsON}$$

In a second step a constant output current  $I_{DC}$  is estimated which equals  $I_{RcsON}$ :

$$I_{DC} = I_{RcsON} \tag{4-71}$$

$$I_{DC} = I_{RcusOFF} - I_{RcsOFF}$$

With equation 4-70 and 4-71  $I_{RcsON}$  is expressed as stated in equation 4-72:

$$I_{RcsON} = (1 - D) I_{RcusOFF} \tag{4-72}$$

In a last step the RMS value of the current  $I_{Rcs}$  is computed:

$$I_{RcsRMS} = \sqrt{\frac{1}{T_S} [(I_{RcsON})^2 D T_S + (I_{RcsOFF})^2 (1 - D) T_S]} \tag{4-73}$$

The current  $I_{Rcs}$  is gauged in the PSIM simulation and demonstrated in figure 4.27. It can be seen that the measurement follows the equations 4-70 and 4-72.

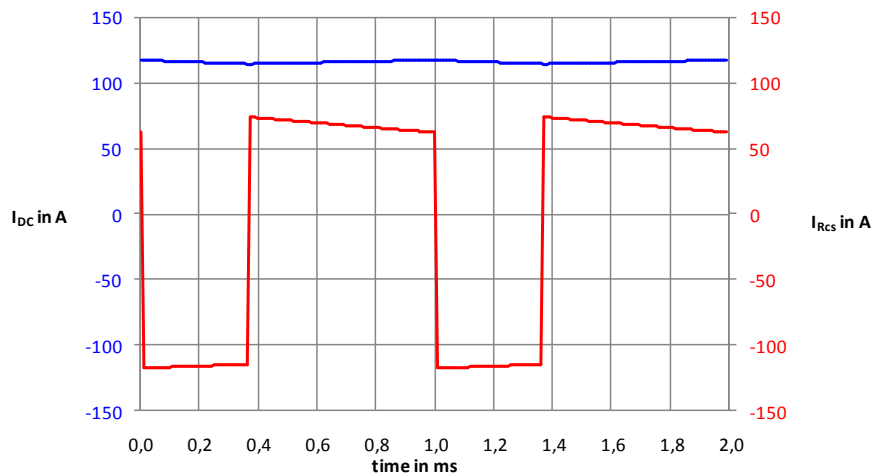


Figure 4.27 Comparison of the output current  $I_{DC}$  and the current  $I_{Rcs}$

The manufacturer of inductors, capacitors and transformers provide values for parasitic elements of their products. They are stated in the next table 4.4:

Parameter	Value
$R_{lfs}$	1 m $\Omega$
$R_{cfs}$	1 m $\Omega$
$R_{cup}$	1 m $\Omega$
$R_{fe}$	131 $\Omega$
$R_{cus}$	1 m $\Omega$
$R_{cs}$	1 m $\Omega$

Table 4.4 Parameters of the parasitic elements



The relationship between input and output parameters is the same as in a Buck-boost converter. Hence, the values for duty ratio  $D$  and transformer ratio  $n$  considered before can also be taken here. Again, assuming a current ripple of 10% of the average value  $I_{dc}$ , a value for the inductor  $L_1$  is obtained:

$$L_1 = \frac{1}{2 \cdot 0,1} \frac{U_{dcnominal}}{I_{dcnominal}} DT_s = 0,89 \text{ mH} \quad 4-79$$

Capacitors  $C_{1p}$  and  $C_{1s}$

It is assumed at first that the HF-transformer is not part of the circuit (see chapter 2.4.4) to calculate the capacitors  $C_{1p}$  and  $C_{1s}$ . They are treated as if they were one, called  $C_1$ . The voltage across this capacitor during the on-state of the switch is shown in equation 4-80 [25]:

$$\frac{dU_{C1}}{dt} = -\frac{I_{DC}}{C_1} \quad 4-80$$

With equation 4-81 the ripple magnitude of the capacitor voltage can be calculated. The slope of the voltage during the first switching state and its length is known. With  $\Delta U_{C1}$  as ripple to peak value and two times  $\Delta U_{C1}$  as peak to peak value, it yields [25]:

$$2\Delta U_{C1} = \frac{I_{DC}}{C_1} DT_s \quad 4-81$$

$$2\Delta U_{C1} = \frac{I_{dc}}{C_1} (1 - D)T_s$$

The relationship between the capacitor voltage  $U_{C1}$  and the input voltage  $U_{dc}$  of the converter is represented in equation 4-82.

$$U_{C1} = \frac{U_{dc}}{1 - D} \quad 4-82$$

A voltage ripple of 1% compared to the average value  $U_{dc}$  is estimated and the same value for the duty ratio  $D$  is taken as stated in the foregoing. Finally, the capacitor  $C_1$  is computed considering equation 4-81 and 4-82.:

$$C_1 = \frac{1}{2 \cdot 0,01} \frac{I_{dcnominal}}{U_{dcnominal}} (1 - D)^2 T_s = 35 \text{ mF} \quad 4-83$$

In a next step the capacitor  $C_1$  separated into two equal ones which are serial connected. Their value is stated in equation 4-84:

$$C_1 = \frac{C \cdot C}{C + C} = \frac{C}{2} \quad 4-84$$

$$\rightarrow C = 2C_1$$

If the HF-transformer is part of the circuit, it is placed between the two capacitors which in total have the same value as  $C_1$  again. The capacitor on the primary side of the transformer  $C_{1p}$  is equal to  $C$

mentioned above. But for the capacitor on the secondary side the winding ratio of the transformer  $n$  has to be considered:

$$C_{1p} = 2C_1 = 70mF \quad 4-85$$

$$C_{1s} = \frac{2C_1}{n^2} = 57,14\mu F$$

*Inductor  $L_2$  and capacitor  $C_2$*

The second inductor in the circuit  $L_2$  is evaluated during the time the switch is turned off. The current flowing through the inductor is shown in equation 4-86:

$$\frac{di_{L2}}{dt} = -\frac{U_{L2}}{L_2} \quad 4-86$$

The slope of the current  $i_{L2}$  is known and its duration is also given. Again,  $\Delta i_{L2}$  is a ripple to peak value and two times  $\Delta i_{L2}$  is a peak to peak value, so  $\Delta i_{L2}$  is estimated as the following:

$$2\Delta i_{L2} = \frac{U_{L2}}{L_2} (1 - D)T_S \quad 4-87$$

Solving equation 4-86 for  $L_2$ , the stated equation 4-88 is achieved:

$$L_2 = \frac{U_{L2}}{2\Delta i_{L2}} (1 - D)T_S \quad 4-88$$

The calculation of the capacitor  $C_2$  relies on the equality of charge. It is caused by the voltage change across the capacitor  $\Delta u_{C2}$  and the integral of capacitor current  $i_{C2}$  [25] is considered again. The charge generated by the voltage drop  $\Delta u_{C2}$  is the product of the peak to peak value of this voltage and the value of the capacitor  $C_2$ .

$$q = 2\Delta u_{C2}C_2 \quad 4-89$$

The equal charge is expressed by the integral of capacitor current  $i_{C2}$  over time. As stated in [25], it is calculated as follows:

$$q = \int i_{C2}dt = \frac{1}{2}i_{C2} \frac{T_S}{2} \quad 4-90$$

The integration time is half the switching period  $T_S$  due to the fact that the capacitor current  $i_{C2}$  is positive during half of the switching period.

The equation for filter capacitor  $C_2$  yields:

$$C_2 = \frac{1}{8} \frac{i_{C2}}{\Delta u_{C2}} T_S \quad 4-91$$

For an exact calculation of the two parameters  $L_2$  and  $C_2$  the following assumptions must be made:

- The voltage across the inductor  $L_2$  during the off-state equals the output voltage  $U_{DC}$  and a ripple  $U_{DCripple}$  which is estimated to be 1% of the  $U_{DC}$ :

$$U_{L_2} = U_{DC} + U_{DCripple} = U_{DC} + 0,01 \cdot U_{DC} = U_{DC}(1,01) \quad 4-92$$

- The voltage change across the capacitor  $C_2$  is  $U_{DCripple}$ :

$$\Delta u_{C_2} = U_{DCripple} = 0,01 \cdot U_{DC} \quad 4-93$$

- The current ripple in the inductor current  $\Delta i_{L_2}$  is equal to the capacitor current  $i_{C_2}$  and assumed to be 10% of the output current  $I_{DC}$ .

$$\Delta i_{L_2} = i_{C_2} = 0,1 \cdot I_{DC} = 0,1 \cdot I_{dc} \frac{1-D}{Dn} \quad 4-94$$

Finally the values for  $L_2$  and  $C_2$  regarding the assumptions stated above are computed:

$$L_2 = \frac{U_{L_2}}{2\Delta i_{L_2}}(1-D)T_s = \frac{1}{2 \cdot 0,1} \frac{U_{DC}(1,01)}{I_{dcnominal}} nDT_s = 656,74 \text{ mH} \quad 4-95$$

$$C_2 = \frac{1}{8} \frac{i_{C_2}}{\Delta u_{C_2}} T_s = \frac{0,1}{8 \cdot 0,01} \frac{I_{dcnominal}}{U_{DC}} \frac{1-D}{Dn} T_s = 4,8 \mu\text{F} \quad 4-96$$

#### L-C filter

The input filter is configured in a similar way as the L-C filter used in the Buck-boost converter (see section 4.6.2.1). Merely the capacitor current is estimated to be 10% of the nominal input current  $I_{dc}$ . The values obtained in the calculations yield:

$$L_f = \frac{0,1 U_{dcnominal}}{2 \cdot 0,001 I_{dcnominal}} DT_s = 8,9 \text{ mH} \quad 4-97$$

$$C_f = \frac{1}{2} \frac{0,1 \cdot I_{dcnominal}}{0,01 \cdot U_{dcnominal}} (1-D)T_s = 7 \text{ mF} \quad 4-98$$

### 4.6.3.2 Simulation of the ideal Cúk converter

The Simulation of the ideal Cúk converter is again done in PSIM in order to prove that the converter operates in an applicable way with parameter values for the electrical devices calculated before (see section 4.6.3.1). The converter is simulated while working under nominal conditions. The output voltage  $U_{DC}$  and current  $I_{DC}$  are measured and shown in figure 4.29. Both reach the end value in applicable time and do not start swinging.

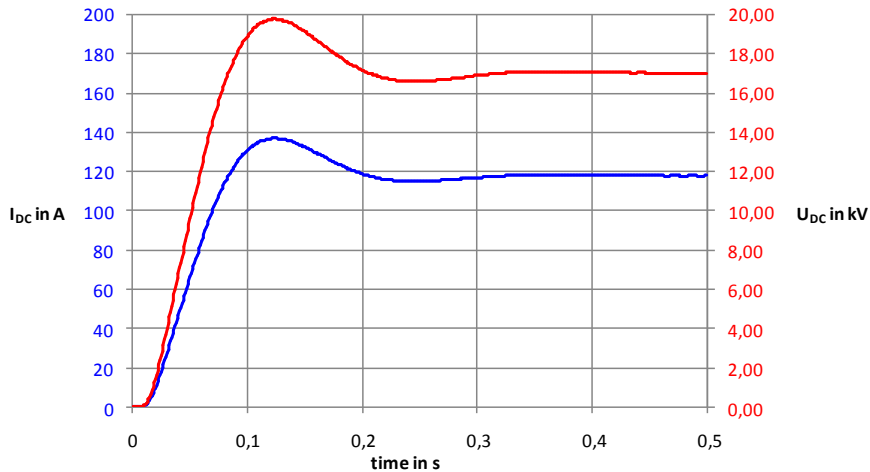


Figure 4.29 Output voltage  $U_{DC}$  and current  $I_{DC}$  of the Cúk converter

The input current  $I_{DC}$  before and after the L-C filter is also measured (figure 4.30). It can be seen that the input current ripple is small, so the influence of the converter on the generator and the turbine is negligible.

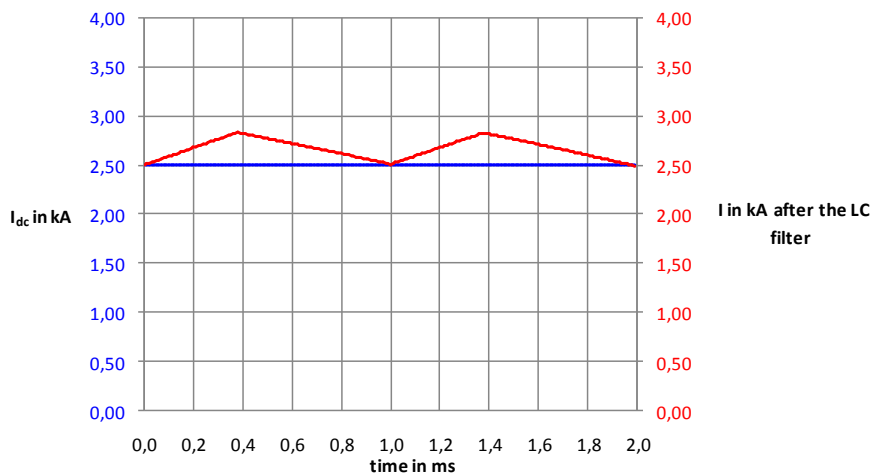


Figure 4.30 Current before and after the L-C filter

The simulation demonstrates that the converter operates in a suitable way with the computed parameter values.

### 4.6.3.3 Modeling the Cúk converter

Similar to the Buck-boost converter the Cúk converter is modeled with its parasitic elements. All explanations and assumptions made for the Buck-boost converter regarding parasitic elements and nomenclature of currents and voltages are also adopted here. Figure 4.31 and 4.32 illustrate the circuit in both states where the currents and voltages are different.

ON

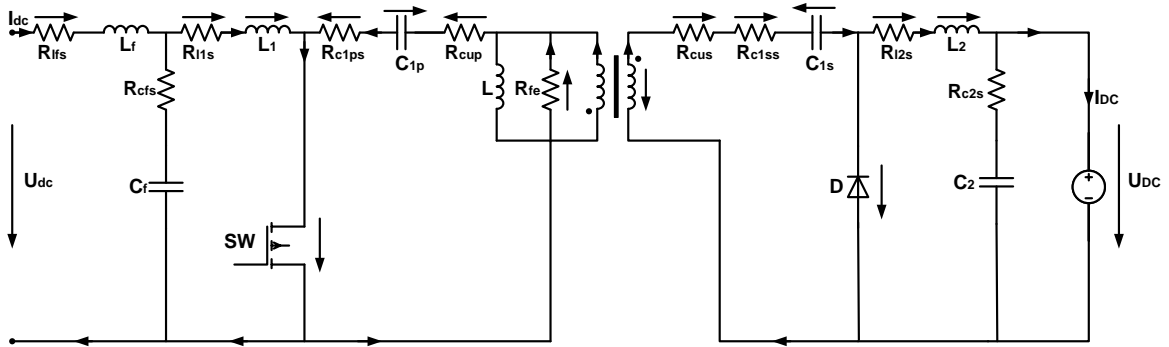


Figure 4.31 Cúk converter with parasitic elements during the on-state

OFF

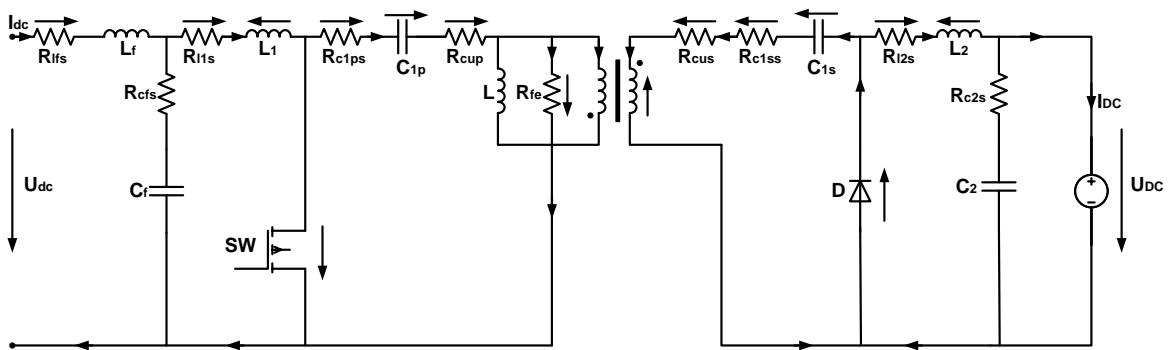


Figure 4.32 Cúk converter with parasitic elements during the off-state

Losses of the filter inductance  $P_{lf}$

The losses  $P_{lf}$  are computed in the same way as in the Buck-boost converter and are described in equation 4-99. The same assumptions regarding the voltage drop across this inductance is made (see section 4.6.2.3 and figure 4.33).

$$P_{lf} = R_{lfs} I_{RlfsRMS}^2 \quad 4-99$$

$$P_{lf} = R_{lfs} I_{dc}^2$$

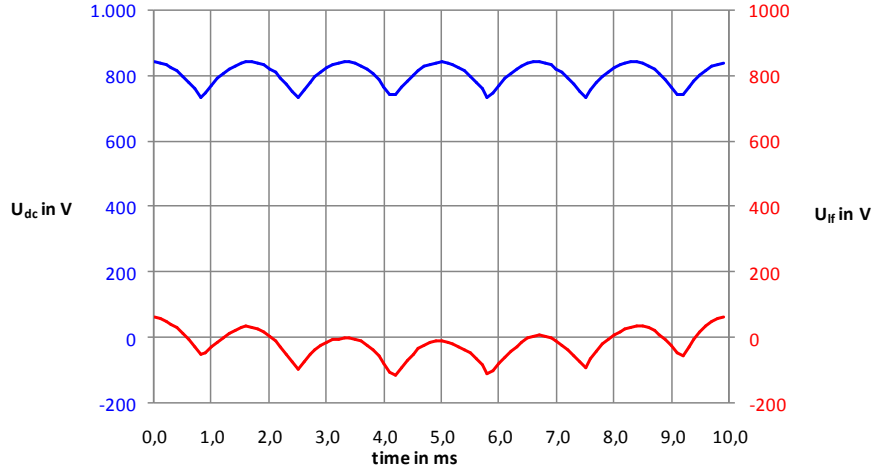


Figure 4.33 Comparison of the input voltage  $U_{dc}$  and the voltage drop  $U_{if}$  across the inductor  $L_f$

*Losses of the filter capacitor  $P_{lcf}$*

The resistor  $R_{cfs}$  stands for these losses which are expressed in the next equation:

$$P_{lcf} = R_{cfs} I_{RcfsRMS}^2 \quad 4-100$$

For the calculation of the current  $I_{RcfsRMS}$  the behavior of the current  $i_{Rcfs}$  must be deemed. It is demonstrated in figure 4.34 which is achieved by the real time simulation of the Cúk converter in PSIM. The current  $i_{Rcfs}$  is a triangle curve and equals the ripple current on  $I_{Rl1s}$ . This ripple is neglected in the computation of the inductance losses in  $L_1$  because the ripple is small compared to the input current  $I_{dc}$  (figure 4.34). The current  $\Delta i_{Rcfs}$  which is the peak value is obtained by equation 4-101.

$$\frac{di_{Rcfs}}{dt} = \frac{U_{L1ON}}{L_1} \quad 4-101$$

$$\Delta i_{Rcfs} = \frac{U_{L1ON}}{2L_1} DT_S$$

$$\Delta i_{Rcfs} = \frac{U_{dc} - U_{Rlfs} - U_{Rl1s} - U_{SWON}}{2L_1} DT_S$$

$$\Delta i_{Rcfs} = \frac{U_{dc} - I_{dc}(R_{lfs} + R_{l1s}) - U_{SWON}}{2L_1} DT_S$$

The RMS value of triangle current which is assumed to be symmetric is achieved as follows [27]:

$$I_{RcfsRMS} = \frac{\Delta i_{Rcfs}}{\sqrt{3}} \quad 4-102$$

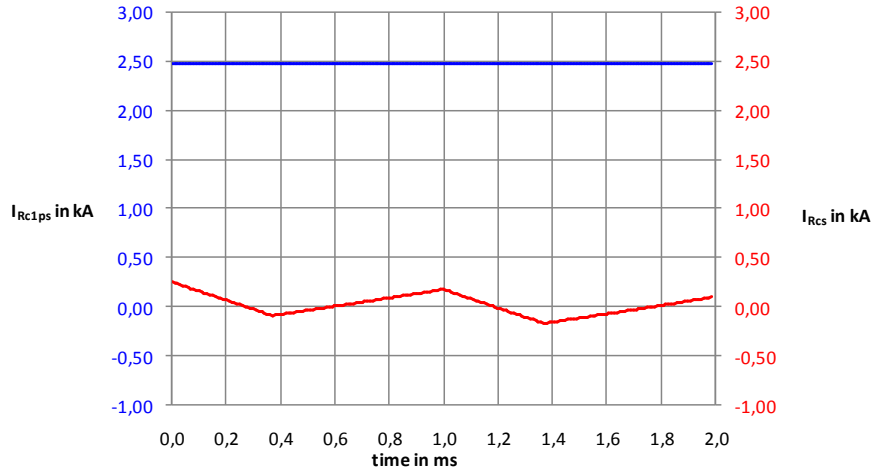


Figure 4.34 Comparison of the input current  $I_{dc}$  and the current  $I_{Rcs}$

*Losses of the first inductance  $P_{ll1}$*

The current  $I_{Rl1s}$  is equal to the input current  $I_{dc}$  if  $i_{Rcfs}$  is not taken into account as explained before. The equation describing the losses  $P_{ll1}$  yields:

$$P_{ll1} = R_{l1s} I_{Rl1sRMS}^2 \quad 4-103$$

$$P_{ll1} = R_{l1s} I_{dc}^2$$

*Losses of the first capacitor  $P_{lc1p}$  on the primary side of the transformer*

These losses are expressed in the next equation:

$$P_{lc1p} = R_{c1ps} I_{Rc1psRMS}^2 \quad 4-104$$

Both switching states are deemed for the calculation of the current  $I_{Rc1psRMS}$ . While the switch is turned off (figure 4.32) the current flowing through the resistor  $I_{Rc1psOFF}$  equals the input current  $I_{dc}$ . A constant voltage across the filter capacitor  $C_{1p}$  is estimated. Hence, the charge  $q_{OFF}$  stored during the off-state equals the charge  $q_{ON}$  which is the emitted while the switch is turned on. The following relationship is obtained:

$$q_{ON} = q_{OFF} \quad 4-105$$

$$I_{Rc1psON} \cdot D \cdot T_S = I_{Rc1psOFF} \cdot (1 - D) \cdot T_S$$

$$I_{Rc1psON} = \frac{1 - D}{D} I_{dc}$$

With the knowledge of both currents during the RMS value  $I_{Rc1psRMS}$  depending on the input current  $I_{dc}$  is expressed by equation 4-106.

$$I_{Rc1psRMS} = \sqrt{\frac{1}{T_S} [(I_{Rc1psON})^2 D T_S + (I_{Rc1psOFF})^2 (1 - D) T_S]} \quad 4-106$$

The behavior of the current  $I_{Rc1ps}$  is demonstrated in figure 4.35, it follows the equations 4-105.

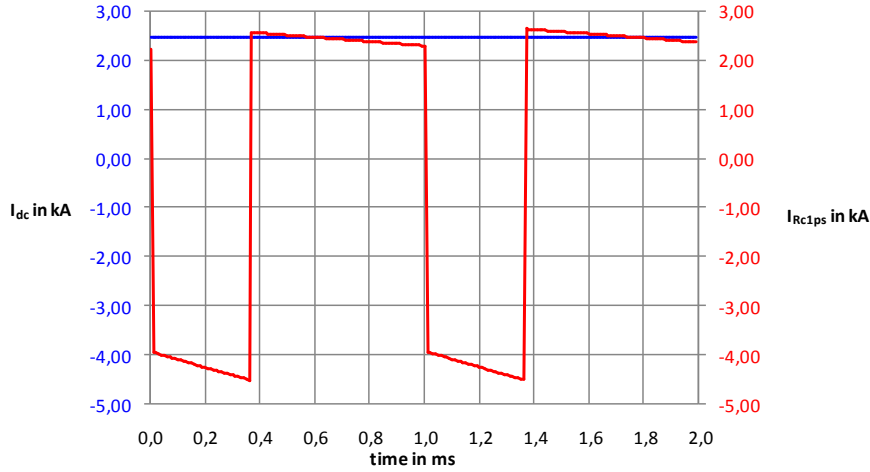


Figure 4.35 Comparison of the input current  $I_{dc}$  and the current  $I_{Rc1ps}$

Copper losses of the transformer on the primary side  $P_{IRcup}$

The currents  $I_{Rcup}$  and  $I_{Rc1ps}$  are the same. The relationship expressing the losses in  $R_{cup}$  yields:

$$P_{IRcup} = R_{cup} I_{RcupRMS}^2 \quad 4-107$$

$$P_{IRcup} = R_{cup} I_{Rc1psRMS}^2$$

Iron losses of the transformer  $P_{IRfe}$

These losses are computed with the voltage drop across the main inductance  $U_{RfeRMS}$  and the resistor  $R_{fe}$ .

$$P_{IRfe} = \frac{U_{Rfe}^2}{R_{fe}} \quad 4-108$$

The voltage across  $R_{fe}$  while the switch is on  $U_{RfeON}$  is computed under the assumption of a constant voltage  $U_{C1p}$ :

$$U_{RfeON} = U_{C1p} - U_{RcupON} - U_{Rc1sON} - U_{SWON} \quad 4-109$$

$$U_{RfeON} = U_{C1p} - I_{Rc1psON} (R_{c1ps} + R_{cup}) - U_{SWON}$$

In a second step, the voltage drops across the inductance  $L_1$  are explained in the two switching states:

$$U_{L1ON} = U_{dc} - U_{RlfsON} - U_{Rl1sON} - U_{SWON} \quad 4-110$$

$$U_{L1ON} = U_{dc} - I_{dc}(R_{lfs} + R_{l1s}) - U_{SWON}$$

$$U_{L1OFF} = U_{C1p} + U_{Rc1psOFF} + U_{RcupOFF} + U_{RfeOFF} + U_{RlfsOFF} + U_{Rl1sOFF} - U_{dc} \quad 4-111$$

$$U_{L1OFF} = U_{C1p} + I_{dc}(R_{c1ps} + R_{cup} + R_{lfs} + R_{l1s}) + U_{RfeOFF} - U_{dc}$$

Considering the equality of voltage time areas during both switching states in the inductance  $L_1$ , equation 4-112 is obtained:

$$U_{L1ON} \cdot D \cdot T_S = U_{L1OFF} \cdot (1 - D) \cdot T_S \quad 4-112$$

$$U_{L1OFF} = \frac{D}{1 - D} U_{L1ON}$$

With equation 4-109, 4-119, 4-111 and 4-112 a formula for  $U_{C1p}$  is achieved:

$$U_{C1p} = \frac{1}{1 - D} U_{dc} - \frac{1}{1 - D} I_{dc}(R_{lfs} + R_{l1s}) - I_{dc}(R_{c1ps} + R_{cup}) - U_{RfeOFF} - \frac{D}{1 - D} U_{SWON} \quad 4-113$$

Assuming that the products of voltage across the main inductance and time are equal in both switching states the relationship between  $U_{RfeON}$  and  $U_{RfeOFF}$  yields:

$$U_{RfeON} \cdot D \cdot T_S = U_{RfeOFF} \cdot (1 - D) \cdot T_S \quad 4-114$$

$$U_{RfeOFF} = \frac{D}{1 - D} U_{RfeON}$$

Finally, an equation merely relying on input variables is obtained for  $U_{RfeON}$  with 4-113 and 4-114:

$$U_{RfeON} = U_{dc} - I_{dc}(R_{lfs} + R_{l1s}) - \frac{1 - D}{D} I_{dc}(R_{c1ps} + R_{cup}) - U_{SWON} \quad 4-115$$

In a last step  $U_{RfeRMS}$  is calculated:

$$U_{RfeON} = \frac{1}{T_S} \sqrt{(U_{RfeON})^2 D T_S + (U_{RfeOFF})^2 (1 - D) T_S} \quad 4-116$$

The measurement of the voltage  $U_{Rfe}$  proves the equations mentioned before (figure 4.36).

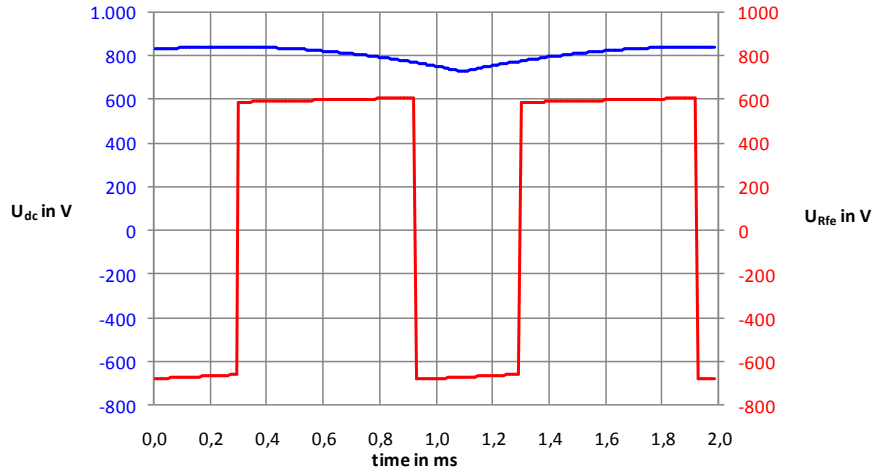


Figure 4.36 Comparison of the input voltage  $U_{dc}$  and the voltage  $U_{Rfe}$

*Losses of the Switch  $P_{ISW}$*

The computation of the switch losses  $P_{ISW}$  is done in the same way as in the Buck-boost converter. They are separated in conduction  $P_{ISWcon}$  and switching losses  $P_{ISWsw}$ :

$$P_{ISW} = P_{ISWcon} + P_{ISWsw} \quad 4-117$$

$$P_{ISWcon} = V_{(TO)} I_{Fav} + r_T I_{FRMS}^2$$

$$P_{ISWsw} = (E_{on} + E_{off}) \frac{U_{CEOFF}}{V_{CE}} f_S$$

With:

- $V_{(TO)}$ : threshold voltage which is equal to  $U_{SWON}$
- $r_T$ : slope resistance
- $I_{Fav}$ : average forward current
- $I_{FRMS}$ : RMS forward current
- $E_{rr}$ : reverse recovery energy
- $E_{on}$ : turn on energy per pulse
- $E_{off}$ : turn off energy per pulse
- $V_{CE}$ : nominal collector emitter voltage
- $f_S$ : switching frequency

The conduction losses rely on the average  $I_{SWAV}$  and the RMS value  $I_{SWRMS}$  of the switch current  $I_{SW}$ . The current  $I_{SW}$  is the sum of  $I_{Rc1psON}$  and  $I_{Rl1sON}$  and so  $I_{SWAV}$  and  $I_{SWRMS}$  yield:

$$I_{SWAV} = \frac{1}{T_S} \int_0^{DT_S} (I_{Rc1psON} + I_{Rl1sON}) dt \quad 4-118$$

$$I_{SWAV} = (I_{Rc1psON} + I_{Rl1sON})D$$

$$I_{SWRMS} = \sqrt{\frac{1}{T_S} \int_0^{DT_S} (I_{Rc1psON} + I_{Rl1sON})^2 dt}$$

$$I_{SWRMS} = (I_{Rc1psON} + I_{Rl1sON})\sqrt{D}$$

In figure 4.37 the current  $I_{SW}$  is illustrated. It can be seen that the behavior of  $I_{SW}$  predicted by the equations 4.118 is similar to the measurement in the PSIM simulation.

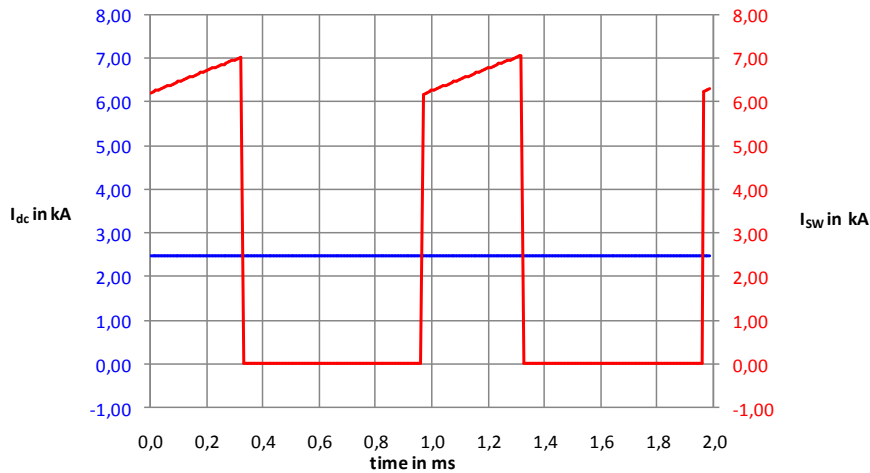


Figure 4.37 Comparison of the input current  $I_{dc}$  and the current  $I_{sw}$

The reverse voltage between collector and emitter of the IGBT while it is turned off  $U_{CEOFF}$  is obtained in equation 4-120.

$$U_{CEOFF} = U_{l1OFF} - U_{Rl1sOFF} - U_{RlfsOFF} + U_{dc} \tag{4-120}$$

$$U_{CEOFF} = U_{l1OFF} + U_{dc} - I_{dc}(R_{lfs} + R_{l1s})$$

The voltage  $U_{CE}$  is illustrated in figure 4.38.

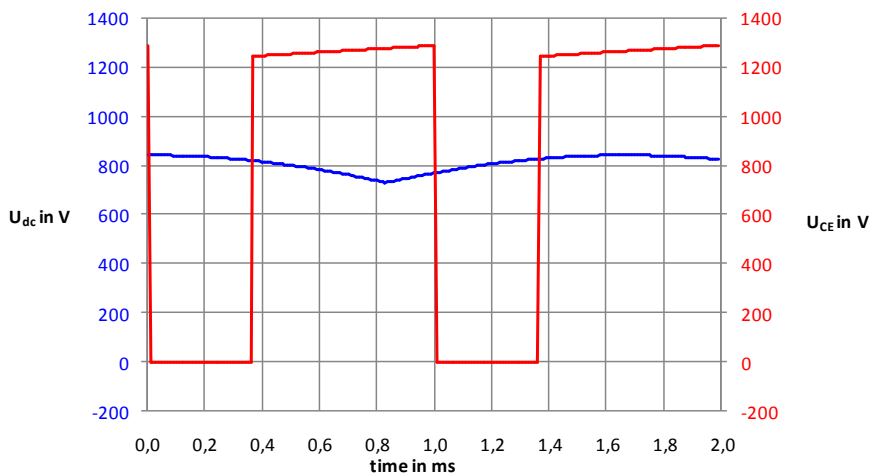


Figure 4.38 Comparison of the input voltage  $U_{dc}$  and the voltage  $U_{ce}$

The data of an applicable IGBT is stated in table 4.5. The parameters are examples of an IGBT which is used in this technical context. They do not belong to a certain device.

<b>Parameter</b>	<b>Value</b>
$V_{CE}$	1500 V
$V_{(TO)}$	0,6 V
$r_T$	0,65 mΩ
$E_{on}$	0,7 mJ
$E_{off}$	0,8 mJ

**Table 4.5 Values of the IGBT parameters**

*Copper losses of the transformer on the secondary side  $P_{I_{Rcus}}$*

The copper losses are explained in the following equation:

$$P_{I_{Rcus}} = R_{cus} I_{RcusRMS}^2 \quad \mathbf{4-121}$$

The transformer in a Buck-boost converter stores energy during one of the switching states. The main inductance and the current flowing through it are important for the functionality of the converter and cannot be neglected. In contrast to this, the transformer used in a Cúk converter transfers merely power from the primary to the secondary side. If a transformer core with a high permeability is used, the magnetization current through the main inductance is small and is neglected here [22]. Relying on this assumption the current running through the ideal side of the transformer  $I_p$  is calculated as follows:

$$I_{pON} = I_{RcupON} - \frac{U_{RfeON}}{R_{fe}} \quad \mathbf{4-122}$$

$$I_{pOFF} = I_{RcupOFF} - \frac{U_{RfeOFF}}{R_{fe}}$$

The transformer ratio  $n$  is taken into account to compute the current  $I_{Rcus}$ :

$$I_{RcusON} = \frac{1}{n} \left( I_{RcupON} - \frac{U_{RfeON}}{R_{fe}} \right) \quad \mathbf{4-123}$$

$$I_{RcusOFF} = \frac{1}{n} \left( I_{RcupOFF} - \frac{U_{RfeOFF}}{R_{fe}} \right) \quad \mathbf{4-124}$$

At last, the RMS value of the current  $I_{Rcus}$  is obtained by the following expression:

$$I_{RcusRMS} = \sqrt{\frac{1}{T_S} [(I_{RcusON})^2 D T_S + (I_{RcusOFF})^2 (1 - D) T_S]} \quad \mathbf{4-125}$$

The gauged current  $I_{Rcus}$  (figure 4.39) has the same behavior and values as expressed in the equations above.

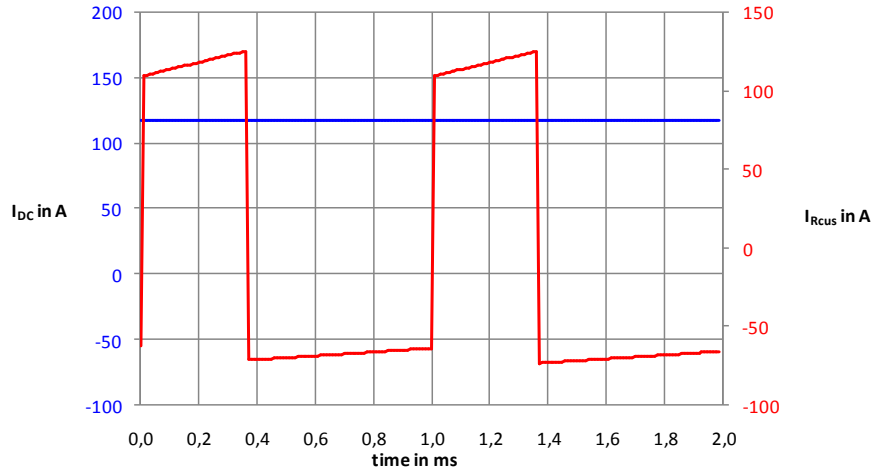


Figure 4.39 Comparison of the output current  $I_{DC}$  and the current  $I_{Rcus}$

*Losses of the first capacitor  $P_{lc1s}$  on the secondary side of the transformer*

The losses of the capacitor  $C_{1s}$  are explained in equation 4-126. The current  $I_{Rc1ssRMS}$  and the current  $I_{RcusRMS}$  are the same.

$$P_{lc1s} = R_{c1ss} I_{Rc1ssRMS}^2 \quad 4-126$$

$$P_{lc1s} = R_{c1ss} I_{RcusRMS}^2$$

The curve of the current  $I_{Rcus}$  is gauged in the PSIM simulation and is illustrated in figure 4.39.

*Losses of the second inductor  $P_{lI2}$*

The losses  $P_{lI2}$  are characterized by the resistor  $R_{l2s}$ . The relationship describing these losses yields:

$$P_{lI2} = R_{l2s} I_{Rl2sRMS}^2 \quad 4-127$$

If a constant current  $I_{Rl2s}$  in both switching states is deemed, the RMS value of  $I_{Rl2s}$  is equal to the current  $I_{RcusON}$ :

$$I_{Rl2sRMS} = I_{RcusON} \quad 4-128$$

*Losses of the diode  $P_{lD}$*

There are again switching  $P_{lDsw}$  and conduction losses  $P_{lDcon}$  (compare section 4.6.1):

$$P_{lD} = P_{lDcon} + P_{lDsw} \quad 4-129$$

$$P_{lDcon} = V_{(TO)} I_{Fav} + r_T I_{FRMS}^2$$

$$P_{IDsw} = E_{rr} \frac{U_{CAON}}{V_{CA}} f_S$$

With:

- $V_{(TO)}$ : threshold voltage
- $r_T$ : slope resistance
- $I_{Fav}$ : average forward current
- $I_{FRMS}$ : RMS forward current
- $V_{CA}$ : nominal cathode anode voltage
- $E_{rr}$ : reverse recovery energy
- $f_S$ : switching frequency

The current  $I_D$  is the sum of  $I_{RcusOFF}$  and  $I_{RcusON}$  and so  $I_{SWAV}$  and  $I_{SWRMS}$  yield:

$$I_{DAV} = \frac{1}{T_S} \int_0^{(1-D)T_S} (I_{RcusON} + I_{RcusOFF}) dt \quad \text{4-130}$$

$$I_{DAV} = (I_{RcusON} + I_{RcusOFF})(1 - D)$$

$$I_{DRMS} = \sqrt{\frac{1}{T_S} \int_0^{(1-D)T_S} (I_{RcusON} + I_{RcusOFF})^2 dt} \quad \text{4-131}$$

$$I_{DRMS} = (I_{RcusON} + I_{RcusOFF})\sqrt{(1 - D)}$$

In order to prove the equations mentioned before the current  $I_D$  is measured in the PSIM simulation and shown in figure 4.40.

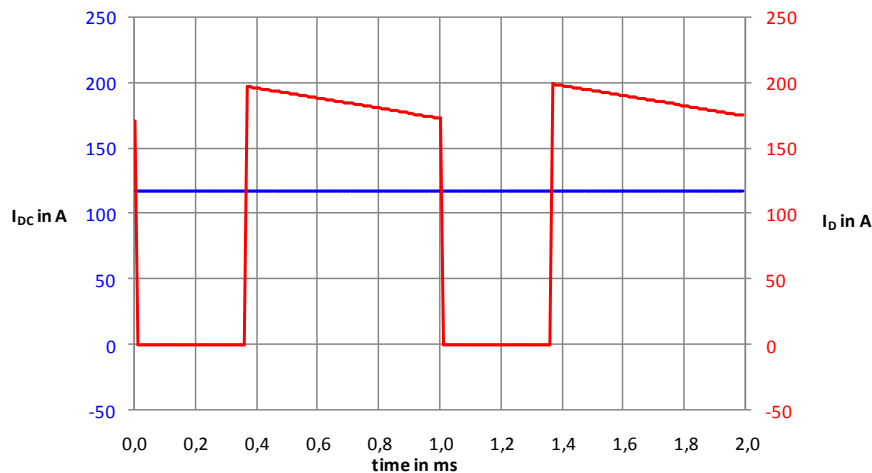


Figure 4.40 Comparison of the output current  $I_{DC}$  and the diode current  $I_D$

The voltage between cathode and anode of the diode during the on-state is computed in equation 4-132:

$$U_{CAON} = U_{DC} + U_{RI2SON} + U_{I2ON} \quad 4-132$$

$$U_{CAON} = U_{DC} + I_{RI2SON}R_{I2s} + U_{I2ON}$$

The voltage  $U_{CA}$  is shown in figure 4.41.

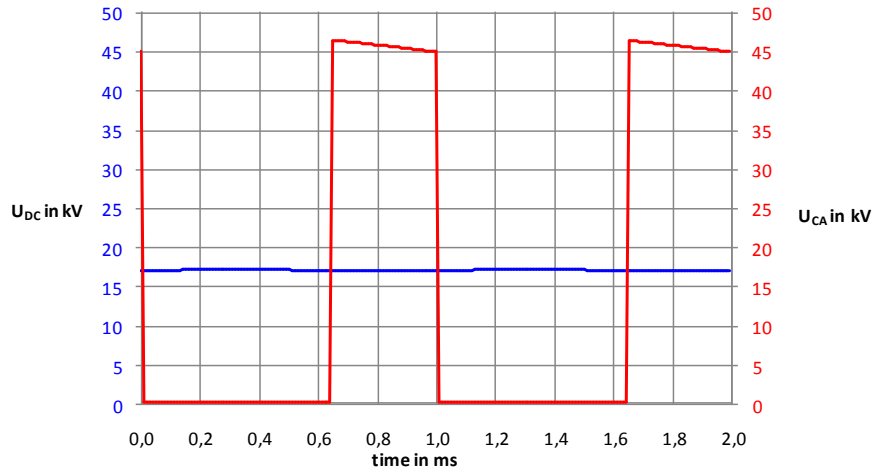


Figure 4.41 Comparison of the input voltage  $U_{DC}$  and the voltage  $U_{CA}$

The data of an applicable diode is shown in table 4.6. The parameters are examples of a diode used in this technical context and do not belong to a certain device.

Parameter	Value
$V_{CA}$	1700 V
$V_{(TO)}$	0,6 V
$r_T$	0,75 m $\Omega$
$E_{rr}$	0,2 mJ

Table 4.6 Values for the diode parameters

The maximum reverse voltage of the diode  $V_{CA}$  is too small for the usage in a Cúk converter. A serial connection of several diodes is necessary. The number of diodes  $x$  is computed with a 50% safety margin:

$$x = \frac{1,5 \cdot U_{CAON}}{V_{CA}} = \frac{1,5 \cdot 46kV}{1,7kV} \approx 41 \quad 4-133$$

In the end, the equation for the power losses of all serial connected diodes  $P_{IDall}$  yields:

$$P_{IDall} = x \cdot P_{ID} \quad 4-134$$

Losses of the second capacitor  $P_{Ic2}$

For the losses of the second capacitor the current  $I_{Rc2s}$  has to be determined (equation 4-135).

$$P_{Ic2} = R_{c2s} I_{Rc2sRMS}^2 \quad 4-135$$

The calculation of  $P_{Ic2}$  is done similarly to the losses of the filter capacitor  $C_f$ . The current  $i_{Rc2s}$  is deemed to be a triangle curve. It is demonstrated in figure 4.42 where it is gauged in the PSIM model of the Cúk converter. The current  $i_{Rc2s}$  equals the ripple current on  $I_{Rl2s}$ . This ripple is neglected in the computation of the inductance losses because the ripple is small compared to the current  $I_{Rl2s}$ . The current  $\Delta i_{Rc2s}$  which is the peak value is achieved by equation 4-136.

$$\frac{di_{Rc2s}}{dt} = \frac{U_{L2OFF}}{L_2} \quad 4-136$$

$$\Delta i_{Rc2s} = \frac{U_{L2OFF}}{2L_2} (1 - D) T_S$$

$$\Delta i_{Rc2s} = \frac{U_{DC} + U_{Rl2s} + U_{DON}}{2L_2} (1 - D) T_S$$

$$\Delta i_{Rc2s} = \frac{U_{DC} + I_{Rl2s} R_{l2s} + U_{DON}}{2L_2} (1 - D) T_S$$

The RMS value of triangle current which is considered to be symmetric is stated in following equation:

$$I_{Rc2sRMS} = \frac{\Delta i_{Rc2s}}{\sqrt{3}} \quad 4-137$$

The current  $I_{Rc2s}$  is gauged in the PSIM simulation and shown in figure 4.42.

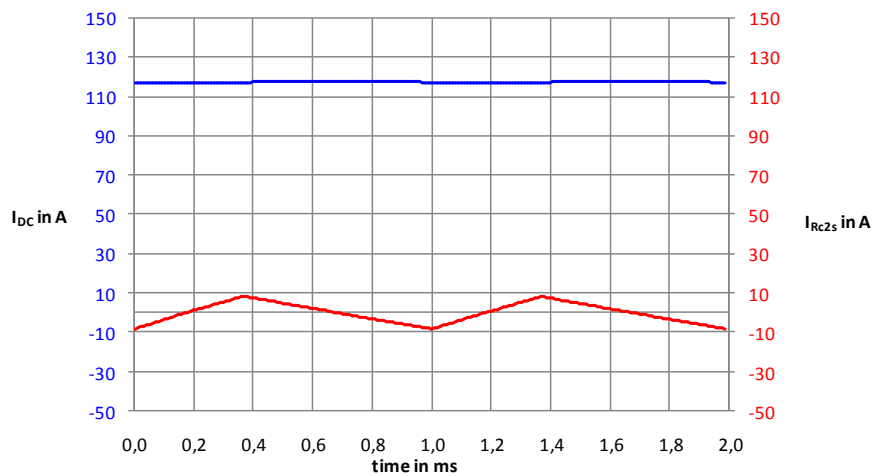


Figure 4.42 Comparison of the output current  $I_{DC}$  and the diode current  $I_{Rc2s}$

Similar to the Buck-boost converter the manufacturer of inductors, capacitors and transformer provide values for the parasitic elements as stated in the next table 4.7:

<b>Parameter</b>	<b>Value</b>
$R_{lfs}$	1 m $\Omega$
$R_{cfs}$	1 m $\Omega$
$R_{l1s}$	1 m $\Omega$
$R_{c1ps}$	1 m $\Omega$
$R_{cup}$	1 m $\Omega$
$R_{fe}$	131 $\Omega$
$R_{cus}$	1 m $\Omega$
$R_{c1ss}$	1 m $\Omega$
$R_{l2s}$	1 m $\Omega$
$R_{c2s}$	1 m $\Omega$

**Table 4.7 Parameters of the parasitic elements**

#### 4.6.4 Summary

In chapter 4 the wind turbines systems chosen in chapter 2 are modeled in the steady state theory. At first, the wind, the rotor, the gear box and the generator are expressed in mathematical equations and for each of them a model is built. The sum of these four parts of a wind turbine system is the input interface for the two converter types. The output interface is a voltage source modeling the DC-DC link to the shore.

In a second step, the Buck-boost and the Cúk converter are modeled. It is explained how the converters are configured while assuming circuits without losses. After that, the most important parasitic elements are added to the circuits of both converters and the power losses for each element are computed. Currents and voltages are measured in a real time simulation of the converters made in PSIM to prove equations and assumptions. In the end, all values to describe the parasitic elements and the used semiconductors are stated.

The two converters can be simulated relying on the models mentioned above and the performance factors, efficiency and annual energy production, can be investigated. Both are done in chapter 5.

## 5 Simulation and evaluation of the results

In this chapter both wind turbine system models based on the Buck-boost and the Cúk converter and developed in chapter 4 are simulated in the steady state theory. As part of the simulation the controlling variables duty ratio  $D$  and power coefficient of the wind turbine  $c_p$  are iterated. The algorithm this iteration relies on is explained in this chapter. Two performance factors are investigated. The first one is efficiency and the second one is annual energy production of the wind turbine system. Both factors are described in detail and based on these the two converters are compared. Finally, both converter concepts are evaluated depending on the results of the simulation. The more suitable converter type in this technical context of the described wind turbine system is selected.

### 5.1 Simulation

Here the simulation and the algorithm behind it are explained. As mentioned before an iteration of the duty ratio  $D$  and the power factor  $c_p$  is necessary. The reasons for these iterations are elucidated in the following.

#### 5.1.1 Iteration of the duty ratio $D$

During the modeling in chapter 4 merely the ideal calculation for the duty ratio is used (see chapter 4 section 4.6.2 and section 4.6.3). The losses of the converters are not taken into account because they are not known when the duty ratio is calculated. The losses are computed with the duty ratio  $D$ . Both the losses and the duty ratio depend on each other. Hence, the real duty ratio must be adjusted regarding the losses of the converter and vice versa.

##### 5.1.1.1 Calculation of the real duty ratio in a Buck-boost converter

The Buck-boost converter always fulfills equation 5-1 where input power equals the sum of output power and losses.

$$P_{coninput} = P_{conoutput} + P_{conlosses} \quad 5-1$$

$$U_{dc}I_{dc} = U_{DC}I_{DC} + P_{conlosses}$$

Solving equation 5-1 for  $I_{DC}$  the result yields:

$$I_{DC} = \frac{U_{dc}I_{dc} - P_{conlosses}}{U_{DC}} \quad 5-2$$

Based on the equations stated in chapter 4 (see section 4.6.2.3) the transfer-function for the output current  $I_{DC}$  with  $I_{dc}$  as an input is calculated:

$$I_{DC} = I_{dc} \left( \frac{(1-D)R_{fe} + \frac{R_{cup}}{D} + R_{lfs}}{DnR_{fe}} \right) - \frac{U_{dc} - U_{SWON}}{DnR_{fe}} \quad 5-3$$

If equation 5-2 and 5-3 are solved for  $D$ , the real duty ratio as function of the variables  $U_{dc}$ ,  $I_{dc}$  and  $U_{DC}$  can be obtained (5-4). The calculation software Derive is used for this computation and the result is not stated here (see M-file "mainBB.m" on the attached CD).

$$D = f(U_{dc}, I_{dc}, U_{DC}) \quad 5-4$$

### 5.1.1.2 Calculation of the real duty ratio in a Cúk converter

The equation 5-1 and 5-2 mentioned in the previous section are also correct according to the Cúk converter. Again the transfer-function for the output current  $I_{DC}$  relying on equations stated in chapter 4 (see section 4.6.3.3) with  $I_{dc}$  as an input is computed:

$$I_{DC} = I_{dc} \left( \frac{(1-D)(R_{fe} + R_{c1ps} + R_{cup}) + D(R_{l1s} + R_{lfs})}{DnR_{fe}} \right) - \frac{U_{dc} - U_{SWON}}{nR_{fe}} \quad 5-5$$

After solving equation 5-2 and 5-5  $D$ , the real duty ratio as function of the variables  $U_{dc}$ ,  $I_{dc}$  and  $U_{DC}$  can be obtained (5-6). Again Derive is used for this calculation and the result is not stated here (see M-file "mainCuk.m" on the attached CD).

$$D = f(U_{dc}, I_{dc}, U_{DC}) \quad 5-6$$

### 5.1.2 Iteration of the power factor $c_p$

Similar to the duty ratio  $D$  the power factor  $c_p$  needs to be iterated. Below nominal wind speed the power factor  $c_p$  is kept at its maximum to assure that as much power as possible is harnessed from the wind. When reaching wind speeds above nominal more power is available. But the wind turbine system cannot handle more power and so the power factor  $c_p$  is reduced (see chapter 2, section 2.1.3.2 and Appendix). In order to guarantee a converter output power of 2 MW at wind speeds above nominal wind speed, a new power factor has to be computed. Equation 5-7 describes how the new  $c_p$  value is calculated (compare chapter, section 2.1.2).

$$c_p = \frac{2MW + P_{lall}}{\frac{1}{2}\rho r_b^2 \pi v^3} \quad 5-7$$

The entire losses of the wind turbine system  $P_{lall}$  are itself a function of the power factor. This is the reason why the power factor must be iterated at wind speeds greater than nominal. The  $c_p$  values of the look up table are adjusted.

### 5.1.3 Algorithm behind the simulation

The algorithm is illustrated in figure 5.1. Firstly, all models developed in chapter 4 run once with the power coefficient from the look up table (Appendix), the ideal duty ratio  $D_{ideal}$  and a wind speed ramp as input. The ramp starts at a wind speed of 0 m/s and ends at 30 m/s. At the beginning of the loop the entire losses of the system  $P_{lall}$  are calculated and as stated in equation 5-7 a new power coefficient is obtained. If the  $c_p$  value is bigger than the possible maximum it is adjusted to the maximum. All models run again with the real duty ratio. After passing through the loop a hundred times both variables duty ratio and power factor are iterated sufficiently well. Finally both performance factors, efficiency and annual energy production, are calculated.

## 5. Simulation and evaluation of the results

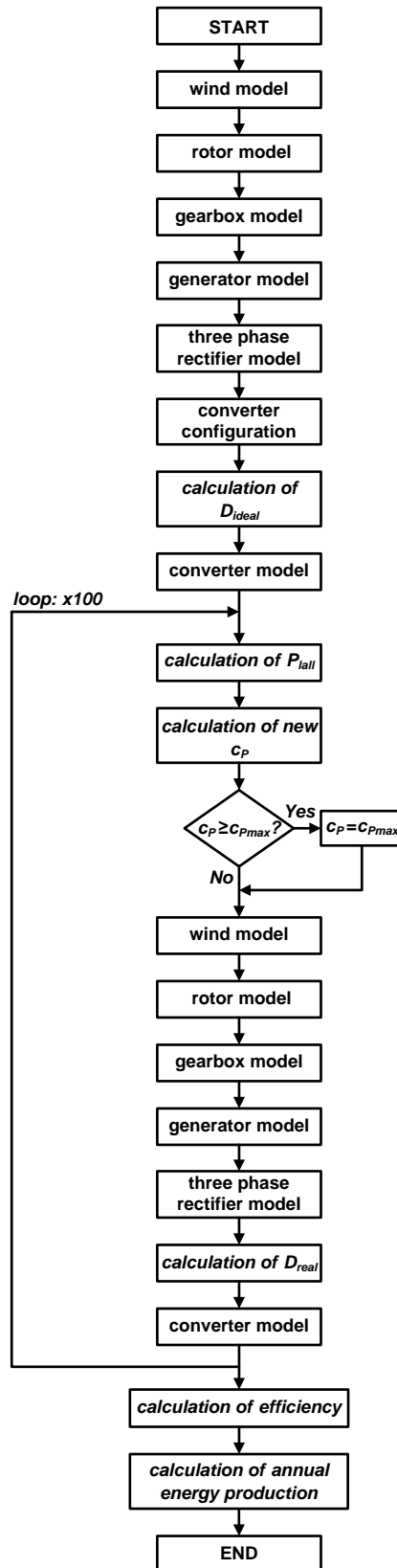


Figure 5.1 Simulation algorithm

Figure 5.2 shows input power, losses and output power of the Buck-boost converter with adjustment of the variables ( $c_p$  and  $D$ ). Merely the curves of the Buck-boost converter are deemed here due to the Cúk converter is based on the same simulation algorithm. The figure proves that the simulation algorithm explained above is operating correctly. With adjustment of  $c_p$  and  $D$  (figure 5.2), the output power is kept constant to 2 MW when enough wind power is available. Input power is the sum of output power plus losses of the converter.

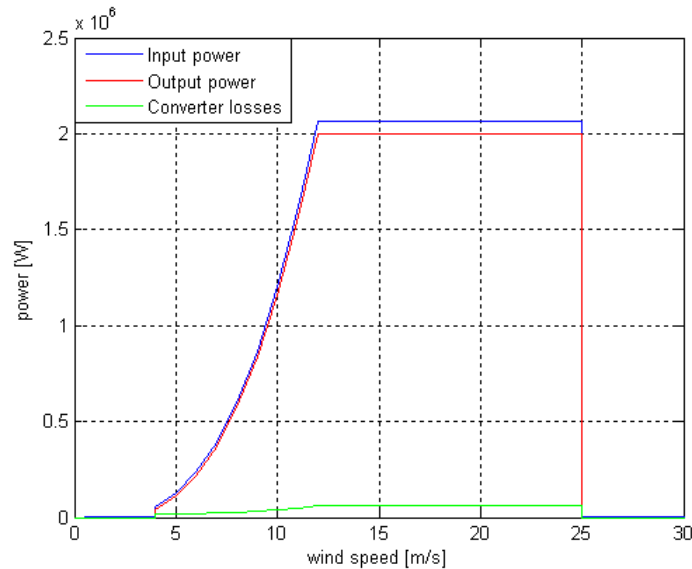


Figure 5.2 Input and output power and losses with adjustment of the variables  $c_p$  and  $D$

## 5.2 Performance factors and evaluation

In this section the two performance factors, efficiency and annual energy production of the investigated wind turbine systems, are explained. The Buck-boost and the Cuk converter are compared according to these two factors. It is evaluated which one of them is the more suitable application in the context of the described wind turbine concept (see chapter 2).

### 5.2.1 Efficiency

This performance factor is the ratio of input and output power of wind turbine system 5-8.

$$\eta = \frac{P_{convter\ output}}{P_{turbine}} \quad 5-8$$

Figure 5.3 demonstrates the efficiency of each wind turbine system regarding the converter type as function of the wind speed. Comparing the curves of both converters there is no big difference between them. A more detailed investigation is necessary.

## 5. Simulation and evaluation of the results

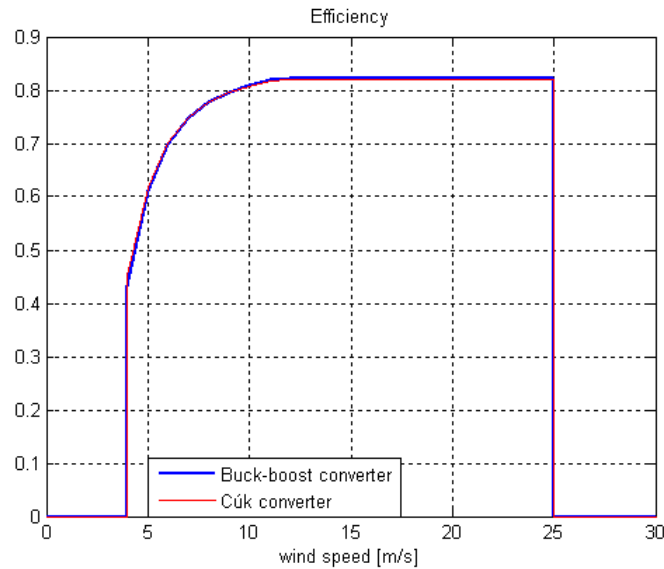


Figure 5.3 Efficiencies of the wind turbine system based on the Buck-boost and the Cúk converter

The efficiency during partial load is most interesting while investigating this performance factor. Partial load means that the output power is below its nominal value of 2 MW. It occurs in a wind speed range between 4 and 12 m/s. Here, efficiency is a keystone because there is not more power available that can be harnessed from the wind. During full load when the output power has its nominal value, losses are compensated by more power harnessed from the wind. Efficiency is less important here because there is more power available as actually used.

In figure 5.4 the efficiencies during partial load of both converters are set in comparison. The Buck-boost converter has lower efficiency in a wind speed range between 4 and 8,5 m/s while the Cúk converter shows a smaller efficiency value above 8,5 m/s. It is not possible to decide which one of the converters is the more suitable application according to the performance factor efficiency. Another performance factor is needed.

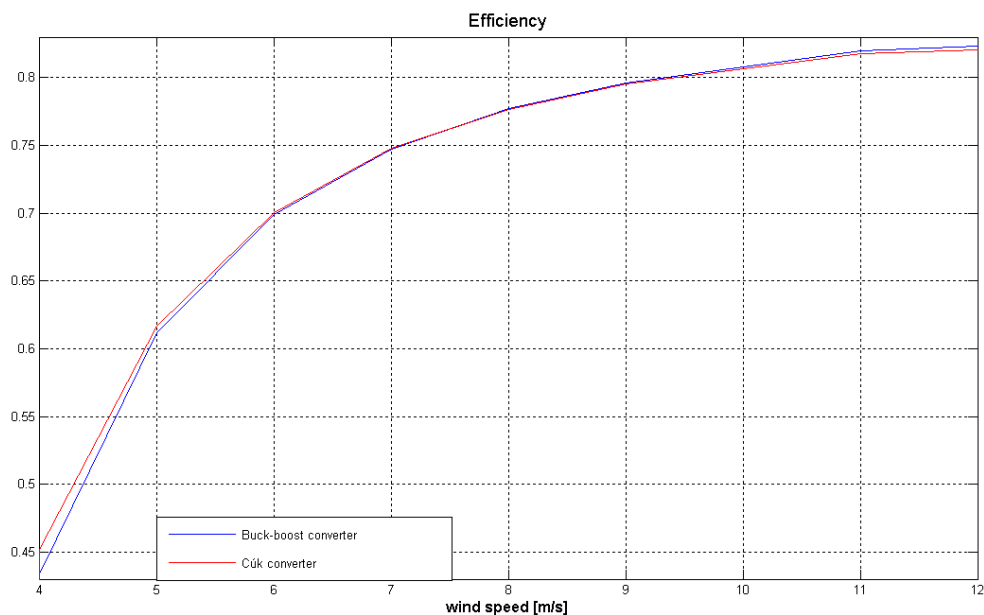


Figure 5.4 Comparison of both efficiencies

### 5.2.2 Annual energy production

The annual energy production of a wind turbine system depends on the wind speed distribution over the year at the place where the wind turbine is situated. The Weibull distribution function (5-9) of the wind speed which is commonly used to describe the wind speed distribution is also utilized in this report [1].

$$f_{Weibull}(v) = \frac{c}{a} \left(\frac{v}{a}\right)^{c-1} e^{-\left(\frac{v}{a}\right)^c} \quad 5-9$$

The parameters c and a depend on the location of the wind turbine. In this report an offshore site (IEC I) is discussed. The parameter values and the average wind speed are stated in table 5.1 [28].

Parameter	Value
a	11,38
c	2
V <sub>average</sub>	10,1 m/s

Table 5.1 Parameter values for the Weibull distribution function

In figure 5.5 the Weibull distribution function relying on the selected parameters is illustrated. It shows the probability for a certain wind speed as function of the wind speed.

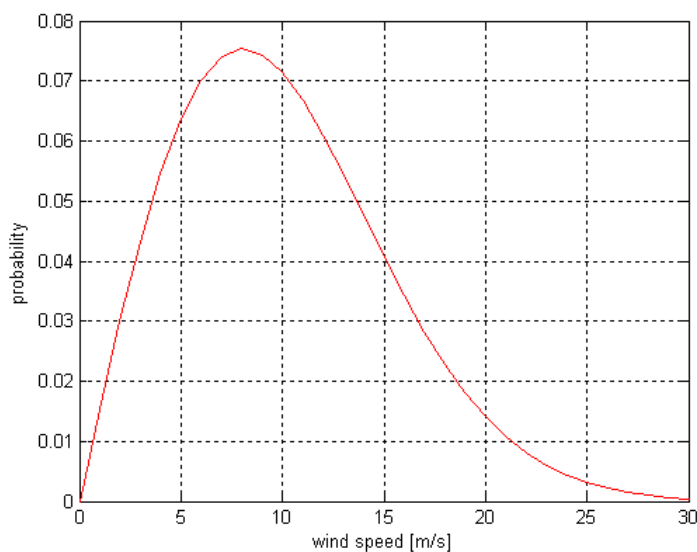


Figure 5.5 Weibull distribution function

In order to achieve an annual energy distribution as function of the wind speed, the Weibull distribution is multiplied with the number of hours the wind turbine is operating and the power output of the wind turbine as function of the wind speed. It is stated in [28] that an offshore wind turbine produces power 8122 hours per year. The simulation explained in the foregoing part of this chapter delivers the power output of each wind turbine system. For the Buck-boost and the Cúk converter the annual energy distribution is demonstrated in figure 5.6 and 5.7.

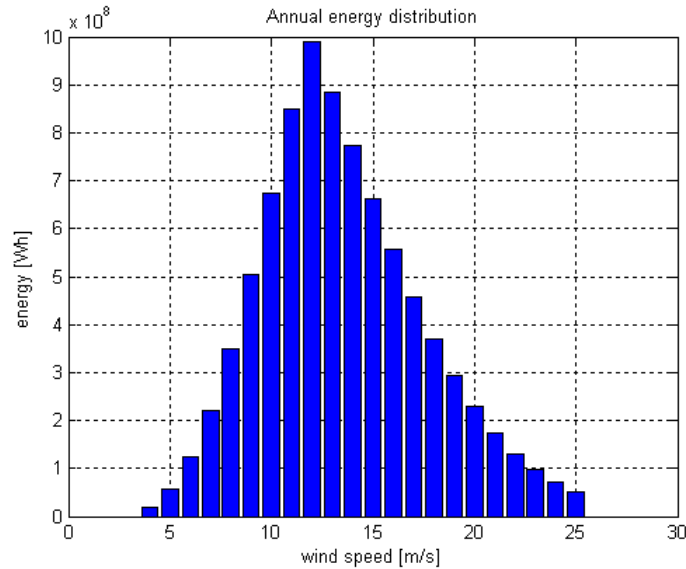


Figure 5.6 Annual energy distribution of the wind turbine system based on a Buck-boost converter

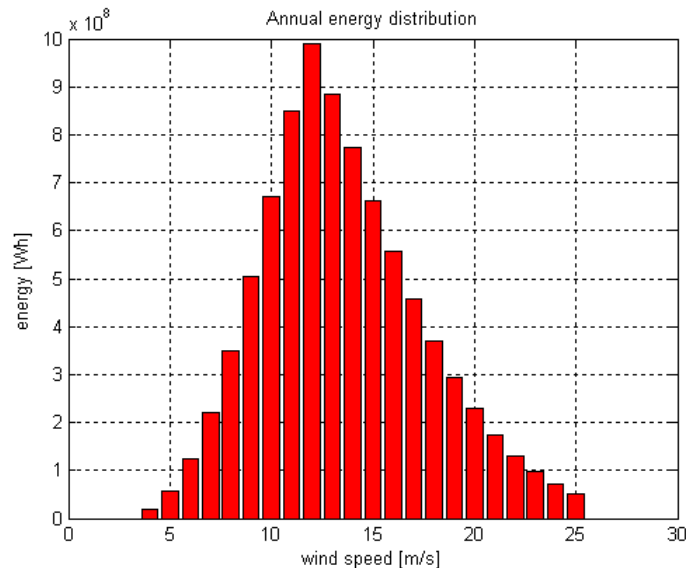


Figure 5.7 Annual energy distribution of the wind turbine system based on a Cúk converter

The amount of energy produced by the wind turbine system which is the annual energy production is obtained by the sum of energy over wind speed. The following values for the annual energy production of each converter are achieved:

Wind turbine system with a Buck-boost converter: 8,5376 GWh

Wind turbine system with a Cúk converter: 8,5356 GWh

The system based on a Buck-boost converter produces 2 MWh more energy than the system relying on the Cúk converter. This is the amount of energy a single person needs approximately in a private household per year. Although the difference in the annual energy production is not big, the Buck-boost converter is the more suitable application in this technical context described in chapter 2. A reason for the higher annual energy output of the Buck-boost converter could be found in the number of parts needed in it. The Buck-boost converter is made of six electrical devices ( $L_r$ ,  $C_r$ , transformer, switch, diode, and C; see section 4.6.2.1, figure 4.15). In comparison to that the Cúk

## ***5. Simulation and evaluation of the results***

converter consists of ten electrical parts ( $L_f$ ,  $C_f$ ,  $L_1$ , switch,  $C_{1p}$ , transformer,  $C_{1s}$ , diode,  $L_2$  and  $C_2$ ; see section 4.6.3.1, figure 4.28). If more electrical devices are part of the circuit more parasitic elements must be considered and more losses occur.

But it must be taken into account that the converter is only one part of a wind turbine system. If conditions like the wind distribution for instance are changing the comparison of the two investigated wind turbine systems could have a different result. Another important aspect are the parameter values of the parasitic elements. If there is a change among these values the result of the comparison of the two converters could differ from the achieved one too.

## 6 Conclusion

During this project a wind turbine system is explained and its parts are selected for the use in an offshore wind farm with an HVDC-link to the shore line.

The following parts are selected:

- Variable speed turbine
- Synchronous generator equipped with permanent magnets
- AC-DC converters with a high frequency transformer and a three phase rectifier
  - o Buck-boost converter
  - o Cúk converter
- Serial DC-DC interconnection of the wind turbines
- DC-link to the shore line

All parts are modeled in the steady state theory. But the main focus is set on the AC-DC converter models. Based on all models two wind power systems are simulated in Matlab. According to the performance factors efficiency and annual energy production which are the results of the simulation, both converters are compared. The comparison relying on the factor efficiency is not possible. The results of the simulation are not clear in this case. The Buck-boost converter shows a slightly higher annual energy production as the Cúk converter.

But the comparison of both converters is not the main goal of this thesis. It is the development of AC-DC-converter models in the steady state theory and this goal is reached in this thesis. The result of the comparison depends on the wind distribution and the values of parasitic elements. If they change the result could be different. That is the reason why the simulation tool made of the models is more important than the result of the comparison.

### 6.1 Further work

In this section is suggested what kind of changes can be made to improve the results of the project:

1. Different parameter values for the parasitic elements can be considered to investigate their impact on the performance factors. This offers the opportunity to inspect the impact of the quality of the parts used in the circuits of the converters.
2. Neglected parasitic elements can be taken into account.
3. Other wind distributions can be used as input.
4. Different high frequency transformers and so other switching frequencies can be considered.
5. Other AC-DC converter concepts which are not introduced in this report can be deemed.

## References

- [1]. Quaschnig, Volker. *Regenerative Energiesysteme*. München : Hanser, 2007.
- [2]. Lewald, Norbert. *Umweltverträgliche Erzeugung elektrischer Energie - Windkraftanlagen*.
- [3]. Marques, André Madeira. *Design, Control, Simulation and Energy Evaluation of a DC Offshore Wind Park*. Instituto Superior Técnico, Universidade Técnica de Lisboa : s.n., 2009.
- [4]. Lei Shuai, Ana - Irina Stan, Tiberiu Mihai Stanciu, Daniel Ioan Stroe. *Variable speed wind turbine equipped with synchronous generator*. Aalborg University : s.n.
- [5]. F. Blaabjerg, Z. Chen, R. Teodorescu, F. Iov. *Power Electronics in Wind Turbine Systems*. Aalborg University, Institute of Energy Technology : s.n., 2006.
- [6]. Anca D. Hansen, Lars H. Hansen. *Market penetration of wind turbine concepts over the years*. Force Technology, Lyngby, Denmark; Risø National Laboratory, Wind Energy Department; Roskilde, Denmark : s.n., 2007.
- [7]. Paola Bresesti, Wil L. Kling, Ralph L. Hendriks, Riccardo Vailati. *HVDC Connection of Offshore Wind Farms to the Transmission System*. University of Eindhoven : s.n., March 2007.
- [8]. Jorge Varela Barreras, Fernando Valderrey Sánchez. *A fast method to evaluate annual energy production of different off-shore wind farm configurations connected to a VSC-HVDC line transmission including evaluation of a new variable speed wind turbine concept based on RCC-Wrig*. Aalborg University, Institute of Energy Technology, Denmark : s.n., 2009.
- [9]. D. Jovcic, N. Strachan. *Offshore wind farm with centralised power conversion and DC interconnection*. University of Aberdeen : s.n.
- [10]. Lundberg, Stefan. *Configuration studies of large wind parks*. Chalmers University of Technology, Department of Electric Power Engineering, Göteborg Sweden : s.n., 2003.
- [11]. Lazaridis, Lazaros P. *Economic Comparison of HVAC and HVDC Solutions for Large Offshore Wind Farms under Special Consideration of Reliability*. Royal Institute of Technology, Department of Electrical Engineering, Stockholm : s.n., 2005.
- [12]. D. Jovcic, J.V. Milanovic. *Offshore Wind Farm Based on Variable Frequency Mini-Grids with Multiterminal DC Interconnection*. University of Aberdeen, University of Manchester : s.n.
- [13]. F. Iov, M. Ciobotaru, F. Blaabjerg. *Power Electronics Control of Wind Energy in Distributed Power Systems*. DK-9220 Aalborg East, Denmark : s.n.
- [14]. Dr.-Ing, Leibfried Porf. *Energieübertragung und Netzregelung*. Universität Karlsruhe : s.n.
- [15]. Ned Mohan, Tore M. Undeland, William P. Robbins. *Power electronics*. USA : s.n., 2003.
- [16]. Robert Warren Erickson, Dragan Maksimović. *Fundamentals of power electronics*. USA : Kluwer Academic Publishers, 2004.
- [17]. Bhim Singh, Brij N. Singh, Amrisha Chandra, Kamal Al-Haddad, Ashish Pandey, Dwarka P. Kothari. *A Review of Single-Phase Improved Power Quality AC-DC Converters*. 2003.
- [18]. Max, Lena. *Energy Evaluation for DC/DC Converters in DC-Based Wind Farms*. CHALMERS UNIVERSITY OF TECHNOLOGY Göteborg, Sweden : s.n., 2007.
- [19]. Malinowski, Mariusz. *Sensorless Control Strategies for Three - Phase PWM Rectifiers*. Warsaw University of Technology : s.n., 2001.
- [20]. Giersch, Harthus, Vogelsang. *Elektrotechnik für Fachschulen*. Stuttgart : B. G. Teubner, 1982.
- [21]. Kenji Amei, Yukichi Takayasu, Takahisa Ohji, Masaaki Sakui. *A Maximum Power Control of Wind Generator System Using a Permanent Magnet Synchronous Generator and a Boost Chopper Circuit*. Faculty of Engineering, Toyama University, 3190 Gofuku, Toyama : s.n., 2002.
- [22]. Vogelmann, Heinrich. *Einführung in die Elektrotechnik*. Universität Karlsruhe : s.n., 2001.
- [23]. Dr. Dušan Graovac, Marco Pürschel, Andreas Kiep. *MOSFET Power Losses Calculation Using the Data-Sheet Parameters*. s.l. : Infineon, 2006.
- [24]. Braun, Prof. Dr.-Ing. Michael. *Netzgeführte Stromrichter*. Universität Karlsruhe : s.n., 2009.
- [25]. Robert W. Erickson, Dragan Maksimovic. *Fundamentals of Power Electronics*. University of Colorado : s.n., 2001.
- [26]. Garcia, Nelson. *Determining Inductor Power Losses*. s.l. : Coilcraft, 2005.

- [27]. Hering, Bressler, Gutekunst. *Elektronik für Ingenieure und Naturwissenschaftler*. Heidelberg : Springer Verlag, 2005.
- [28]. Helle, Lars. *Modeling and Comparison of Power Converters for Doubly Fed Induction Generators in Wind Turbines*. Aalborg University, Denmark : s.n., 2007.

## List of figures

- Figure 2.1 Power coefficient  $C_p$  as a function of the tip speed ratio  $\lambda$  and the pitch angle  $\theta$  [3] 4
- Figure 2.2 Power versus wind speed [4] 5
- Figure 2.3 Fixed speed wind power system with different control mechanisms [5] 6
- Figure 2.4 Wind turbine with a wound rotor induction generator and resistance control [5] 6
- Figure 2.5 Limited speed wind power system with a doubly-fed induction generator [5] 7
- Figure 2.6 Variable speed wind power system with a squirrel cage induction generator [5] 8
- Figure 2.7 Variable speed wind power system with a synchronous generator [5] 8
- Figure 2.8 Variable speed wind power system with a permanent magnet synchronous generator 8
- Figure 2.9 Variable speed wind power system with a Multi-pole synchronous generator [5] 8
- Figure 2.10 Variable speed wind power system with a Multi-pole PM-synchronous generator [5] 9
- Figure 2.11 General topology of an off shore wind farm 11
- Figure 2.12 Offshore wind farm based on an AC-AC concept [10] 12
- Figure 2.13 Offshore wind farm based on an AC-DC concept [10] 12
- Figure 2.14 Offshore wind farm based on a DC-DC concept with parallel connection [10] 13
- Figure 2.15 Offshore wind farm based on a DC-DC concept with serial connection [10] 13
- Figure 2.16: Boost converter 15
- Figure 2.17: Off and on state of the boost converter [15] 15
- Figure 2.18: Buck boost converter 17
- Figure 2.19: Off and on state of the buck boost converter [15] 17
- Figure 2.20 Buck boost converter with a HF transformer 18
- Figure 2.21 Cúk converter 18
- Figure 2.22 Off and on state of the Cúk converter [15] 19
- Figure 2.23 Cúk converter with high frequency transformer [17] 20
- Figure 2.24 Full-bridge converter 20
- Figure 2.25 Active three phase rectifier 21
- Figure 4.1 Overview of the entire model 26
- Figure 4.2 Block diagram of the wind 26
- Figure 4.3 Power coefficient  $c_p$  as function of the wind speed  $v$  27
- Figure 4.4 Rotational speed of the rotor  $\omega_R$  as function of the wind speed  $v$  27
- Figure 4.5 Block diagram of the rotor 28
- Figure 4.6 Rotor torque  $T_R$  as function of the wind speed  $v$  28
- Figure 4.7 Block diagram of the gear box 28
- Figure 4.8 One phase circuit of a synchronous generator 29
- Figure 4.9 Space vector diagram of the synchronous generator 29
- Figure 4.10 Block diagram of the synchronous generator 30
- Figure 4.11 Output voltage  $U_s$  and  $I_s$  as function of the wind speed  $v$  32
- Figure 4.12 Model of the DC-DC connection as block a) and as circuit b) 32
- Figure 4.13 Block diagram of the synchronous generator 33
- Figure 4.14 Block diagram of the three phase rectifier 34
- Figure 4.15 Circuit of the Buck-boost converter 35
- Figure 4.16 Output voltage  $U_{DC}$  and current  $I_{DC}$  of the Buck-boost converter 38
- Figure 4.17 Currents before and after the L-C filter 39
- Figure 4.18 Buck-boost converter with parasitic elements during the on-state 39
- Figure 4.19 Buck-boost converter with parasitic elements during the off-state 40
- Figure 4.20 Comparison of the input voltage  $U_{dc}$  and the voltage drop  $U_{lf}$  across the inductor  $L_f$  41
- Figure 4.21 Comparison of the input current  $I_{dc}$  and the current  $I_{Rcs}$  42
- Figure 4.22 Comparison of the input current  $I_{dc}$  and the current  $I_{Rcup}$  43
- Figure 4.23 Comparison of the input voltage  $U_{dc}$  and the voltage  $U_{Rfe}$  44
- Figure 4.24 Comparison of the input voltage  $U_{dc}$  and the voltage  $U_{CE}$  45
- Figure 4.25 Comparison of the output current  $I_{DC}$  and the current  $I_{Rcus}$  46
- Figure 4.26 Comparison of the input voltage  $U_{DC}$  and the voltage  $U_{CA}$  48
- Figure 4.27 Comparison of the output current  $I_{DC}$  and the current  $I_{Rcs}$  49
- Figure 4.28 Circuit of the Cúk-converter 50
- Figure 4.29 Output voltage  $U_{DC}$  and current  $I_{DC}$  of the Cúk converter 54

- Figure 4.30 Current before and after the L-C filter 54
- Figure 4.31 Cúk converter with parasitic elements during the on-state 55
- Figure 4.32 Cúk converter with parasitic elements during the off-state 55
- Figure 4.33 Comparison of the input voltage  $U_{dc}$  and the voltage drop  $U_{if}$  across the inductor  $L_f$  56
- Figure 4.34 Comparison of the input current  $I_{dc}$  and the current  $I_{Rcs}$  57
- Figure 4.35 Comparison of the input current  $I_{dc}$  and the current  $I_{Rc1ps}$  58
- Figure 4.36 Comparison of the input voltage  $U_{dc}$  and the voltage  $U_{Rfe}$  60
- Figure 4.37 Comparison of the input current  $I_{dc}$  and the current  $I_{SW}$  61
- Figure 4.38 Comparison of the input voltage  $U_{dc}$  and the voltage  $U_{CE}$  61
- Figure 4.39 Comparison of the output current  $I_{DC}$  and the current  $I_{Rcus}$  63
- Figure 4.40 Comparison of the output current  $I_{DC}$  and the diode current  $I_D$  64
- Figure 4.41 Comparison of the input voltage  $U_{DC}$  and the voltage  $U_{CA}$  65
- Figure 4.42 Comparison of the output current  $I_{DC}$  and the diode current  $I_{Rc2s}$  66
- Figure 5.1 Simulation algorithm 70
- Figure 5.2 Input and output power and losses with adjustment of the variables  $c_p$  and  $D$  71
- Figure 5.3 Efficiencies of the wind turbine system based on the Buck-boost and the Cúk converter 72
- Figure 5.4 Comparison of both efficiencies 72
- Figure 5.5 Weibull distribution function 73
- Figure 5.6 Annual energy distribution of the wind turbine system based on a Buck-boost converter 74
- Figure 5.7 Annual energy distribution of the wind turbine system based on a Cúk converter 74

## Appendix

wind speed	C <sub>p</sub>	$\omega_R$
m/s	[-]	RPM
0	0,000	0,00
1	0,000	0,00
2	0,000	0,00
3	0,000	0,00
4	0,463	9,00
5	0,466	10,28
6	0,466	11,57
7	0,466	12,85
8	0,466	14,13
9	0,467	15,42
10	0,464	16,70
11	0,454	16,70
12	0,412	16,70
13	0,325	16,70
14	0,261	16,70
15	0,212	16,70
16	0,175	16,70
17	0,145	16,70
18	0,123	16,70
19	0,104	16,70
20	0,089	16,70
21	0,077	16,70
22	0,067	16,70
23	0,059	16,70
24	0,052	16,70
25	0,046	16,70